The Petrophysical Implications of Stromatolites Structures on Reservoir Quality of The Dam Formation, Saudi Arabia

BY

Jaber Muharrag

A Thesis Presented to the

COLLEGE OF GRADUATE AND INTERDISCIPLINARY STUDIES

KING FAHD UNIVERSITY OF PETROLEUM & MINERALS

DHAHRAN, SAUDI ARABIA

In Partial Fulfillment of the
Requirements for the Degree of

MASTER OF SCIENCE

In

Geology

December 2024

KING FAHD UNIVERSITY OF PETROLEUM & MINERALS

DHAHRAN- 31261, SAUDI ARABIA

DEANSHIP OF GRADUATE STUDIES

This thesis, written by **Jaber Muharrag** under the direction of his thesis advisor and approved by his thesis committee, has been presented and accepted by the Dean of Graduate Studies, in partial fulfillment of the requirements for the degree of **MASTER OF SCIENCE IN GEOLOGY.**

Hassah

Dr. Hassan A. Eltom
(Advisor)

Dr. John D Humphrey
Department Chairman

Dr. Ammar El-Husseiny
(Member)

Dr. Fawwaz Alkhaldi
(Member)

Prof. Suliman Saleh Al-Homidan
Dean of Graduate Studies

Date

2024

I dedicate this thesis to my family who supported me throughout my life to reach where I have reached today. They have unconditionally prioritized my needs over their own needs to facilitate me to succeed in life, and I could not feel more thankful.

I also dedicate this thesis to my friends and the special people in my life who never failed to offer their emotional and mental support whenever I felt the pressure was overwhelming.

I am confident that my father and mother are always proud of me on personal and professional level, and I hope this work only further consolidates this trust.

ACKNOWLEDGMENTS

I would like to start by thanking Dr. Khalid Al-Ramadan, the programs director of the geosciences department, who helped paint the pathway when I first joined the geology master's program at KFUPM and offered his guidance for me and my colleagues whenever needed.

My biggest appreciation is to my advisor Dr. Hassan Eltom who supported me ever since he became my advisor and throughout the program. We worked together on multiple projects and his help went beyond what is expected, and I always felt he was there to support me during each phase of developing my thesis project, and for that I'm greatly thankful. Dr. Hassan taught me how to successfully conduct scientific research that holds significant value, and how to formulate those results into professional writing that can be published in highly ranked journals.

I would like to thank Dr. Ammar El-Husseiny, a committee member of my thesis project, for his support in enhancing my research methodology, scientific reasoning and conclusion, and the petrophysical aspects of the analysis. His support in conducting the appropriate petrophysical testing and the means to get those tests conducted is also greatly appreciated. I would like to thank Dr. Fawwaz Al-Khaldi, an external committee member from Saudi Aramco, for his guidance and continuous consultation during different stages of the research project. He contributed significantly to the two papers that resulted from this research, especially in the write up, revision, and the construction of figures.

I extend my sincere appreciation to those that helped me conduct the fieldwork and the lab testing and analysis starting by Dr. Moaz Salih, Dr. Nabil Saraih, Mr. Ahmed Refaat, Mr. Ahmed Naji, Mr. Nanda Syahputra, Mr. Bandar Al-Otaibi, and Mr. Habeeb Al-Abbass.

Lastly, I would like to thank Saudi Aramco for sponsoring my education financially, and also following up with my progress closely to make sure I succeed in this program.

TABLE OF CONTENTS

LIST OF TABLES

LIST OF FIGURES

LIST OF ABBREVIATIONS

CASB	:	Columnar Above Sequence Boundary
CBSB	:	Columnar Below Sequence Boundary
CF	:	Columnar Form
CT	:	Computed Tomography
HL	:	Horizontally Linked
CBSB	:	Columnar Below Sequence Boundary
$\mathbf{K_{air}}$	:	Air Permeability
$\mathbf{K_H}$	:	Horizontal Permeability
$\mathbf{K_V}$	:	Vertical Permeability
NMR	:	Nuclear Magnetic Resonance
TR	:	Transported
$\mathbf{V_p}$	:	Primary Wave Velocity
XRD	:	X-ray Diffraction

ABSTRACT

Full Name : [Jaber Ibrahim Muharrag]

Thesis Title : [THE PETROPHYSICAL IMPLICATIONS OF STROMATOLITES STRUCTURES ON RESERVOIR QUALITY OF THE DAM FORMATION, SAUDI ARABIA]

Major Field : [Geology]

Date of Degree : [December 2024]

This study investigates the relationship between stromatolite morphology, stratigraphic context, and petrophysical properties in carbonate strata, focusing on samples from the Miocene-aged Dam Formation in Saudi Arabia. A total of 60 core plug samples, comprising columnar stromatolites (CF) collected above and below a sequence boundary (SB) (40 samples, evenly split) and laterally linked stromatolites (LL, 20 samples), were analyzed using field observations, petrographic techniques, and Nuclear Magnetic Resonance (NMR) to evaluate porosity, permeability, pore system architecture, and laminae characteristics. CF and LL stromatolites above SB exhibit alternating dense, micrite-rich laminae and highly porous, grain-rich laminae, with porosity ranging from 33.93% to 48.04% for CF forms and 32.28% to 54.90% for LL forms. Permeability varies significantly, ranging from 1.38 mD to 1900.50 mD for CF stromatolites and 13.31 mD to 2017.78 mD for LL stromatolites, with LL forms displaying less variability. Above the SB, stromatolites formed in transgressive system tracts under fluctuating energy conditions exhibit higher permeability due to grain-dominated sediments deposited during high-energy events, whereas low-energy conditions produce mud-dominated sediments with reduced permeability. In contrast, CF form stromatolites below the SB, deposited in restricted environments, feature mud-supported fabrics modified by diagenesis, resulting

in more uniform pore structures and narrower permeability ranges. These differences are reflected in bimodal NMR distributions above the SB and unimodal distributions below, highlighting variability in pore system architecture and fluid flow behavior. While petrographic and NMR analyses provided valuable insights, they alone could not fully explain the observed permeability variability, emphasizing the critical roles of pore connectivity and laminae orientation. This research underscores the importance of stromatolite morphology, depositional history, and stratigraphic context in controlling petrophysical properties and fluid flow dynamics, offering significant implications for reservoir characterization in carbonate systems.

ملخص الرسالة

الاسم الكامل: جابر إبراهيم محرق

عنوان الرسالة: التداعيات البتروفيزيائية لبنيات الستروماتوليت على جودة الحقل في تكوين دام في المملكة العربية السعودية

التخصص: جيولوجيا

تاريخ الدرجة العلمية: ماجستير

اتُحقق هذه الدراسة في العلاقة بين أشكال الستروماطوليت والسياق الطبقي والخصائص البتروفيزيائية في الصخور الكلسية، مع التركيز على عينات من تكوين دام الميوسيني في المملكة العربية السعودية. تم تحليل ستين عينة أسطوانية أساسية، تشمل ستروماطوليت عمودي الشكل مأخوذ من فوق وتحت الحد الطبقي (أربعون عينة مقسمة بالتساوي) وستروماطوليت مرتبط بشكل جانبي (عشرون عينة)، باستخدام الملاحظات الميدانية والتقنيات البتروغرافية والرنين المغناطيسي النووي لتقييم المسامية والنفاذية وهندسة نظام المسام وخصائص الطبقات. أظهرت الستروماطوليتات العمودية والمترابطة طبقات متناوبة بين طبقات غنية بالمكريت الكثيف وأخرى غنية بالحبيبات وذات مسامية عالية، حيث تتراوح المسامية بين 33.93% و48.04% للستروماطوليتات العمودية وبين 32.28% و54.90% للستروماطوليتات المترابطة. وتتنوع النفاذية بشكل كبير، حيث تتراوح بين 1.38 ملي دارسي و1900.50 ملي دارسي للستروماطوليتات العمودية وبين 13.31 ملي دارسي و2017.78 ملي دارسي للستروماطوليتات المترابطة، مع تفاوت أقل في الأخيرة.

فوق الحد الطبقي، تشكلت الستروماطوليتات في فترات النظام الانتقالي تحت ظروف مياه متقلبة، مما أدى إلى ترسب رواسب غنية بالحبيبات في الظروف ذات الطاقة الحركية العالية للمياه، بينما أدت الظروف ذات الطاقة الحركية المنخفضة للمياه إلى تراكم رواسب غنية بالطين وتقليل النفاذية. في المقابل، أظهرت الستروماطوليتات تحت الحد الطبقي التي تشكلت في بيئات مياه راكضه أنسجة مدعومة بالطين تم تعديلها بواسطة عمليات التحجر، مما أدى إلى هياكل مسامية أكثر انتظامًا ونطاقات نفاذية أضيق. تعكس هذه الاختلافات توزيعًا ثنائي الطور للرنين المغناطيسي النووي فوق الحد الطبقي وتوزيعًا أحادي الطور تحته، مما يبرز تفاوتًا في هندسة نظام المسام وسلوك تدفق السوائل.

على الرغم من أن التحليلات البتروغرافية والرنين المغناطيسي النووي قدمت رؤى قيمة، إلا أنها لم تتمكن بمفردها من تفسير التنوع الملحوظ في النفاذية، مما يبرز الأدوار المهمة لاتصال المسام واتجاه الطبقات. تؤكد هذه الدراسة أهمية أشكال السترومالطوليت والسياق الترسيبي والتاريخ الطبقي في التحكم في الخصائص البتروفيزيائية وديناميكيات تدفق السوائل، مما يوفر دلالات مهمة لتوصيف المكامن في الأنظمة الكلسية

CHAPTER 1

INTRODUCTION

1.1 Introduction

Stromatolites, a term derived from two words meaning "layered rocks" or "laminated beds", are sedimentary structures formed by biogenic activity of photosynthetic algae, through sediments accretion and aragonite precipitation to build these structures (Hofmann, 1973; Awramik, 1992a; Walter, 1976). Laminae is a key component of stromatolites that form entirely through microbial interaction, and when preserved, represent ancient microbial biofilaments or mats (Andres and Reid, 2006). In any free-standing body of water, these structures can form when the rate of sedimentation surpasses the destructive effects of wave activity or burrowing organisms, given that the conditions are suitable for the survival of stromatolites-building microbes (Walter, 1976). The oldest known stromatolites, reported in the literature, are found in 3.7-billion-year-old metamorphic rocks from the Isua Supracrustal Belt in Greenland, providing evidence of benthic microbial activity and early signs of life (Nutman et al., 2016). Stromatolites exhibit various morphologies shaped by environmental physical processes, reflecting microbial adaptations to changing conditions (Allwood et al., 2009). A study of modern stromatolites from Highborne Cay, Bahamas, compared semi-horizontal ridges to columnar morphologies, finding that ridges form typically occurs in shallow, high-energy

waters with frequent burial, while columnar form develops in deeper, low-energy waters with less burial activity (Andres and Reid, 2006).

Stromatolites have multiple documented occurrences in the subsurface of Saudi Arabia, particularly within Jurassic and Miocene strata (Hughes, 2010; Muharrag et al., 2024). Modern intertidal stromatolites have also been recently reported on Sheybarah Island, located in the northwest of Saudi Arabia (Vahrenkamp et al., 2024). Stromatolites have also been reported in Miocene-equivalent strata from neighboring countries to the stromatolite-bearing Dam Formation in Saudi Arabia. For instance, stromatolites are present in the Dam Formation in Qatar as stromatolitic bands and in the Fatha Formation in northern Iraq in a domal form (Muharrag et al., 2024). These stromatolites occurrences could offer valuable insights into the geospheres of these localities during their time of deposition (Awramik, 1992a).

1.2 Objectives

1.2.1 Problem statement

While numerous studies have examined stromatolites from sedimentological and stratigraphic perspectives, relatively few have thoroughly investigated their impact on petrophysical properties (Muharrag et al., 2024). As laminae are a fundamental component of stromatolite structures, they are expected to influence fluid storage and flow, either positively or negatively. The studies in the literature that explored the potential for such effects either focused on strata of different composition and geological age compared to this study, or were not thorough in linking the effects to specific morphologies or stratigraphical significance. Therefore, this study seeks to fill this knowledge gap by

evaluating whether stromatolites affect petrophysical properties differently based on their forms and stratigraphic positions, and by exploring the underlying reasons for these variations.

1.2.2 Hypothesis

To achieve the goal of this study, two hypotheses were proposed for assessment:

- ***Petrophysical properties vary with different stromatolites morphologies***
- ***Petrophysical properties of the same stromatolites' morphology vary relative to their stratigraphic position, relative to a major sequence boundary***

Two forms were examined and compared to test the first hypothesis: the **horizontally laminated form** with occasional small ridges, and the **columnar form** of isolated stromatolite heads. The columnar form was selected to evaluate the second hypothesis, as it was extensively present both below and above, and near a major sequence boundary.

1.3 Study area

This study investigates stromatolites found in the Dam Formation outcrops located in the Al-Lidam area of eastern Saudi Arabia (Fig. 1). These outcrops are represented by geographically dispersed hills that make the type locality of the formation, with the most well-preserved outcrop displaying only a portion of the formation. The Dam Formation consists of early Miocene clastic and carbonate rocks, interspersed with thin layers of evaporites that become thicker further east on the Arabian Peninsula (Fig. 2). The formation was originally deposited as distal foreland carbonates and proximal foreland

clastics linked to the ancient Neo-Tethys Ocean and the collision between the Arabian and Asian plates, which led to the Zagros Belt orogeny (Beydoun, 1993; Alkhaldi et al., 2021). Previous studies have documented stromatolite occurrences in the study area as part of facies comprising stromatolites, thrombolites, and ooids (Alkhaldi, 2009; Bashri et al., 2017; Alkhaldi et al., 2021; Ali et al., 2021). Various morphologies have been documented, reflecting diverse physical conditions, including horizontal stromatolites, linked hemispheroids, digitate heads, and isolated columns. The lamination was described previously as fine to medium quartzose packstone (Alkhaldi et al., 2021), but microscopic analysis revealed varying textures with alternating dominance of peloidal, quartz, and mud components (Muharrag et al., 2024). This facies is interpreted to represent tidal flat to intertidal environments (Alkhaldi et al., 2021).

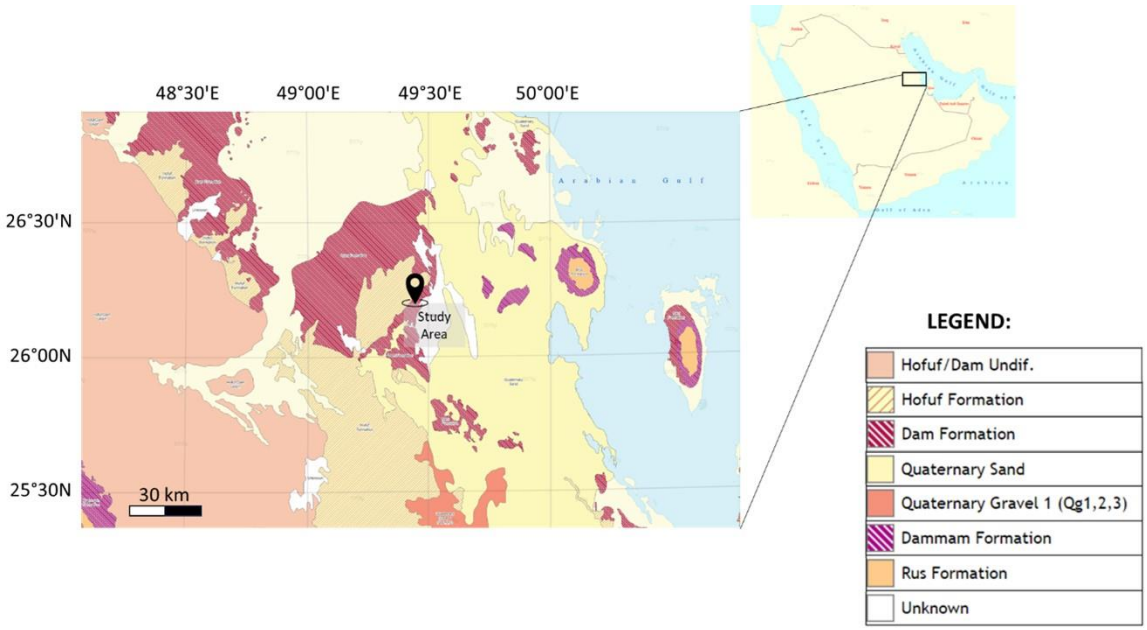

Figure 1: A base map of Dam Formation showing the outcrop study area. Other prominent formations are displayed on the map (modified after USGS).

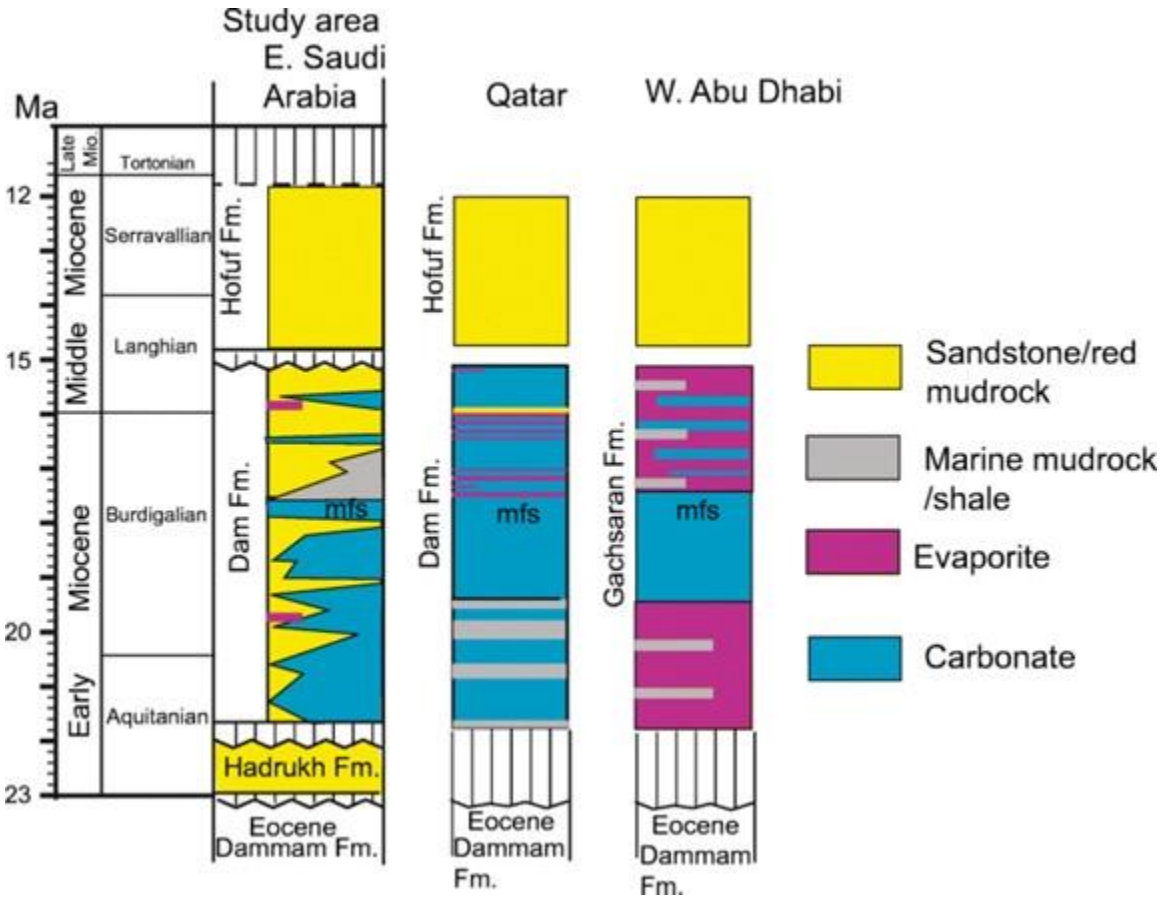

Figure 2: Dam Formation stratigraphic column showing the predominant compositions in Saudi Arabia, Qatar, and Abu Dhabi (Alkhaldi et al., 2021).

1.4 Methodology

To accurately assess the influence of stromatolites on petrophysical properties, it is essential to understand the surrounding strata, environmental conditions, and preservation processes. It is also crucial to assess the apparent lamination and rock constituents directly in situ at the outcrop location. The process began with a field investigation at the outcrop site, documenting the various stromatolite morphologies and their stratigraphic positions. Extensive sampling was conducted, taking into account the stromatolite structures and the orientation of their laminations relative to the strata.

The lab evaluation stage involved preparing the samples by coring the rock specimens into 1-inch diameter rock plugs. The rock plugs were initially examined using non-destructive testing, beginning with computerized tomography (CT) scanning to evaluate the internal structures of the samples. Nuclear magnetic resonance testing was run after saturating the samples in distilled water to assess the micro to macro porosity ratios. Both ends of the rock plug samples were polished to create flat, even surfaces for velocity measurements. The velocity testing was conducted by measuring the arrival time of primary waves (Vp). Thin sections were prepared by trimming the top of each sample and mounting them with blue-dyed epoxy. Petrographic analysis was then performed using microscopy to examine the various rock constituents and textures. Additionally, X-ray diffraction (XRD) testing was carried out to determine the mineralogical composition of the rocks.

The subsequent stage focused on statistically and graphically processing the data to interpret its implications. This began with an analysis of variance (ANOVA) to determine whether there were statistically significant differences within and between the groups in

the quantitative analysis. The data were then visualized through graphs to identify potential relationships between various parameters. Finally, all the results were integrated, and evidence-based proposals were made regarding the effects of stromatolites on the petrophysical properties of similar rock formations.

CHAPTER 2

Petrophysical implications of stromatolite morphologies: A case study of the Dam Formation, Saudi Arabia

Abstract

This study examines how stromatolite morphologies influence the porosity and permeability of carbonate strata, focusing on columnar (CF) and laterally linked (LL) forms. By emphasizing the critical role of morphology in shaping porosity, permeability, and pore system architecture, the research integrates field observations with laboratory analyses of 40 core plug samples collected from the Miocene-aged Dam Formation in Saudi Arabia. These analyses include petrographic and Nuclear Magnetic Resonance (NMR) techniques to assess rock texture, laminae characteristics, pore types, and pore size distribution. Porosity and permeability measurements were analyzed in conjunction with detailed rock characterization derived from both field and laboratory data. The findings reveal that both CF and LL stromatolite forms can be classified as coarse-grained stromatolites, comparable to examples from both modern and ancient settings. Both forms exhibit alternating dense, micrite-rich laminae and highly porous, grain-rich laminae. The grain-rich laminae are primarily composed of ooids, peloids, skeletal grains, and quartz, with well-preserved interparticle, intraparticle, and moldic porosity. In contrast, the micrite-rich laminae are characterized by clotted micrite, clotted peloids, and sinuous biofilms preserved on lamina tops. Fenestral and vuggy porosity are present in both lamina

types. Despite having relatively narrow porosity ranges—33.93% to 48.04% for CF stromatolites and 32.28% to 54.90% for LL stromatolites—both forms exhibit wide permeability ranges. Permeability in CF stromatolites ranges from 1.38 mD to 1900.50 mD, whereas LL stromatolites range from 13.31 mD to 2017.78 mD. Notably, LL stromatolites display less variable permeability compared to the highly variable CF forms. Although petrographic and NMR analyses provided valuable insights into the factors influencing permeability, the results demonstrate that these techniques alone cannot fully explain the observed permeability variability especially in the LL form. The findings suggest that additional factors, such as pore connectivity and laminae orientation, might play a significant role in controlling permeability. Proposed scenarios of laminae configuration in the samples suggest that these configurations may be the most critical factor influencing the measured permeability in stromatolites. This research has significant implications for reservoir characterization, providing a deeper understanding of fluid flow behavior in carbonate systems containing stromatolites.

Keywords: Porosity and permeability; Vuggy porosity; Fenestral porosity; microporosity; Carbonate reservoirs

2.1 Introduction

Stromatolites are one of the sedimentary structures, dating back to over 3.5 billion years, offering valuable clues about the origins of life on Earth (Awramik, 1992; Grotzinger and Knoll, 1999; Allwood et al., 2007; Noffke and Awramik, 2013). These are microbial structures that form through the buildup of biofilms of trapped sediments by photosynthetic cyanobacteria (Riding, 2002; Dupraz et al., 2009; Noffke, 2009; Noffke and Awramik,

2013; Noffke et al., 2013; Suarez-Gonzalez et al., 2014). They typically form in a wide range of environments with shallow water conditions such as subtidal, lagoons or tidal flats (Walter, 1976; Riding, 2002). They especially flourish in hypersaline or oxygen-deprived environments due to the absence of grazers such as gastropods (Dupraz et al., 2009; Noffke et al., 49 2013; Ibarra and Corsetti, 2016).

Stromatolites can develop in various morphologies depending on several factors, including the type of algae forming them, sediment availability, environmental conditions (Riding, 2002; Andres and Reid, 2006), relative position to the photic zone and oxygen levels (Jahnert and Collins, 2012; Reid et al., 2024). For instance, in shallow calm water they could grow into columnar forms, while in more dynamic, high-energy environments they tend to form sheet-like layers capable of withstanding these agitated conditions (Riding, 2002; Jahnert and Collins, 2012). Notably, stromatolite morphology is not exclusively determined by environmental conditions; similar forms can develop in distinct lithofacies, and different forms can coexist within the same lithofacies (Walter, 1976). These morphological variations play a crucial role in controlling fluid storage and flow properties, which are essential for understanding carbonate reservoir quality (Corbett et al., 2015; Ceia et al., 2022). However, research on the relationship between stromatolite morphology and petrophysical properties remains limited, leaving a critical gap in our understanding of their role in carbonate systems.

In a previous study, Muharrag et al. (2024) explored how stromatolites influence petrophysical properties within stratigraphic contexts using samples from the Dam Formation in eastern Saudi Arabia. That study revealed significant differences in porosity, permeability, and pore system architecture above and below a sequence boundary (SB).

Stromatolites above the SB, formed in transgressive system tracts, displayed higher permeability due to grain-dominated sediments, whereas stromatolites below the SB, deposited in restricted environments, exhibited more uniform pore systems with narrower permeability ranges due to diagenetic processes. These findings emphasized the importance of stratigraphic context in determining the petrophysical variability of stromatolites.

Building on these insights, the present study investigates the impact of stromatolite forms on petrophysical properties above the SB within a transgressive system tract. In addition to the columnar forms (CF) previously examined by Muharrag et al. (2024), fieldwork identified an additional stromatolite forms: laterally linked (LL) form. This research seeks to answer two key questions: How do stromatolites in general impact the petrophysical properties when they exist above a BS? And how does such impact vary based on the morphology of the stromatolite (CF versus LL)? By addressing these questions, this study aims to deepen our understanding of the role stromatolite morphology plays in shaping the petrophysical characteristics of carbonate systems. The findings provide valuable insights with significant implications for reservoir characterization and fluid flow predictions. These two questions, while interconnected, explore distinct dimensions of stromatolite influence on petrophysical properties. The first question investigates the general impact of stromatolites on petrophysical properties when they occur above a SB, emphasizing their broader role in influencing reservoir characteristics in this specific stratigraphic context. The second question builds on this by examining how this impact varies depending on the morphology of the stromatolites, delving into the specific differences between various forms. Together, these questions provide both a generalized understanding and a

morphology-specific analysis of stromatolites' role in shaping the petrophysical characteristics of carbonate systems.

2.2 Study area and geological background

The Dam Formation in Saudi Arabia (Fig. 3A, B), deposited during the Miocene, represents a transitional depositional environment where siliciclastic sediments derived from terrestrial erosion mixed with carbonate materials from shallow marine sources (Powers et al., 1966; Bashri et al., 2017; Ali et al., 2021b; Alkhaldi et al., 2021). This formation, strongly influenced by astronomical cycles, is situated above the terrestrial Hadrukh Formation (Fig. 3B), separated by an unconformable boundary, and is subsequently overlain by the Hofuf Formation (Fig. 3B) (Powers et al., 1966; Bashri et al., 2017; Ali et al., 2021b; Alkhaldi et al., 2021). The Dam Formation in outcrop comprises three composite depositional sequences, each characterized by upward-deepening trends (Powers et al., 1966; Bashri et al., 2017; Ali et al., 2021b; Alkhaldi et al., 2021). Figures 3C and 3D illustrate one of these deepening-upward cycles, where grain-dominated oolitic facies and stromatolites are overlain by massive, thick beds of skeletal peloidal wackestone (Bashri et al., 2017).

The stratigraphic sequences in the Dam Formation have been categorized into three primary facies associations: a fossiliferous carbonate group, a siliciclastic unit featuring prominent red beds, and facies rich in oolitic stromatolites (Powers et al., 1966; Bashri et al., 2017; Ali et al., 2021b; Alkhaldi et al., 2021). These distinct facies associations are separated by maximum flooding surfaces that mark significant changes in depositional conditions (Powers et al., 1966; Bashri et al., 2017; Ali et al., 2021b; Alkhaldi et al., 2021).

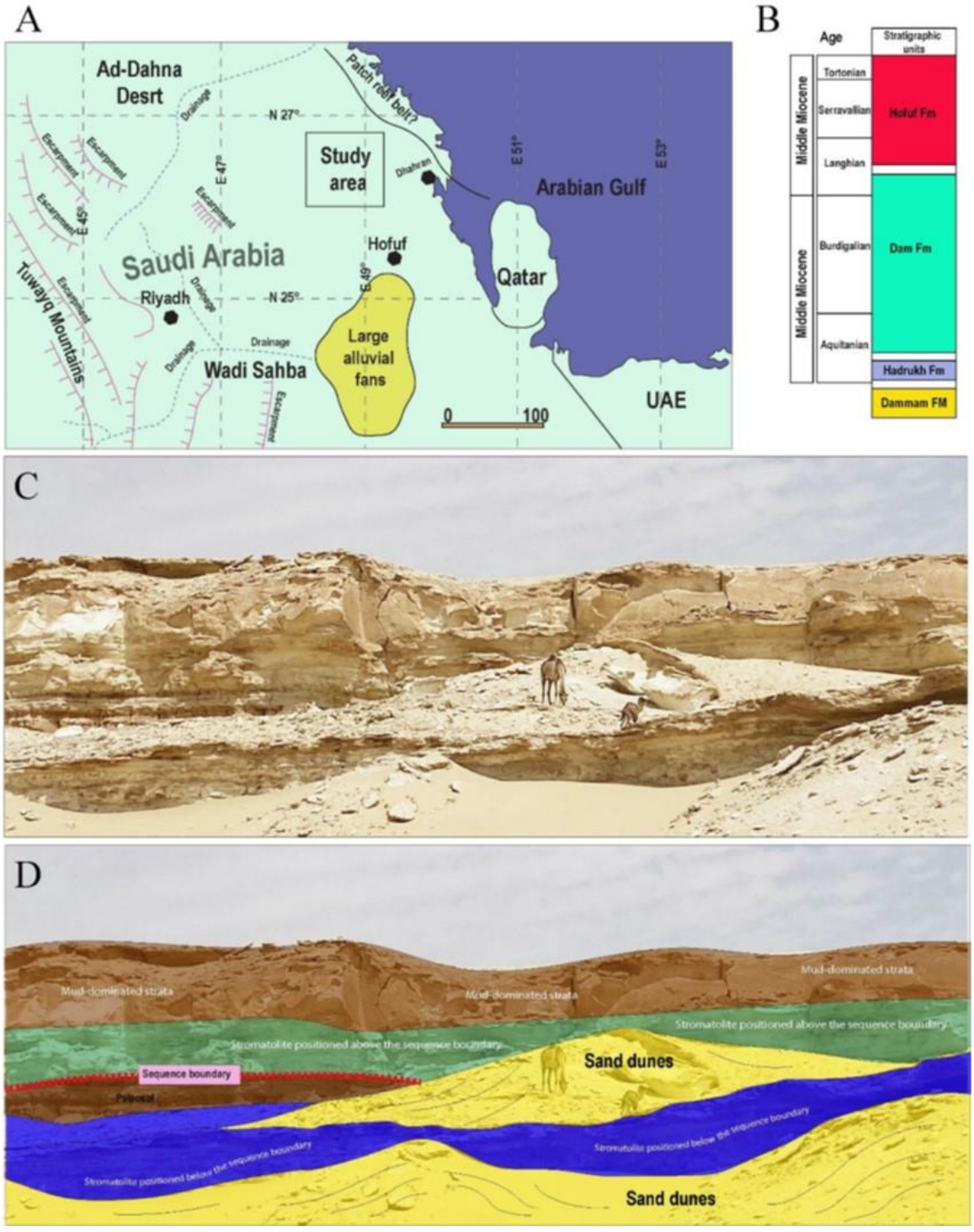

Figure 3: A) Map of eastern Saudi Arabia highlighting the study area. B) Stratigraphic column illustrating the Dam Formation, which overlies the Hudrukh Formation and is overlain by the Hofuf Formation. C and D) Photograph and corresponding annotated photograph of the Dam Formation outcrop. Note the sequence boundary at the top, above which laterally extensive oolitic grainstone and stromatolites are observed. These are overlain by mud-dominated lithofacies, indicating deepening-upward depositional cycles.

In the Al-Lidam region, stromatolites are primarily observed as bindstone structures (Figs. 4, 5), (Bashri et al., 2017). The stromatolites exhibit variations in thickness and recurrence, reflecting changes in depositional environments (Ali et al., 2021a). Notably, stromatolite heads below sequence boundaries tend to be larger in size compared to those above (Muharrag et al., 2024). Above sequence boundaries, three stromatolite morphologies have been identified: columnar forms, typically found in high-energy intertidal zones; horizontally linked forms, associated with low-to-moderate energy conditions near the boundary between intertidal and supratidal zones; and transported forms, indicative of tranquil subtidal settings with disrupted laminations and higher mud content (Alkhaldi et al., 2021).

The Dam Formation correlates with equivalent formations across the Arabian Plate, such as the Al-Nakhash Member in Qatar, the Gachsaran Formation in the UAE, the Mutla Member of the Lower Fars Formation in Kuwait, and the Fatha Formation in Iraq (Al-Saad and Ibrahim, 2002; Hampton et al., 2004; Al-Juboury and McCann, 2008; Sakhavati et al., 2020; Alrefaei et al., 2022). While stromatolites are prominent in certain equivalents, such as the domal structures in the Fatha Formation and stromatolitic bands in Qatar, they are notably absent in formations like the Gachsaran and Lower Fars, despite their similar depositional frameworks. These variations highlight the influence of localized depositional and diagenetic factors within the Miocene sedimentary systems of the Arabian Plate.

2.3 Methodology

The initial task of examining stromatolites forms in the Dam Formation of eastern Saudi Arabia dictated identifying the forms at the outcrop locality and figuring out their

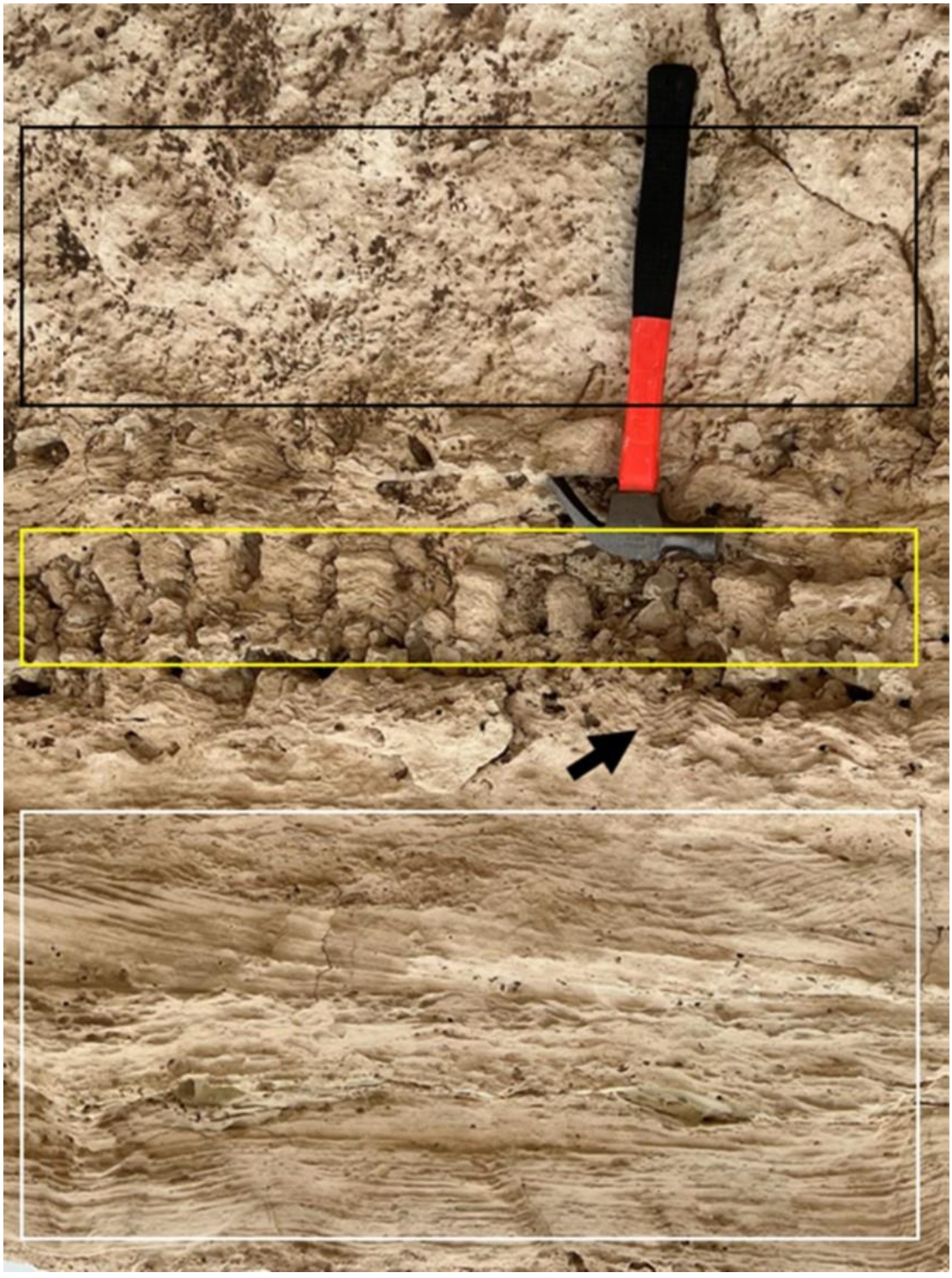

Figure 4: Outcrop photograph showing the two stromatolite forms observed in the Dam Formation (CF and LL). The CF stromatolite form (yellow box) and LL stromatolite form (black arrow) overlying laminated and cross-bedded oolitic grainstone (white box).

Figure 5: Outcrop photograph showing the two stromatolite forms observed in the Dam Formation (CF and LL). The LL stromatolite form exhibits clear lamination, highlighted by white boxes and is overlain by the CF forms (black arrows).

stratigraphic positioning. The two forms (CF and LL) were described in terms of their external shape, sizes, orientation, and the composition of the surrounding matrix. The two forms were then digitally imaged for documentation purposes. Multiple rock boulders were collected from the outcrops of the Dam Formation for laboratory analysis. Samples from the two forms were collected from above a major SB.

A total of 20 core plug samples (1.5 inches in diameter) were taken from the rock specimens for each form (10 horizontal plugs and 10 vertical plugs), resulting in 40 core plug samples across the two forms. Thin-sections were prepared from these samples and scanned using AxioScan and inspected using using ZEISS ZEN 3.8 software for scanned thin section examination. Porosity and permeability were measured on the 40 core plugs using the CMS-300TM core measurement system, which employs a pressure decay permeameter and porosimeter to determine pore volume and non-reactive liquid permeability.

Nuclear magnetic resonance (NMR) testing was performed on all samples using the Oxford GeoSpec+ to analyze the porosity systems within each sample. This method provided additional insights into discrepancies between the rock fabrics and the porosity-permeability data. Since all plug samples were initially dry, they were saturated with distilled water prior to the NMR analysis. The NMR results are presented in a two-axis plot for all samples within each form, superimposed for comparison. The x-axis represents the T_2 relaxation time (measured in milliseconds), which corresponds to the time required for hydrogen nuclei in the sample's water content to return to their equilibrium state after being polarized (Kenyon, 1997). This parameter provides insight into the pore sizes within the

samples, as larger pores typically correlate with longer T_2 times (Kenyon, 1997, El-Husseiny and Knight, 2017). The y-axis indicates incremental porosity, showing the relative contribution of different pore sizes to the total porosity as the measurement progresses. While the x-axis conveys information about pore size, the y-axis highlights the relative abundance of each pore size class, offering a comprehensive view of the pore system in the stromatolite samples.

2.4 Results and discussion

2.4.1 Field observations

Field observations revealed that both CF and LL are frequently associated with high-energy water facies, such as laminated and cross-bedded oolitic grainstones (Fig. 4). Stratigraphically, CF and LL stromatolite forms exhibit a clear relationship. It is common to observe LL stromatolite form overlain by CF stromatolite form, with CF stromatolite form transitioning upward into mud-dominated carbonates that characterized by absence of sedimentary structures (Fig. 4). At the base of beds containing LL stromatolites, stromatolite heads transitioning into LL forms are clearly visible (Fig. 5). Additionally, LL stromatolites are occasionally observed laterally associated with CF stromatolites, although such occurrences are less common (Fig. 5).

The variation in stromatolite forms (CF and LL) can be interpreted through the work of Andres and Reid (2006), who studied modern stromatolites in Highborne Cay, Bahamas. Their research examined columnar stromatolites (equivalent to our CF stromatolite form) and ridge-like stromatolites (equivalent to our LL stromatolite form). Andres and Reid (2006) identified accommodation space, sediment supply, and hydrodynamic conditions as

the primary physical factors influencing stromatolite morphology. These factors are intricately interconnected, and variations in their relative dominance result in different growth forms. Columnar stromatolites typically develop in environments with sufficient accommodation space, with their height constrained by the height of sand waves. In contrast, ridge-like stromatolites form in settings where vertical accommodation space is restricted.

The conceptual model proposed by Andres and Reid (2006) provides a plausible interpretation for our field observations regarding the stratigraphic position of CF and LL stromatolite forms above the SB and their depositional environment. Their association with high-energy water facies, such as laminated and cross-bedded oolitic grainstones (Fig. 4), just above the SB, suggests deposition in shallow-water settings, likely just above the wave base or between the wave base and the storm wave base. The LL stromatolite form, comparable to ridge-like stromatolites described by Andres and Reid (2006), appears to have formed in shallower, higher-energy environments relative to the CF stromatolite form. The distribution of CF stromatolite form likely reflects a deepening-upward trend within the system, where greater accommodation space becomes available. The overlying mud-dominated facies, characterized by the absence of sedimentary structures, further supports the interpretation of a continuous deepening-upward trend within the system.

In addition to Andres and Reid (2006), numerous studies have explored the relationship between stromatolite morphology and environmental conditions (Altermann, 2008; Allwood et al., 2009; Jahnert and Collins, 2012; Bosak et al., 2013; Jahnert and Collins, 2013). While these studies address various aspects of the factors controlling stromatolite development, they generally converge on a common model: high-energy conditions favor

sheet-like stromatolite morphologies, whereas lower-energy settings with greater accommodation space favor more spherical or columnar stromatolite forms. For the purpose of this study, which compares CF and LL stromatolite forms as two morphological end-members in terms of their porosity and permeability, this broad interpretation of depositional environments provides a sufficient background. A more detailed investigation into the specific factors controlling stromatolite development in the Dam Formation can be pursued in future research.

2.4.2 Rock constituents and lamination

Results of the petrographic investigation (Figs. 6-9) revealed that both CF and LL stromatolite forms are dominated by coarse-grained carbonate, resembling coarse-grained carbonate stromatolites described in both the stratigraphic record and modern analogs (Monty, 1976; Awramik and Riding, 1988; Pamela Reid et al., 2003; Suarez-Gonzalez et al., 2014; Suarez-Gonzalez et al., 2019). Both CF and LL stromatolite forms consist of grain-rich laminae and micrite-rich laminae.

The laminations in CF and LL are highly distinct in hands specimens and in their thin section photomicrographs (Figs. 6 and 7), and can be characterized using descriptions proposed for coarse-grained carbonate stromatolites in both modern and stratigraphic records. These laminations are often described as repetitive or alternating (Monty, 1976; Awramik and Riding, 1988; Pamela Reid et al., 2003; Suarez-Gonzalez et al., 2014; Suarez-Gonzalez et al., 2019). The alternating laminations in CF and LL stromatolites are characterized by layers with contrasting microfabrics, such as grain-rich and micrite-rich laminae (Fig. 6). In contrast, repetitive laminations consist of successive laminae with a

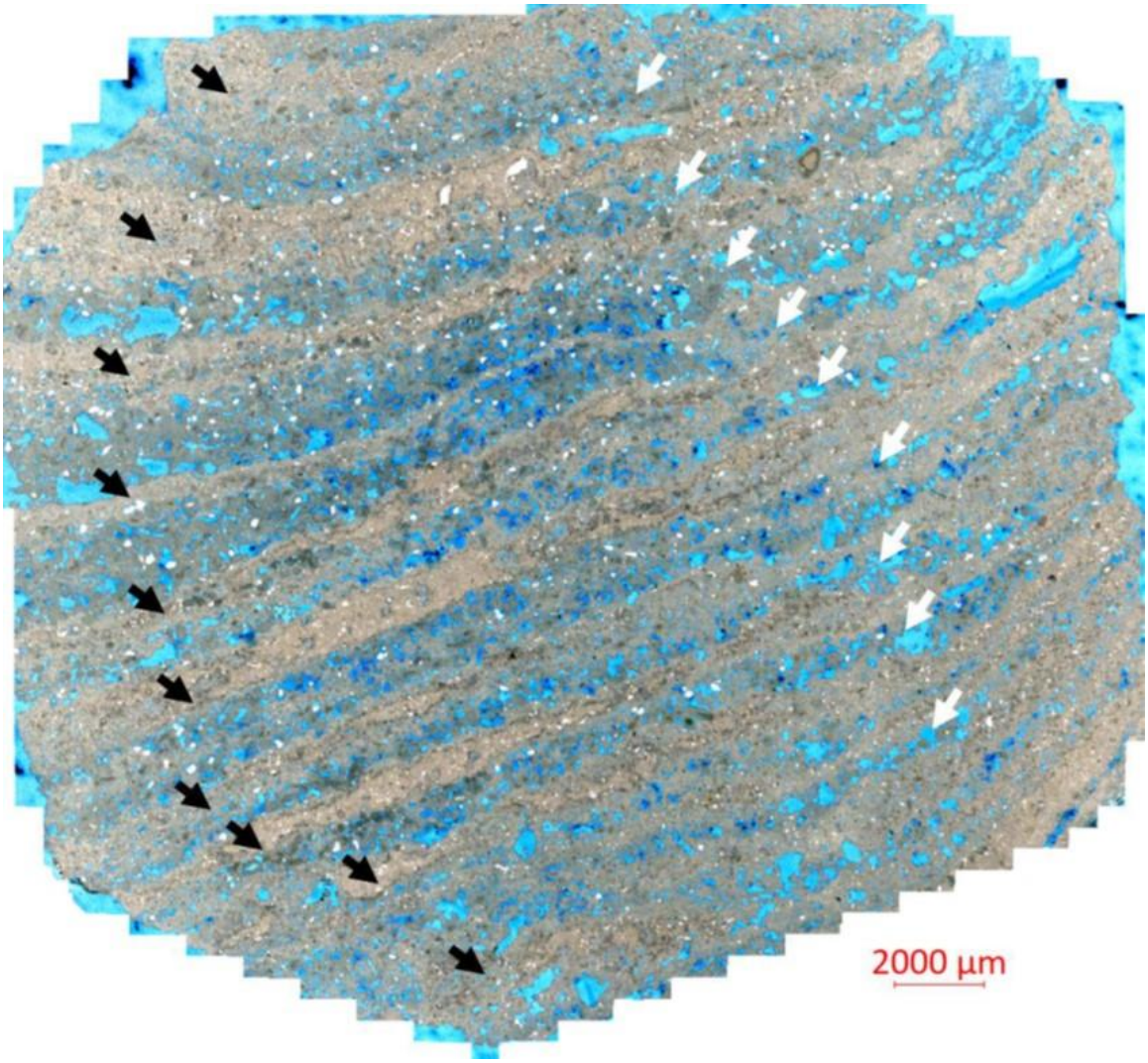

Figure 6: Thin section photomicrograph showing the microtexture of CF stromatolite form. Note the distinct lamination with alternating tan color (Black arrows), tightly bound laminae (micrite-rich) and bluish color (white arrows), porous, grain-rich laminae, reflecting sediment entrapment.

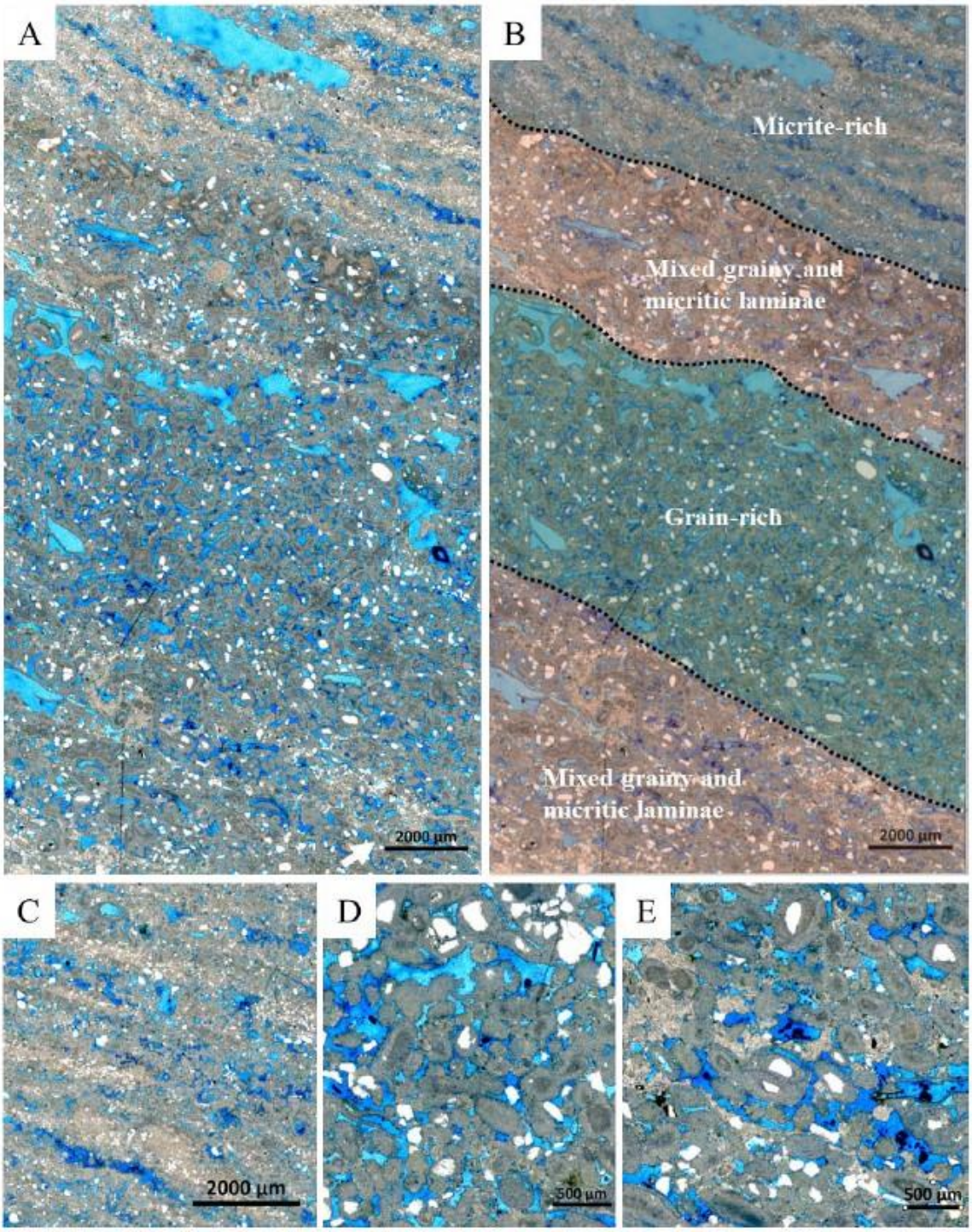

Figure 7: Thin section photomicrographs showing the microtexture and lamination of the LL stromatolite form. (A) and (B) Photomicrograph and annotated version illustrating alternating lamination of micrite-rich laminae, grain-rich laminae, and mixed grainy and micritic laminae. (C), (D), and (E) Close-up views highlighting the micrite-rich laminae, grain-rich laminae, and mixed grainy and micritic laminae, respectively.

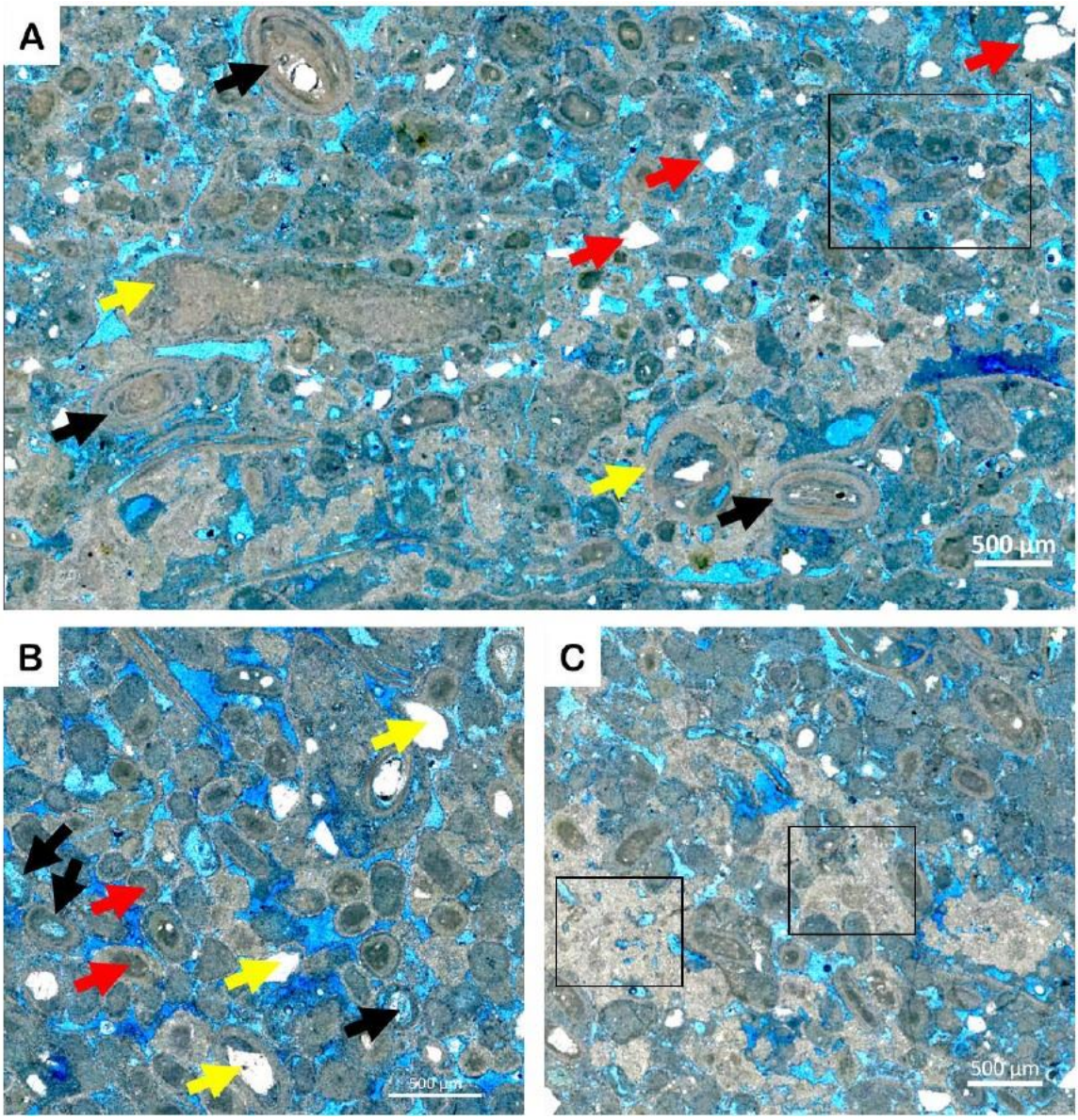

Figure 8: Thin-section photomicrographs illustrating the microtexture of grain-rich laminae. (A) Rock constituents, including ooids (black arrows), quartz grains (red arrows), and skeletal fragments (yellow arrows). (B) Ooid nuclei, preserved as quartz grains (yellow arrows), micritized ooids, or molds of leached nuclei (black arrows). (C) Clotted-peloidal micrite filling intergranular spaces.

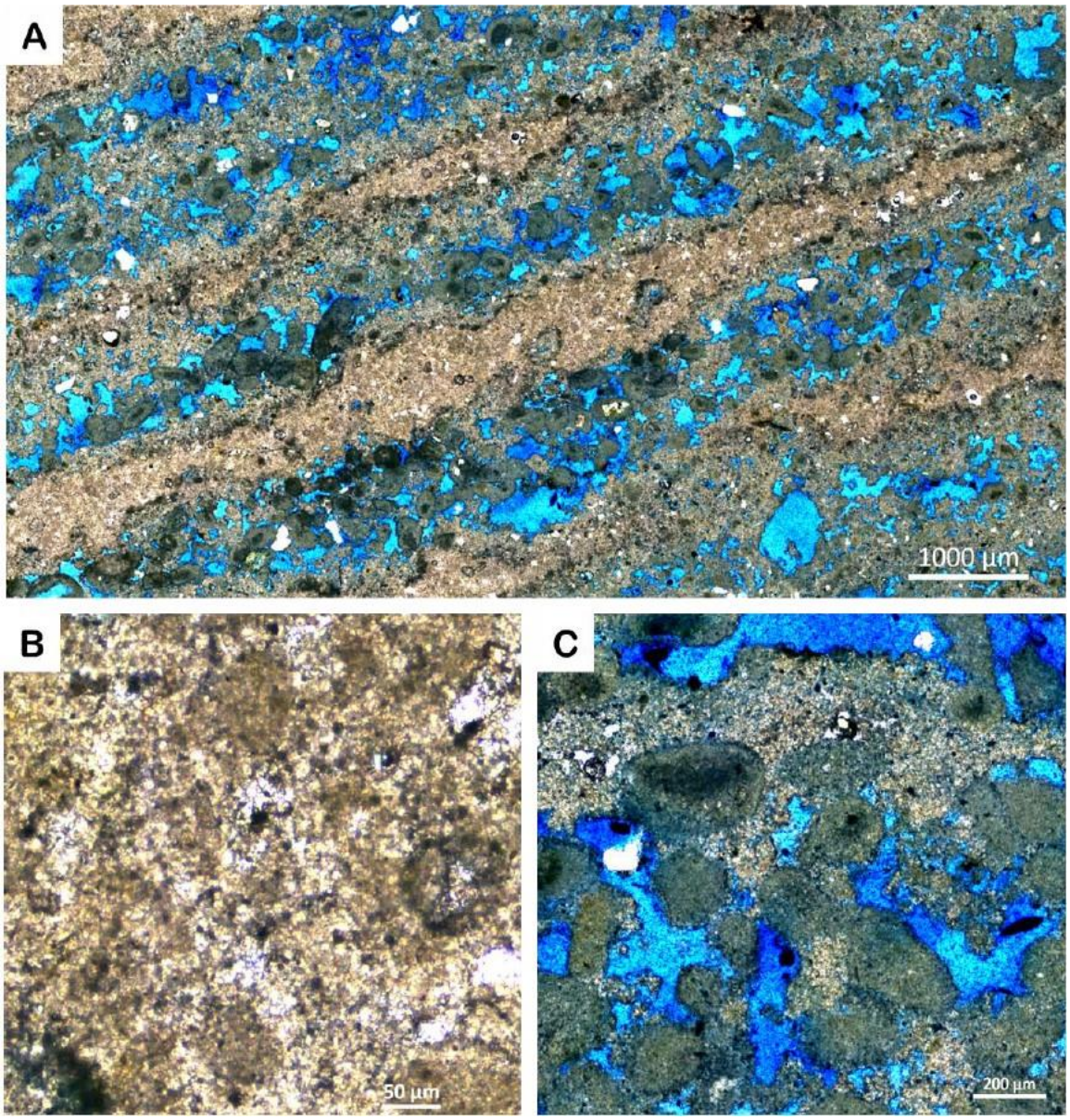

Figure 9: Thin-section photomicrographs illustrating the microtexture of grain-rich laminae. (A) Close-up view of alternating lamination, showing micrite-rich laminae 1 to 2 mm thick and sinuous, continuous biofilms at the very top of each micritic lamina. (B) High-resolution photomicrographs revealing that the clotted micrite is associated with scattered black circular spots, likely representing pyrite crystals. (C) Micrite crusts observed on top of an ooid-dominated interval.

similar microfabric, typically grain-rich laminae, separated by very thin micritic crusts representing hiatal surfaces (Fig. 7).

In the grain-rich laminae, the carbonate grains trapped within both CF and LL stromatolite forms are primarily composed of coated grains, such as pellets, ooids, composite ooids, and peloids, the latter likely representing micritized ooids (Fig. 8A). Skeletal fragments are present but in significantly smaller quantities compared to the coated grains (Fig. 8A). Additionally, silt-sized quartz grains are observed in substantial abundance (Fig. 8A). Ooids are well-sorted and typically have diameters of approximately 200 μm (Fig. 8B). Ooid nuclei are often leached out, leaving moldic pores; however, when nuclei are preserved, they are commonly composed of pellets, muddy peloids or angular quartz grains (Fig. 6B). Generally, the particle porosity of the ooids is preserved but can occasionally be filled with clotted-peloidal micrite (Fig. 8C).

The micrite-rich laminae within both CF and LL stromatolite forms are 1 to 2 mm thick and are primarily composed of clotted peloids and clotted micrite (Fig. 9A). Thin-section micrographs commonly reveal sinuous, continuous biofilms at the very top of each micritic lamina (Fig. 9A). High-resolution photomicrographs show that the clotted micrite is associated with scattered black circular spots, likely representing pyrite crystals (Fig. 9B). Below the biofilms, it is also common to observe thin micrite crusts underlain by grain-rich laminae instead of micrite-rich laminae (Fig. 9C). In some instances, the micrite laminae transition laterally into micrite crusts.

The observations of CF and LL stromatolite lamination styles and composition align closely with the findings of Suarez-Gonzalez et al. (2014) in the Leza Formation, in north

Spain. Suarez-Gonzalez et al. (2014) suggested that coarse-grained carbonate stromatolites, such as those in the Leza Formation, exhibit two distinct lamination styles: alternating lamination and repetitive lamination, both of which are evident in the CF and LL forms of the Dam Formation in our study area (Figs. 6 and 7).

In the alternating laminations the micrite-rich laminae are attributed to microbially induced precipitation of clotted and clotted-peloidal micrite, while grain-rich laminae result from the trapping and binding of carbonate grains as suggested by Suarez-Gonzalez et al. (2014). Repetitive laminations which consist of successive layers with similar microfabrics, typically grain-rich laminae separated by very thin micritic crusts that represent hiatal surfaces (Fig. 7). These crusts are interpreted as having formed during pauses in accretion due to microbial alteration and carbonate precipitation following Suarez-Gonzalez et al. (2014) interpretation. The coexistence of these lamination styles in the CF and LL stromatolites suggests a combination of processes, including grain trapping and binding, microbially induced in-situ calcification, and hiatal crust formation, which are indicative of environmental variability.

As Suarez-Gonzalez et al. (2014) noted, environments with fluctuating seawater and freshwater influence, such as tide-influenced coastal wetlands, may have facilitated the interplay of trapping, binding, and in-situ calcification processes. The CF and LL stromatolites described here were formed in mixed carbonate and siliciclastics setting (Alkhaldi et al., 2021). Thus, it is plausible that the diversity in lamination styles observed is due to variations in accommodation space, hydrodynamics, and microbial activity in such shallow water and mixed system environment.

2.4.3 Pore system

In this study, the carbonate pore system in the two stromatolite forms was characterized based on the classification by Choquette and Pray (1970). Fenestral and vuggy porosity were identified in both micrite-rich and grain-rich laminae (Fig. 10A, B). Interparticle, intraparticle, and moldic porosity were predominant in the grain-rich laminae (Fig. 10C). Microporosity was also observed in the muddy portions of the samples, appearing as a hazy blue hue under thin-section analysis with blue-dyed epoxy, indicating its presence within the background mud-dominated rock texture (Fig. 10D).

In terms of stromatolite forms, the CF form was dominated by interparticle, intraparticle, and moldic porosity, as it develops well-structured grain-rich laminae (Fig. 9A, C). The micrite-rich laminae in this form are often tightly cemented, resulting in reduced pore spaces (Fig. 9A, B), although vugs and fenestral porosity are also commonly present in these laminae (Fig. 10A). The LL stromatolite form, on the other hand, exhibited dominance of vugs and fenestral porosity, particularly within the micrite-rich laminae. The variability in the pore system was clearly reflected in the NMR data (section 2.4.4), which highlighted differences in pore size distribution and porosity across the stromatolite forms.

In terms of size, a significant portion of the fenestral and vuggy porosity exceeds 4 mm in cross-section (Fig. 10A) and is often visible without the aid of a microscope. Another substantial range of these two pores falls between 0.5 mm and 4 mm (Fig. 10B). According to Moore (1989), such pore sizes are classified as megapores and large mesopores. In this study, we collectively refer to these megapores and large mesopores as macropores. On the other hand, interparticle, intraparticle, moldic, fenestral, and vuggy pores (typically associated with carbonate grain size) are usually smaller than 500 μm, usually observed

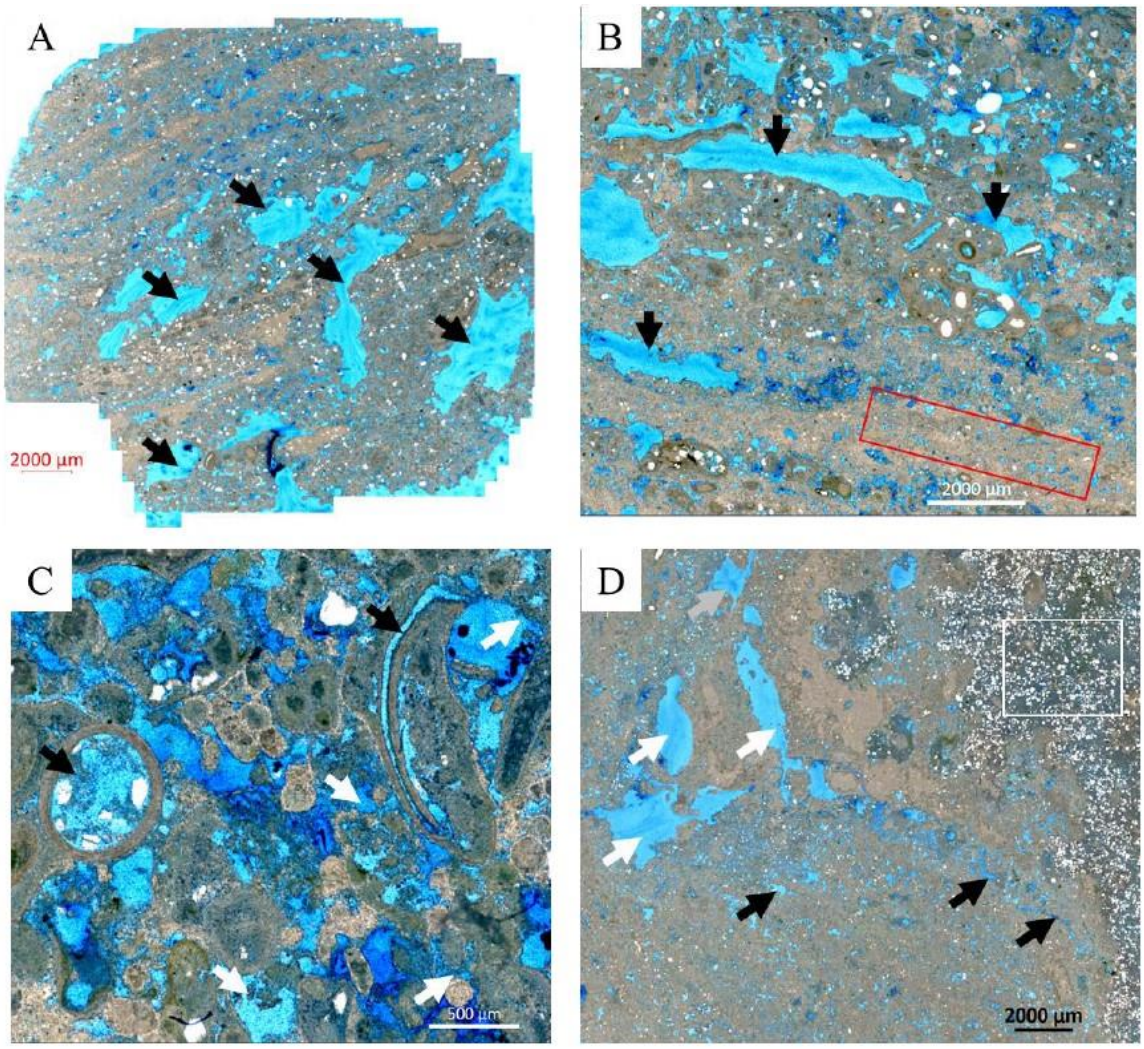

Figure 10: Thin section photomicrographs showing the pore system of CF and LL stromatolite forms. (A) Lamination disrupted by dissolution, resulting in non-fabric selective millimeter-scale vugs (black arrows). (B) Fenestral porosity in both micrite-rich and grain-rich laminae (black arrows). Note different sizes of these fenestral pores (red box). (C) Close-up view of grain-dominated entrapped sediments atop the bound laminae, containing interparticle (white arrows) and moldic pores (black arrows). (D) Top view of a columnar head with a surrounding muddy matrix. Note the fenestral (black arrows) and vuggy porosity (white arrows), and the hazy blue color indicating microporosity (white box).

with less than 200 μm diameter (Fig. 9A, C and Fig. 10C), and are classified as small mesopores based on Moore (1989). For simplicity, we refer to this category of pores as mesopores in our study. Lastly, micropores are defined here as pores smaller than 64 μm, following Moore (1989).

While not always visible in thin-section photomicrographs, these micropores are inferred to exist when the photomicrographs display a hazy blue hue from the dye-impregnated epoxy (Cantrell and Hagerty, 1999) used during sample preparation (Fig. 10D).

2.4.4 Pore size distribution

Most samples of the CF stromatolite form exhibit a bimodal distribution (Fig. 11A), whereas the LL stromatolite form demonstrates a combination of bimodal and wide unimodal distributions, with transitions between peaks that lack distinct boundaries (Fig. 11B). Examples of the NMR distributions, alongside pore system visualizations in thin-section photomicrographs, are displayed in Figures 12 and 13. While the exact correspondence of each peak to its respective porosity system or pore size remains uncertain, combining NMR with petrographic analysis of thin sections can clarify the relationship between the observed peaks and the porosity systems they represent.

a. CF stromatolite form

All samples in the CF stromatolite form, except one, exhibit a bimodal NMR distribution (Fig. 11A). The bimodal distribution is characterized by a first peak ranging from 0 to 100 ms and a second peak ranging from 100 to 1000+ ms (Fig. 11A). The exception, a sample with a unimodal distribution, shows a single peak ranging from 1 to 100 ms. The samples with bimodal NMR distributions can be further divided into two groups based on the

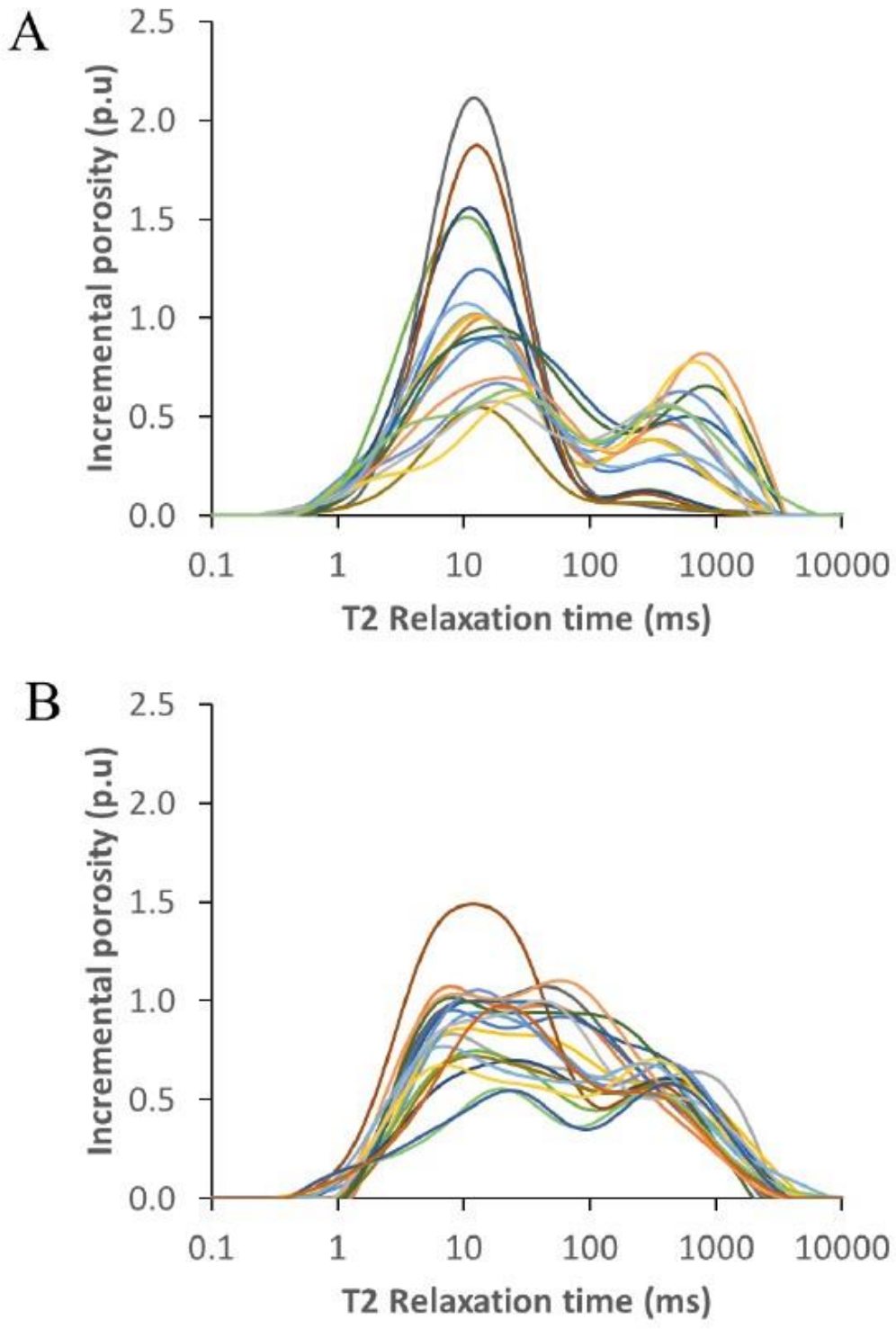

.

Figure 11: Plots illustrating NMR data for the CF stromatolite form (A) and the LL stromatolite form (B). Each plot represents data from 20 samples. Notably, most samples of the CF stromatolite form exhibit a bimodal distribution, whereas the LL stromatolite form demonstrates a combination of bimodal and unimodal distributions, with transitions between peaks that lack distinct boundaries. Examples of the NMR distributions, alongside pore system visualizations in thin-section photomicrographs, are displayed in Figures 12 and 13.

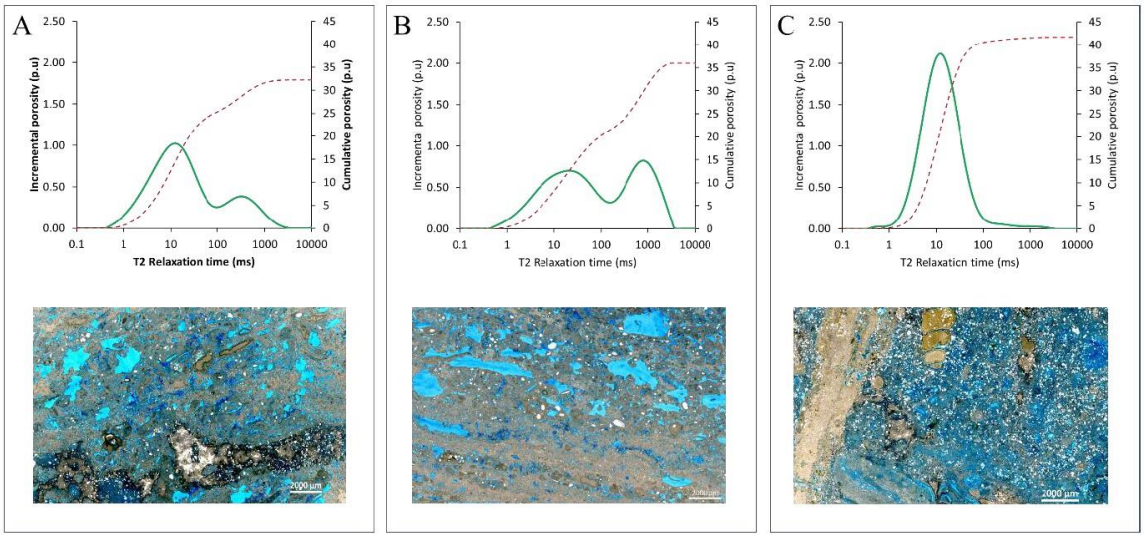

Figure 12: Three panels illustrating the three groups of NMR data and their corresponding thin-section photomicrographs. (A) Group 1: Bimodal distribution dominated by mesopores and macropores. (B) Group 2: Similar to Group 1, but with macropores showing higher relative abundance. (C) Group 3: Unimodal distribution corresponding to micropores, identified in the thin-section photomicrograph as a pervasive hue across the thin-section space, highlighted by blue-dyed epoxy.

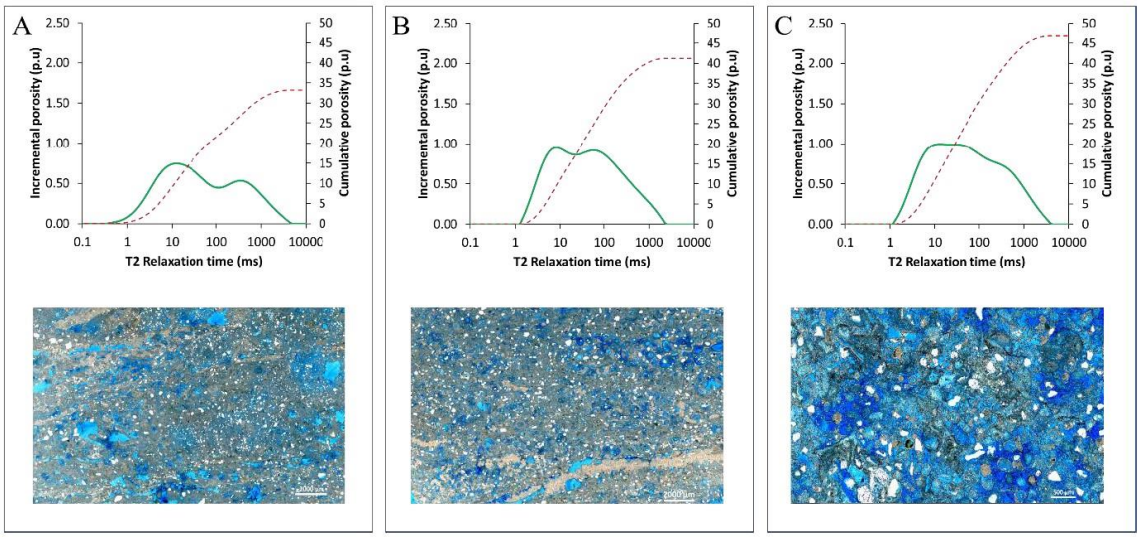

Figure 13: Three panels illustrating the three groups of NMR data and their corresponding thin-section photomicrographs. (A) Group 1: Bimodal distribution dominated by mesopores and macropores. (B) Group 2: Weakly defined bimodal distribution without distinct peaks, where macropores and micropores are equally dominant and contribute to the overall pore system. (C) Group 3: Unimodal distribution where macropores are rarely observed, and the pore system is predominantly composed of micropores and mesopores.

incremental porosity associated with each peak. Group 1 (Fig. 12A) exhibits a markedly higher incremental porosity in the first peak compared to the second, whereas Group 2 (Fig. 12B) shows the opposite pattern, with higher incremental porosity in the second peak. The sample with a single peak and unimodal distribution is classified as a separate group, referred to as Group 3 (Fig. 12C).

Based on petrographic analysis, we interpret the peak ranging from 1 to 100 ms to represent the contribution of micropores and mesopores—pores smaller than 64 μm up to 500 μm, with most ranging from 100 μm to 200 μm in diameter. Ideally, two distinct peaks would represent these two pore systems (micropores and mesopores). However, due to their closely ranged sizes, the NMR system is unable to distinguish between them, resulting in a single peak within this T2 range (1 to 100 ms). The second peak, ranging from 100 to 1000+ ms, reflects larger pores, including large mesopores (0.5 mm 292 to 4 mm) and megapores (>4 mm), collectively referred to here as macropores. This macropore system is clearly distinct in the NMR data from the micropores and mesopores.

This interpretation provides insight into the contribution of different pore systems to total porosity. In Group 1 (Fig. 12A), micropores and mesopores likely contribute more to the total porosity than macropores. In contrast, in Group 2 (Fig. 12B), macropores are likely contribute equally or some times more to the total porosity. In Group 3 (Fig. 12C), where macropores are likely not substantially present, porosity predominantly originates from micropores and mesopores.

b. LL stromatolite form

The LL stromatolite form exhibits significantly lower incremental porosity for micropores and mesopores compared to the CF form (Fig. 11B). Based on T2 relaxation time distributions, the LL samples are classified into three groups. Group 1 (Fig. 13A) exhibits a bimodal distribution similar to Group 1 of the CF stromatolite form, with a dominant first peak (1 to 100 ms) and a secondary peak (100 to 1000+ ms). Group 2 (Fig. 13B) displays a weakly defined bimodal distribution, where the second peak (100 to 1000+ ms) has same or slightly higher incremental porosity than the first peak (10 to 100 ms). Group 3 (Fig. 13C) shows a single, broad peak without clear separation, spanning the entire T2 range (1 to 1000+ ms).

The first peak (1 to 100 ms) is interpreted to represent mesopores, as microporosity is not dominant in the LL form based on petrographic observations. The second peak (100 to 1000+ ms) corresponds to macropores, including large mesopores (0.5 mm to 4 mm) and megapores (>4 mm). The weakly defined bimodal distribution in Group 2 (Fig. 13B) suggests partial connectivity between mesopores and macropores, while the single broad peak in Group 3 (Fig. 13C) may indicate substantial connectivity between these pore systems. This analysis provides further insight into the contribution of different pore systems to total porosity in the LL stromatolite form. In Group 1, mesopores dominate over macropores. In Group 2, macropores are the main contributors, but partial connectivity exists between the two pore systems. In Group 3, enhanced connectivity between mesopores and macropores likely contributes to the broad, single peak observed in the NMR data.

2.4.5 Porosity and permeability distribution

In the CF stromatolite form, the mean porosity is 40.86%, with a standard deviation of 3.74%, and values ranging from 33.93% to 48.04% (Table 1). In contrast, the LL stromatolite form exhibits a higher mean porosity of 44.84%, with a standard deviation of 5.90%, and values ranging from 32.28% to 54.90% (Table 1). For permeability, the CF stromatolite form has a mean of 562.35 mD, with a standard deviation of 784.63 mD, and a wide range of values from 1.38 mD to 1900.50 mD (Table 1). On the other hand, the LL stromatolite form shows a lower mean permeability of 217.40 mD, with a standard deviation of 433.07 mD, and values ranging from 13.31 mD to 2017.78 mD (Table 1). Interestingly, neither the CF nor the LL stromatolite forms display any correlation between porosity and permeability (Fig. 14A).

In the exceedance probability plot (Fig. 14B), the CF stromatolite form exhibits a broader permeability range and higher maximum values compared to the LL form, indicating greater heterogeneity and a wider distribution of permeability values. In contrast, the LL form displays a narrower permeability range with a steeper decline in permeability as exceedance probability increases, reflecting a more homogeneous pore system dominated by lower permeability values (Fig. 14B). A notable trend emerges in the exceedance probability curve (Fig. 14B): at permeability values below 100 mD, the CF stromatolite form consistently exhibits lower permeability than the LL form for any given exceedance probability. However, at permeability values exceeding 100 mD, the CF form consistently shows higher permeability values than the LL form for the same exceedance probabilities. Interestingly, the highest permeability values for both stromatolite forms align with the same exceedance probability.

Sample #	Orientation	Porosity (%)	Density (g/cc)	Permeability (mD)	VP (m/s)
HL-1	H	48.14	2.77	182.91	2343
HL-2	H	47.37	2.80	242.34	2743
HL-3	H	43.00	2.80	144.44	2527
HL-4	H	42.50	2.77	123.36	3291
HL-5	H	46.85	2.79	35.97	1951
HL-6	H	52.52	2.77	132.39	1280
HL-7	H	43.19	2.77	13.31	2280
HL-8	H	42.92	2.78	63.19	2093
HL-9	H	35.61	2.82	97.07	2929
HL-10	H	41.20	2.80	14.45	2626
HL-11	V	45.80	2.80	260.96	2053
HL-12	V	45.43	2.80	2017.78	2509
HL-13	V	39.34	2.81	319.74	3063
HL-14	V	39.10	2.80	258.95	2825
HL-15	V	51.91	2.77	65.76	1322
HL-16	V	54.90	2.77	139.61	1372
HL-17	V	53.16	2.75	86.41	1467
HL-18	V	49.15	2.76	62.62	1562
HL-19	V	42.45	2.78	38.90	2143
HL-20	V	32.28	2.81	47.74	3571
CF-1	H	38.54	2.84	3.11	3186
CF-2	H	36.69	2.83	12.51	3135
CF-3	H	40.39	2.79	1.80	2941
CF-4	H	44.03	2.84	2.25	2544
CF-5	H	41.33	2.83	2.15	2765
CF-6	H	48.04	2.83	794.74	2109
CF-7	H	33.93	2.83	352.43	4500
CF-8	H	42.65	2.82	117.01	3333
CF-9	H	40.40	2.82	273.04	3504
CF-10	H	38.54	2.84	3.11	3186
CF-11	V	38.68	2.83	34.98	3086
CF-12	V	37.94	2.85	22.97	3142
CF-13	V	36.75	2.83	55.83	3133
CF-14	V	40.58	2.83	1.38	3110
CF-15	V	47.30	2.81	2.80	2736
CF-16	V	45.38	2.82	1748.37	2326
CF-17	V	39.01	2.83	1900.50	2048
CF-18	V	43.77	2.84	1784.91	2474
CF-19	V	38.11	2.81	1784.91	3730
CF-20	V	42.79	2.83	1788.97	2308

Table 1: Data showing porosity, grain density, VP, and permeability of stromatolites, grouped as stromatolites horizontally-linked form (HL) and columnar form (CF). Note that some samples were cut in a vertical orientation (marked as V), while others were cut in a horizontal orientation (marked as H).

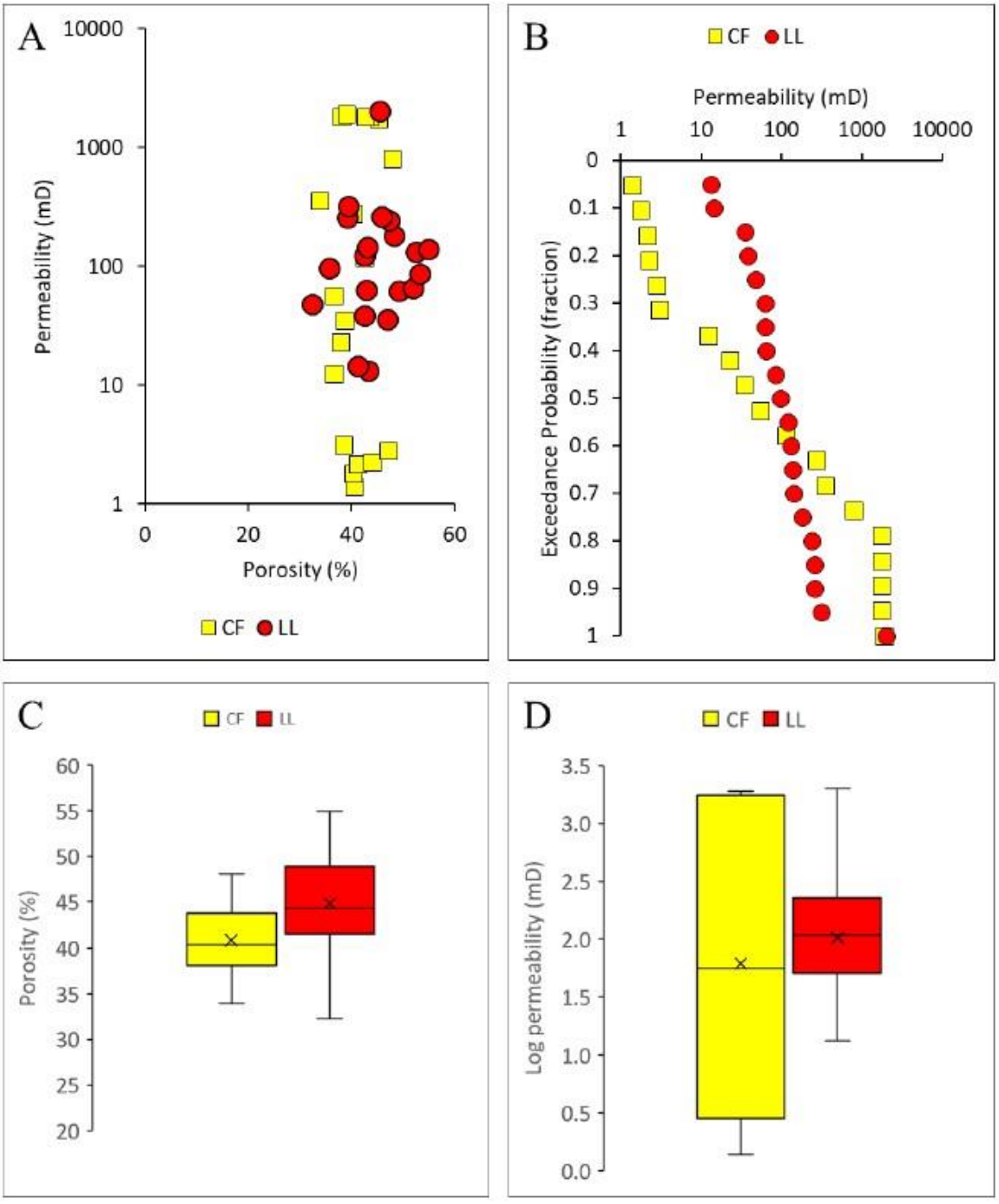

Figure 14: Porosity and permeability variation in the stromatolite forms. (A) Crossplot of porosity and permeability. Note the narrow range of porosity values observed in both forms, corresponding to a very wide range of permeability values, with no apparent relationship between the two variables. (B) Permeability versus its exceedance probability. Note the turning point at 100 mD permeability, before which the CF stromatolite form shows consistently lower values and after which it shows consistently higher values. (C) Box plot showing porosity data. Note the low variability of the data. (D) Box plot showing log permeability data. Note the high variability of the data.

These results highlight the complex trends in the CF stromatolite form. While porosity remains relatively consistent across samples with low variability (Fig. 14C), permeability exhibits a much broader range (Fig. 14D). For instance, in the CF stromatolite form, permeability values range dramatically from as low as 1.38 mD to as high as 1900.50 mD, even in samples with nearly identical porosity (~40%, Table 1). This wide permeability range is evident in both stromatolite forms but is more pronounced in the CF stromatolite form. Notably, this broad range in permeability cannot be attributed solely to sample orientation (horizontal versus vertical plugging, Table 1).

It is plausible to observe high permeability values (up to 1000 mD or more) in rock textures dominated by coarse carbonate sediments, such as those found in the CF and LL stromatolite forms, which exhibit grainstone textures comprising ooids, peloids, and skeletal grains (Figs. 8, 9). Numerous studies in the literature have documented such high permeability values for grainstone rock textures (Ehrenberg et al., 2007). Examples include the prolific Arab-D reservoir in the Middle East and the Khuff Formation and its equivalents in Central and East Asia (Alsharhan, 2006; Lindsay et al., 2006; Knaust, 2013; Esrafili-351 Dizaji and Rahimpour-Bonab, 2014).

However, the occurrence of low permeability values (>5 mD) in grainstone textures associated with coarse-grained stromatolites, despite significantly high porosity (<30%), as observed in certain samples of the CF and LL stromatolite forms, presents a notable challenge to understanding permeability controls. This indicates that factors beyond simple porosity measurements, such as pore size distribution, play a critical role. Results from NMR analysis offer valuable insights into the impact of pore size distribution on

permeability variability in stromatolites, which is further discussed in the following section.

2.4.6 Understanding permeability distribution from NMR data

To analyze the variability of permeability distribution in stromatolite samples using NMR data, T2 log mean (T2 LM) multiplied by porosity (porosity*T2LM) was plotted against permeability values for each stromatolite form (Fig. 15). The objective was to assess whether a significant relationship exists between porosity*T2LM and permeability, as such a correlation would suggest that NMR data, which provide insights into pore size distribution, can effectively explain variations in permeability. The results revealed complex trends. When all samples from both stromatolite forms were plotted together, permeability demonstrated a power-law correlation with an R2 value of 0.62, though with considerable scatter (Fig. 15A). When separated by stromatolite form, the CF stromatolite form exhibited a much stronger power-law correlation with an R2 value of 0.86 (Fig. 15B), whereas the LL form showed no significant correlation, with an R2 value of 0.03 (Fig. 15C). These results suggest that while NMR data (and their indication to pore size distribution) can, to some extent, explain permeability distribution in the CF stromatolite form, it is not as effective in capturing the permeability variability in the LL stromatolite form.

To highlight the variability in the CF stromatolite form, a comparison was made between samples B2 and B17, which exhibit almost identical porosity*T2LM values (Fig. 15B) but vastly different permeability values: 3.1 mD and 117.0 mD, respectively—a difference of approximately two orders of magnitude (Fig. 16). Their porosity values, 38.5% and 42.6%, respectively, show no significant variation. The NMR data for both samples are nearly

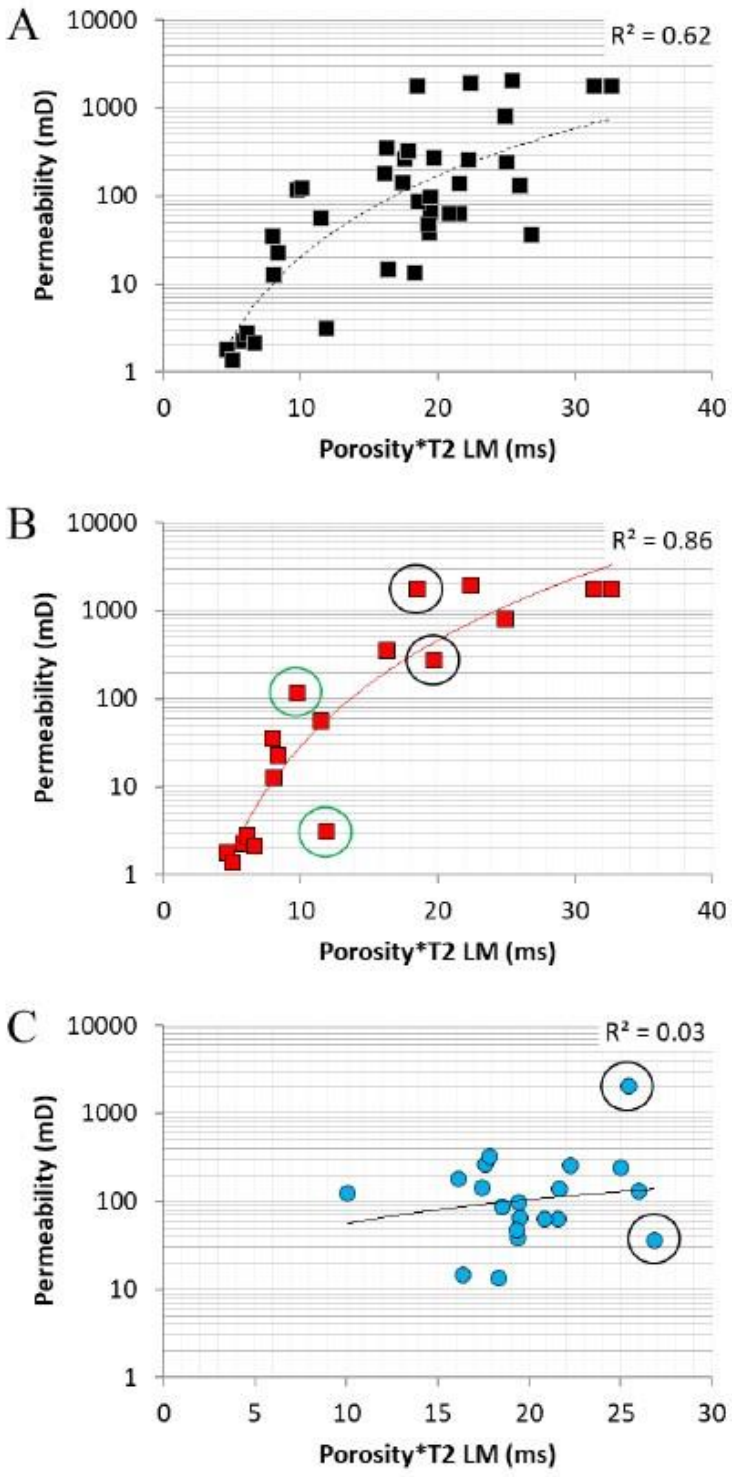

Figure 15: Cross-plots of porosity multiplied by T2 LM and permeability for all data points (A), data representing the CF stromatolite form (B), and data representing the LL stromatolite form (C). In (A), when all samples from both stromatolite forms were plotted together, permeability demonstrated a power-law correlation with porosity multiplied by T2 LM, albeit with considerable scatter. When separated by stromatolite form, the CF stromatolite form (B) exhibited a much stronger power-law correlation with an R2 value of 0.86, whereas the LL stromatolite form (C) showed no significant correlation, with an R2 value of 0.03.

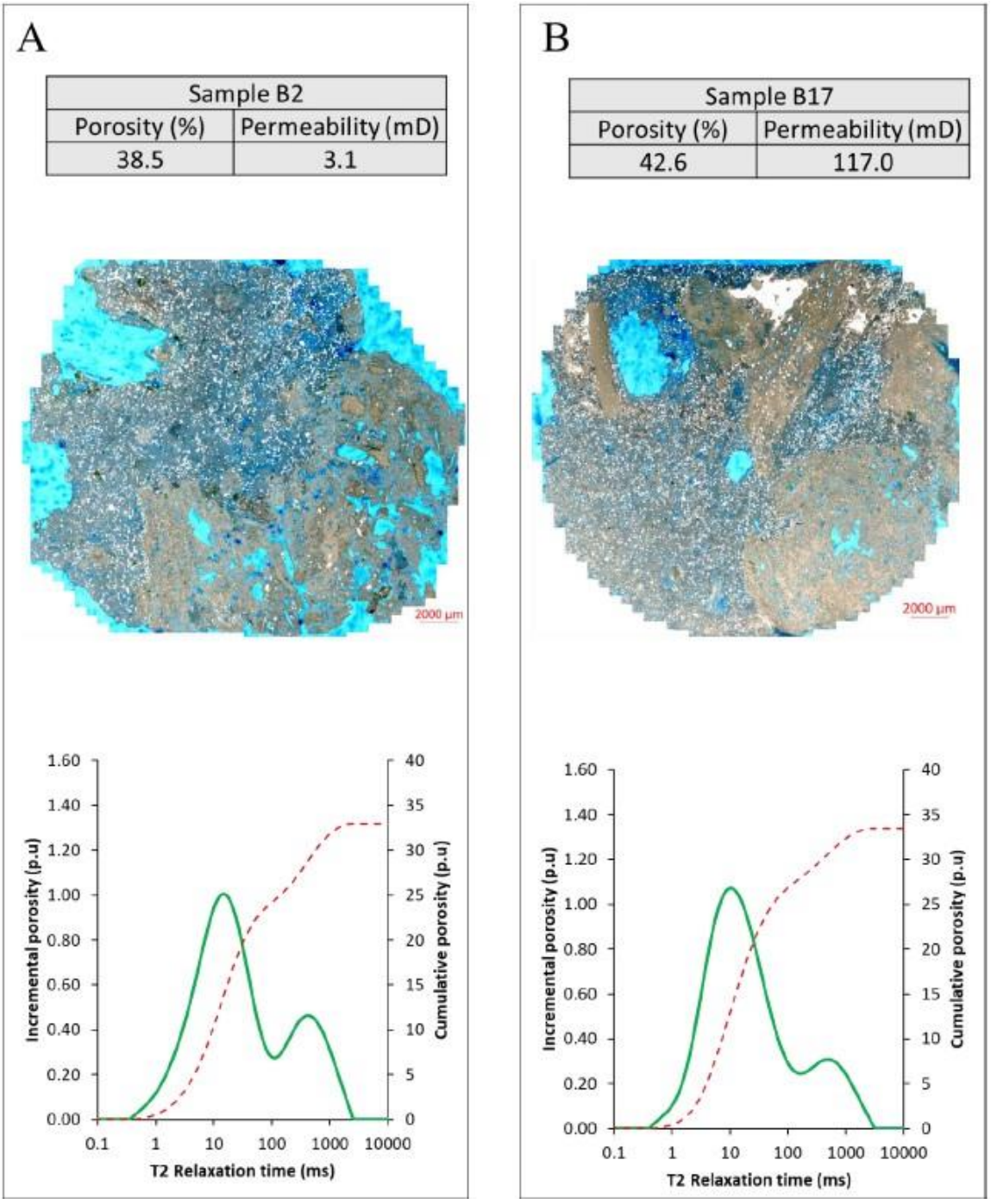

Figure 16: Panel comparison between two samples from the CF stromatolite form, illustrating similar pore types (micropores and macropores) and pore size distribution (bimodal T2 distribution) with nearly identical porosity values but drastically different permeability values, differing by two orders of magnitude.

identical, showing a bimodal distribution with a dominant primary peak (1–100 ms) likely representing micropores and mesopores, and a minor secondary peak (100–1000+ ms) likely associated with macropores (Fig. 16). Petrographic analysis further reveals that both samples are dominated by micropores and mesopores with distinct macropores, reinforcing the expectation that their permeability values should be similar. However, the observed permeability values are significantly different. A similar inconsistency is observed in samples B18 and B11 (Fig. 15B), which also exhibit comparable porosity and NMR characteristics but vastly different permeability values of 273.0 mD and 1748.3 mD, respectively. These findings indicate that factors beyond porosity and pore size distribution may play a crucial role in controlling permeability in the CF stromatolite forms.

In the LL stromatolite form, a comparable analysis of samples D11 and D3 revealed nearly identical porosity*T2LM values (Fig. 15C) but drastically different permeability values: 132 mD and 2017 mD, respectively—a difference of approximately one orders of magnitude (Fig. 17). Notably, the sample with higher porosity (52.5%) exhibited significantly lower permeability compared to the sample with lower porosity (45.4%). Despite their nearly similar porosity*T2LM values (Fig. 15C), and T2 distribution which exhibit a weakly defined bimodal distribution indicative of mesopores and macropores in a potentially connected pore network, the permeability values diverged substantially. Petrographic analysis further revealed no significant differences in the pore systems between these two samples, which would otherwise explain the permeability discrepancy. Similar patterns of large permeability variation despite comparable rock characteristics were observed in other LL samples, underscoring the complexity of the factors controlling permeability in this stromatolite form.

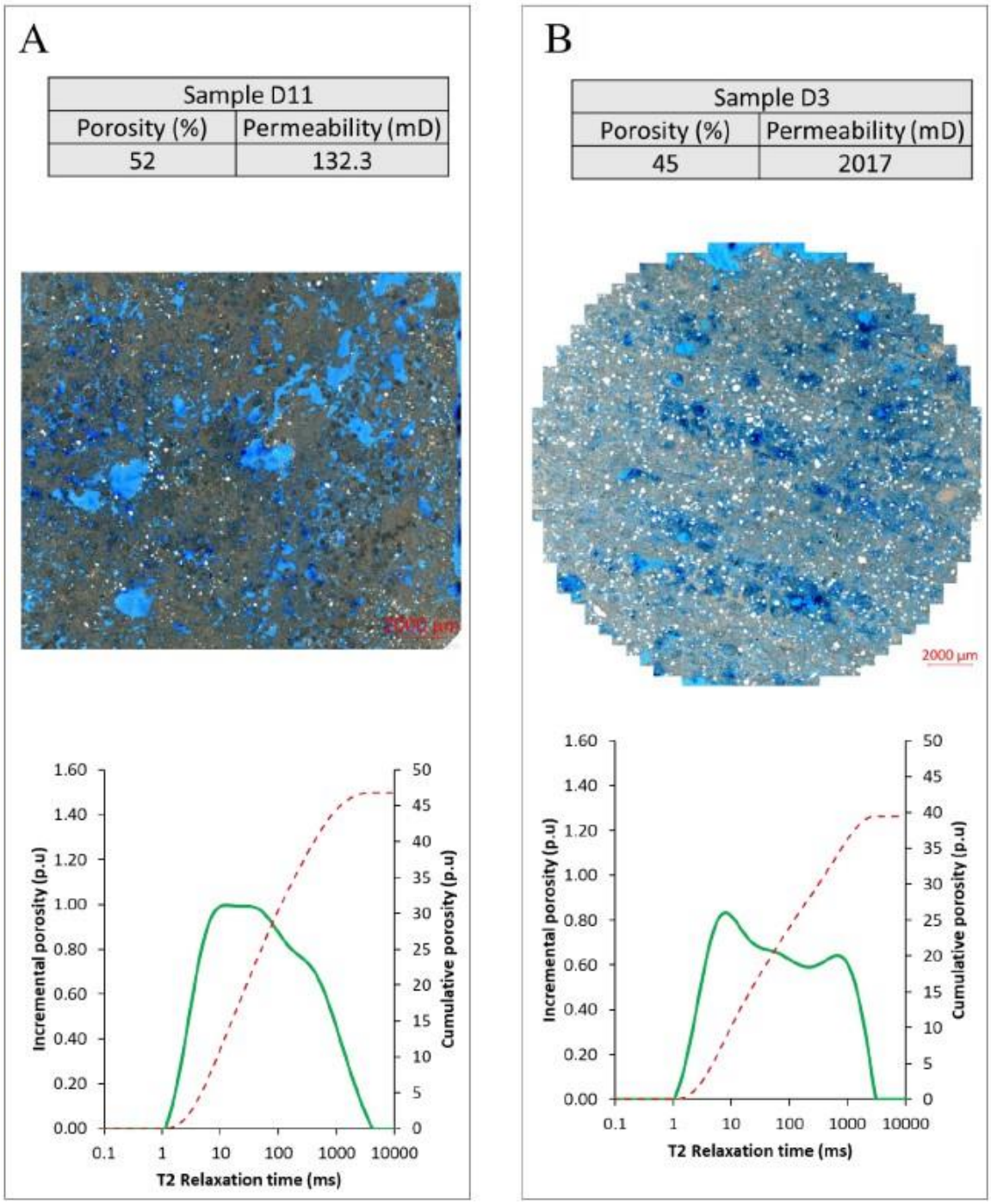

Figure 17: Panel comparison between the sample with the minimum permeability value and the sample with the maximum permeability value in LL stromatolite form. Each panel includes the porosity and permeability values, followed by thin-section photomicrographs and NMR data. Note both samples are dominated by mesopores although NMR data show influence of macropores.

Three key insights emerge from the analysis of permeability data in the context of rock texture, pore type and pore size distribution. First, the scattering in the LL stromatolite form cannot be explained by NMR data. Second, low permeability in some of the CF and LL stromatolite samples cannot be fully explained by petrographic observations or NMR data alone. Third, contrary to expectations based on porosity and pore size distribution, samples with lower permeability sometimes exhibit characteristics suggesting higher permeability potential. These points emphasize the importance of investigating additional factors, such as pore connectivity, microstructural orientation, and the alignment of stromatolite laminae relative to measurement directions, to resolve these discrepancies.

2.4.7 Synthesis

Analyzing permeability distribution in the context of pore size distribution (from NMR data) and rock texture and pore types (from petrographic analysis) reveals two distinct patterns. One pattern can be explained using NMR data and petrographic observations, while the other cannot.

The explainable pattern includes most data from the CF stromatolite form, particularly samples along or close to the line of correlation in Figure 15B. In these cases, low permeability corresponds to low porosity*T2LM values, reflecting the dominance of smaller pores, while high permeability aligns with higher porosity*T2LM values, indicating the prevalence of larger pores. Petrographic analysis supports these findings, showing that samples with low permeability often have mud-dominated textures and microporosity, both of which restrict fluid flow (Fig. 10D). Conversely, intermediate and high permeability values are associated with grain-dominated textures and elevated macroporosity. These observations suggest that the pore system and permeability in CF

stromatolite forms are partially governed by rock texture, which, in turn, is linked to the depositional environment.

As highlighted by Muharrag et al. (2024), variations in rock texture within CF stromatolites are influenced by fluctuating water energy levels in the depositional environment. During high-energy conditions at the onset of transgressive system tracts, grain-dominated sediments accumulated, promoting interparticle and moldic porosity, resulting in high permeability (up to 1900 mD). Conversely, low-energy conditions later in the transgressive phase led to the deposition of mud-dominated sediments, characterized by microporosity and low permeability (as low as 1.8 mD).

However, another pattern emerges in the CF stromatolite form that cannot be explained using the same logic. For instance, samples B2 and B17 exhibit nearly identical pore types, pore sizes, and porosity but display drastically different permeability values (Fig. 16). This contrasting permeability may be attributed to the orientation of micrite-dominated laminae in the samples. In both samples, the grain-dominated laminae are porous and permeable, while the micrite-dominated laminae could have acted as barriers for the sample with low permeability. When the laminae are vertically oriented (and aligned with the direction of gas flow during laboratory measurements), fluid can move continuously through connected porous zones, resulting in higher permeability. In contrast, when the laminae are horizontally oriented, fluid flow is obstructed by the impermeable micrite layers, creating a tortuous pathway or baffle that significantly reduces the effective permeability.

These findings underscore the complexity of permeability in carbonate rocks with stromatolites, as it is influenced not only by pore type, size, and total porosity but also by

the spatial arrangement stromatolite laminae. Structural orientation of stromatolite laminae appears to be a critical factor in determining fluid flow dynamics, highlighting the need for an integrative approach that considers both rock properties and their spatial configuration to fully understand and predict permeability in stromatolitic carbonate systems.

2.4.8 Limitation and way forward

While this study considered horizontal and vertical orientations of laminae by initially cutting horizontal and vertical samples, these classifications proved insufficient for effectively differentiating samples. Challenges in sample scale and sample preparation, such as accurately cutting and determining lamina orientation, likely contributed to this limitation, as stromatolites in both CF and LL forms are highly sinuous and exhibit significant relative inclinations. Furthermore, permeability scattering in the LL stromatolite form could not be explained using any geological scenarios and NMR cannot explain such scattering.

Future research should adopt an integrative approach that considers both the petrophysical properties of stromatolites—such as porosity and permeability, pore type, and pore size—and their spatial laminae configuration, including the interactions between grain-dominated and micrite-dominated laminae. Advanced imaging techniques, such as high-resolution CT scanning, coupled with petrophysical laboratory merriments, NMR and petrographic analysis, can offer valuable insights to support this comprehensive approach. This integration is expected to significantly enhance the accuracy of fluid behavior predictions in reservoirs containing stromatolites.

2.4.9 Summary and conclusions

This study aimed to deepen the understanding of how stromatolite morphology influences the petrophysical properties of carbonate reservoirs, focusing on columnar (CF) and laterally linked (LL) forms in the Dam Formation, Saudi Arabia. Both stromatolite forms exhibit alternating grain-rich and micrite-rich laminae. Grain-rich laminae may significantly contribute to higher permeability through interparticle, intraparticle, and moldic porosity, while micrite-rich laminae may act, to varying degrees, as barriers to fluid flow because they made of clotted fabric with minimum porosity. Both forms also contain large pore systems, such as vugs and fenestral pores, present in both grain-dominated and micrite-dominated laminae. NMR data reflect these characteristics, with the CF stromatolite form typically showing a dominant bimodal distribution and the LL stromatolite form exhibiting a weakly defined bimodal distribution.

Despite similar porosity ranges, both forms display significant permeability variability. While NMR data effectively explain permeability trends in some CF samples by correlating permeability with pore size distribution and rock texture—both of which are influenced by depositional environments—many cases of permeability variability in the CF stromatolite form cannot be fully explained by NMR or petrographic analyses alone. The LL stromatolite form presents even greater challenges, as it exhibits unexplained permeability scattering that remains uncorrelated with pore size distribution or texture.

The spatial configuration of stromatolite laminae emerges as a critical factor that may influence permeability. Vertically aligned porous laminae (grain-dominated lamina) may enable continuous fluid pathways, enhancing permeability, while horizontal alignment of grain-dominated and micrite-dominated laminae may disrupt flow, creating baffle or

tortuous paths and significantly reducing permeability. However, such laminae orientation effects are not captured by either NMR data or petrographic analysis. Future research should integrate advanced imaging techniques such as high-resolution CT scanning with NMR and petrographic analyses to better capture the spatial configuration of laminae and pore systems. This integrative approach is crucial for accurately understanding and predicting fluid behavior in stromatolitic carbonate reservoirs.

CHAPTER 3

Influence of stromatolites on petrophysical properties within stratigraphic contexts: A case study from the Dam Formation, eastern Saudi Arabia

Abstract

Stromatolites, ancient microbial structures, are significant in geological history and important components of carbonate systems. Despite their widespread occurrence, the relationship between stromatolite morphology, stratigraphic context, and petrophysical properties remains underexplored. Based on field observations, and laboratory analysis of 40 samples, this study provides insights into the variation of petrophysical characteristics of stromatolites from the Miocene Dam Formation in eastern Saudi Arabia within different stratigraphic contexts. The results revealed that the stromatolites above and below the sequence boundary (SB) show marked differences in porosity, permeability, and pore system architecture due to varying depositional and diagenetic conditions. Above the SB, stromatolites formed in a transgressive system tract, where fluctuating energy levels influenced sediment types. High-energy conditions in the initial flooding of the transgressive system tract trapped grain dominated sediments, promoting interparticle and moldic porosity, resulting in higher permeability (up to 1900 mD). In contrast, low-energy conditions after the initial flooding in the transgressive system tract led to the accumulation

of mud-dominated sediments, producing microporosity and reducing permeability (as low as1.8 mD). This variability in rock texture and pore system significantly affects fluid flow dynamics, indicating that stromatolites in these settings could exhibit a wide range of reservoir qualities. Below the SB, stromatolites were deposited in restricted environments that favored lateral growth and the entrapment of mud-supported rock fabrics. Diagenesis modified pore systems of these stromatolites by cementing original porosity while generating vuggy porosity through dissolution, resulting in a more uniform pore structure with narrower permeability ranges compared to those above the SB. The unimodal NMR distribution below the boundary, compared to the bimodal distribution above, reflects this more homogeneous pore system, indicating potentially lower but more predictable reservoir quality. This study underscores the importance of stratigraphic context in influencing the petrophysical properties of stromatolites, providing crucial insights for reservoir characterization and predicting fluid flow behavior in carbonate systems.

3.1 Introduction

Stromatolites, organo-sedimentary structures dating back to the Archean Eon, are among the earliest evidence of life on Earth (Buick et al., 1981; Awramik, 1992; Batchelor et al., 2005; Allwood et al., 2007; Schopf et al., 2007; Schopf, 2012). These structures form through the trapping of sediments by microbial mats of ancient cyanobacteria (Walter, 1976; Byerly et al., 1986) and typically thrive in harsh, stress inducing environments such as supratidal flats, where predatory organisms are scarce (Feldmann and McKenzie, 1998; Mary and Woods, 2008; Farías et al., 2011; Kurth et al., 2017). Although often associated with intertidal settings, stromatolites are found across a wide range of depositional

environments, from subtidal to supratidal zones (Walter, 1976; Feldmann and McKenzie, 1998; Słowakiewicz et al., 2013). Modern stromatolites are rare but well-developed in locations like Shark Bay, Western Australia, and the Exuma Cays, Bahamas (Reid et al., 1995). In stratigraphic record, stromatolites are commonly preserved in the Precambrian fossil strata or found at stratigraphic intervals marking mass extinction events, such as the Permian-Triassic boundary (Hoffman, 1976; Schubert and Bottjer, 1992; Grotzinger and Knoll, 1999; Ezaki et al., 2012; Eltom et al., 2017; Boud et al., 2018; Heindel et al., 2018; Eltom et al., 2018). Despite their significance in the fossil record and as indicators of paleoenvironmental conditions, there is a notable gap in understanding the relationship between stromatolite morphology and reservoir characteristics, particularly their impact on porosity, permeability, and pore system architecture within carbonate systems. The assumption that stromatolites exhibit low vertical permeability due to their laminated structures (Sprechmann et al., 2004; Rezende et al., 2013; Proctor et al., 2015) has not been sufficiently explored in relation to sequence boundary (SB) or their effects on reservoir properties such as fluid flow dynamics (Proctor et al., 2015). Additionally, the influence of diagenetic processes like dissolution and cementation on stromatolites' pore systems across different stratigraphic intervals has received limited attention. While stromatolites have been extensively studied in the context of the evolution of life and paleoenvironmental conditions (Knoll et al., 1989; Schopf et al., 2007; Luo and Reitner, 2016), less attention has been paid to their relationship with reservoir properties, particularly regarding porosity, permeability, and pore architecture within carbonate systems. The general assumption is that stromatolites exhibit low vertical permeability compared to horizontal permeability due to their laminated structure (Sprechmann et al., 2004; Rezende et al., 2013; Proctor et

al., 2015). However, the variability in stromatolite morphology relative to SB, and its effect on reservoir properties, remains underexplored (Proctor et al., 2015). Moreover, while diagenetic processes such as dissolution and cementation are known to alter pore systems of stromatolites, their interaction with stromatolites across stratigraphic intervals has been minimally researched. This study aims to fill these gaps by analyzing stromatolite morphology within the Miocene-aged Dam Formation in eastern Saudi Arabia, investigating how their stratigraphic position relative to SB affects petrophysical properties. SB, significant stratigraphic surfaces indicating breaks in deposition, often mark shifts in sedimentation due to sea level changes, creating key unconformities in the rock record (Catuneanu, 2009). The study integrates field investigations, petrographic analysis, petrophysical measurements (porosity, permeability, velocity), and pore system characterization (NMR and petrography) to tests the hypothesis that stromatolite rock textures, porosity, and permeability vary significantly depending on their position relative to SB, ultimately clarifying the impact of stromatolite morphology and stratigraphic context on their reservoir potential.

3.2 Geological setting

The Dam Formation (Fig. 18) formed during the Miocene period as transgressional siliciclastic sediments mixed with carbonate sediments (Powers et al., 1966; Al-Enezi, 2006; Chan et al., 2017; Alkhaldi et al., 2021) coming from shallow marine sources which were linked to astronomical forcing (Alkhaldi et al., 2021). Dam Formation represents transgressional sediments of marine to near-shore sources, deposited on top of the terrestrial-sourced Hadrukh Formation at an unconformable boundary (Martin, 2001;

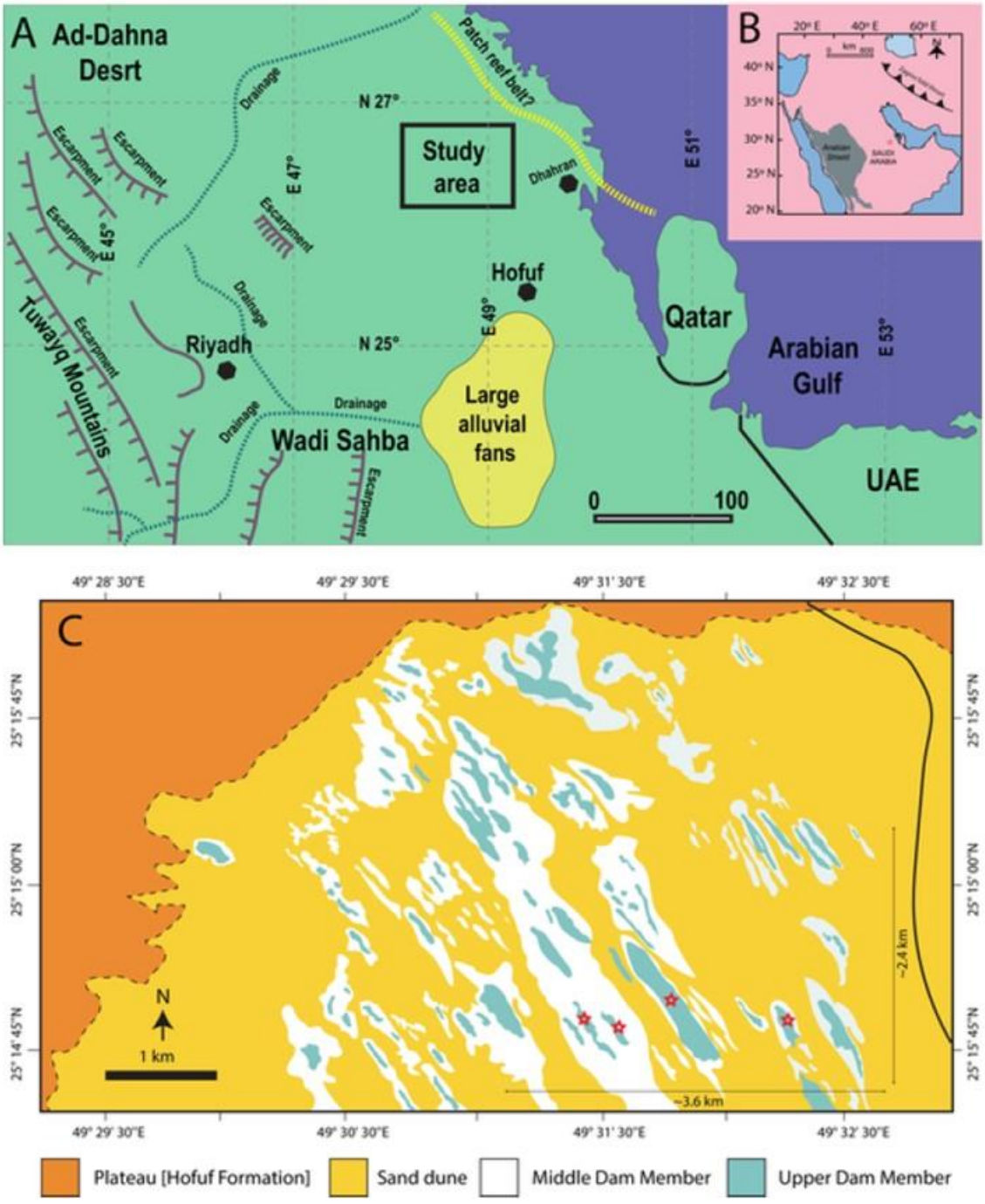

Figure 18: Maps illustrating the study area in eastern Saudi Arabia. A) Regional geological map of eastern Saudi Arabia, highlighting the location of the study area within the Lidam region (black box). B) Map of Saudi Arabia showing the broader location of the study area. C) High-resolution map of the Lidam region, detailing outcrops from the Middle-Upper Miocene and indicating the specific outcrops selected for this study.

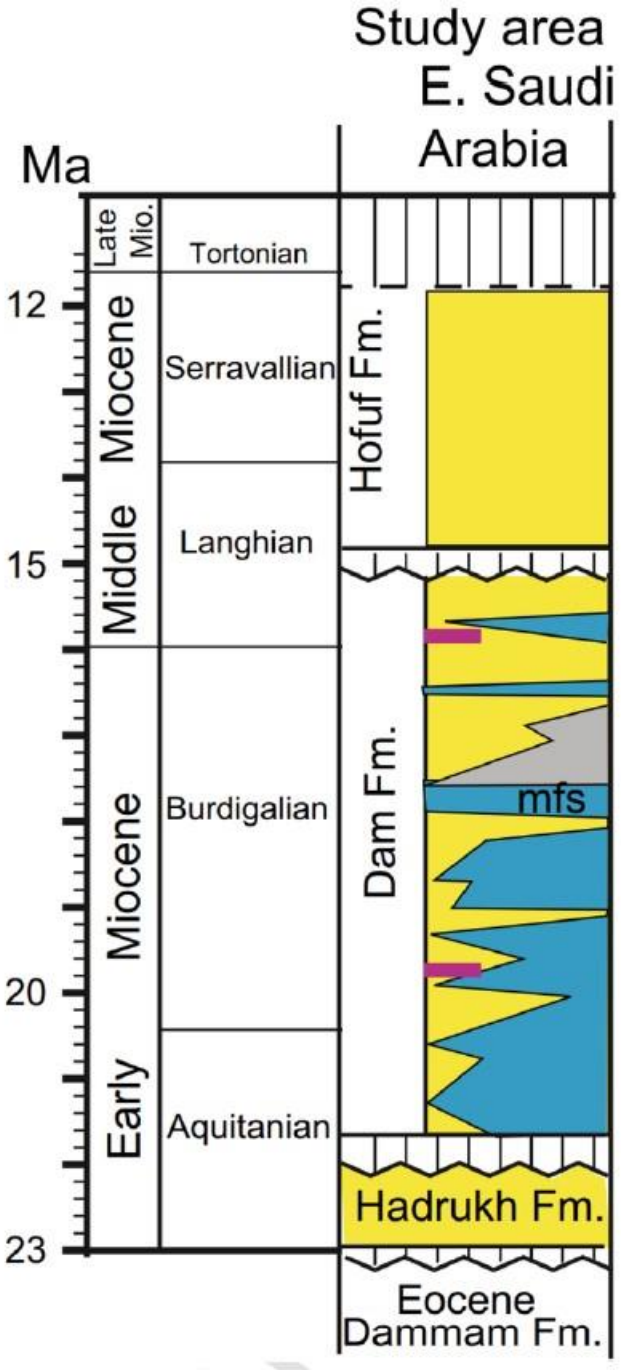

Figure 19: Stratigraphic column of the Early to Middle Miocene, illustrating the Dam Formation, which lies above the Hadrukh Formation and its overlain by the Hofuf Formation.

Bashri et al., 2017; Alkhaldi et al., 2021). The formation was previously divided into three composite sequences that represent deepening upward cycles (Alkhaldi et al., 2021). Hofuf Formation, terrestrial siliciclastic, unconformably overlies the Dam Formation (Martin, 2001; Bashri et al., 2017; Ali et al., 2021a; Ali et al., 2021b; Alkhaldi et al., 2021). Sedimentological development and facies analysis have been previously studied and illustrated by Alkhaldi et al. (2012) who divided the whole sequence of Dam Formation into three separate facies associations consisting of a fossiliferous carbonate group, followed by a siliciclastic group that contains the well-known "red beds", and finally topped by oolitic stromatolites-rich facies association (Fig. 19). All three facies associations are separated by regional Maximum Flooding Surfaces. Our interest falls in the last facies association that contains the stromatolite beds, which is further subdivided into different facies.

Throughout the outcrops that are commonly recognized in Al-Lidam area of Dam Formation (Fig. 18 C), the stromatolites which are mostly forming bindstone (and rarely forming grainstone) occur on different cycles with variable numbers of reoccurrence and thicknesses (Ali et al., 2021a; Ali et al., 2021b). There is a distinct distribution of these morphological forms based on the sequence stratigraphic framework of the Dam Formation, as pointed out by Alkhaldi (2009). The stromatolite heads below the SB of the composite sequences are much larger than the stromatolite heads above the SB (Figs. 20 B and 21). In the Dam Formation, above the SB of each composite sequence, three forms of stromatolites have been documented (Irtem, 1986; Ziegler, 2001; Alkhaldi, 2009; Bashri et al., 2021): 1) Columnar form (stromatolite heads, (Fig. 21 A)): Located in the middle to lower part of the intertidal zone, this form is characterized by a high-energy environment,

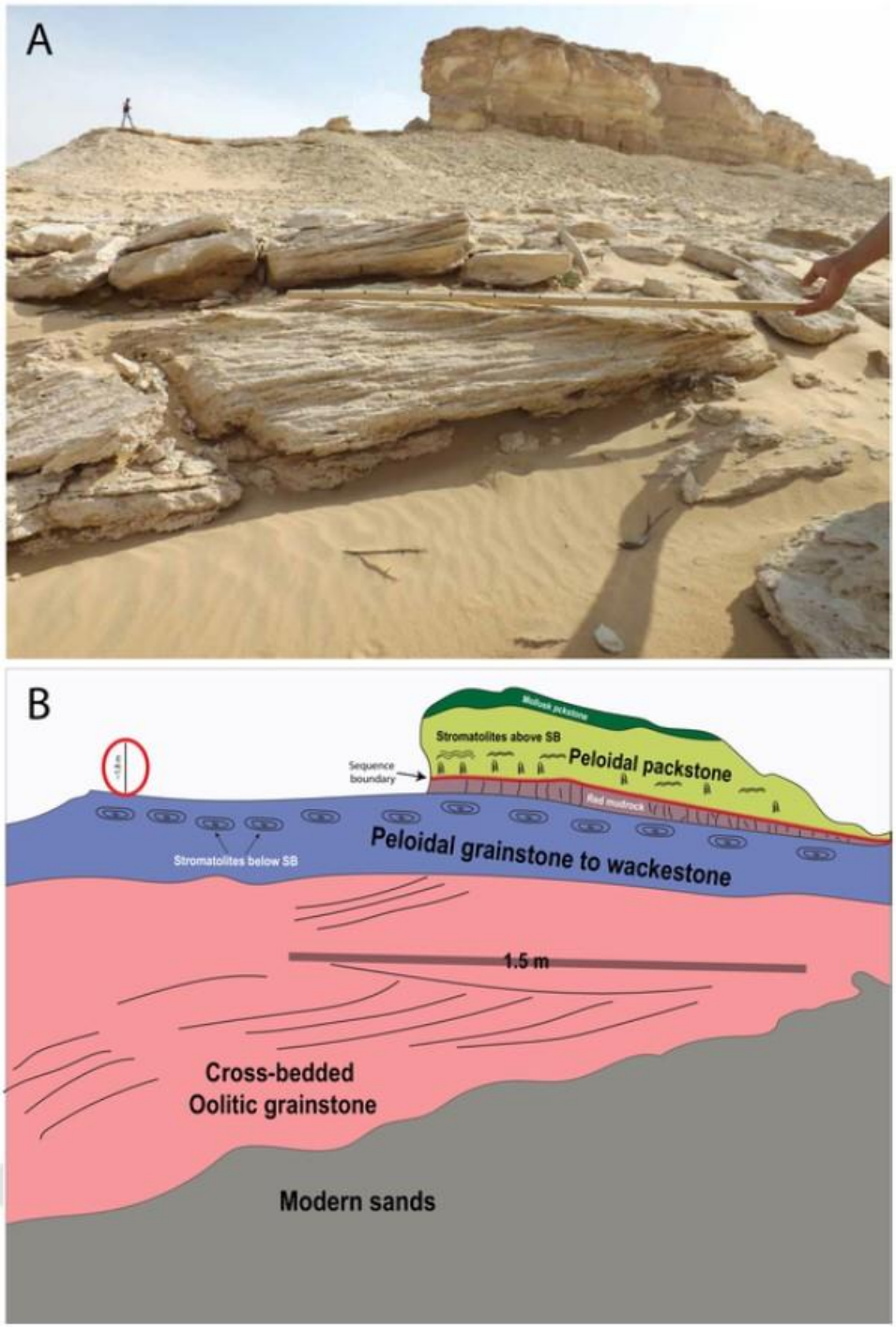

Figure 20: Photograph and its annotated version depicting one of the studied outcrops in the Lidam area, highlighting the strata above and below the SB. Examples of stromatolites from above and below this SB are shown in Figs. 20–23.

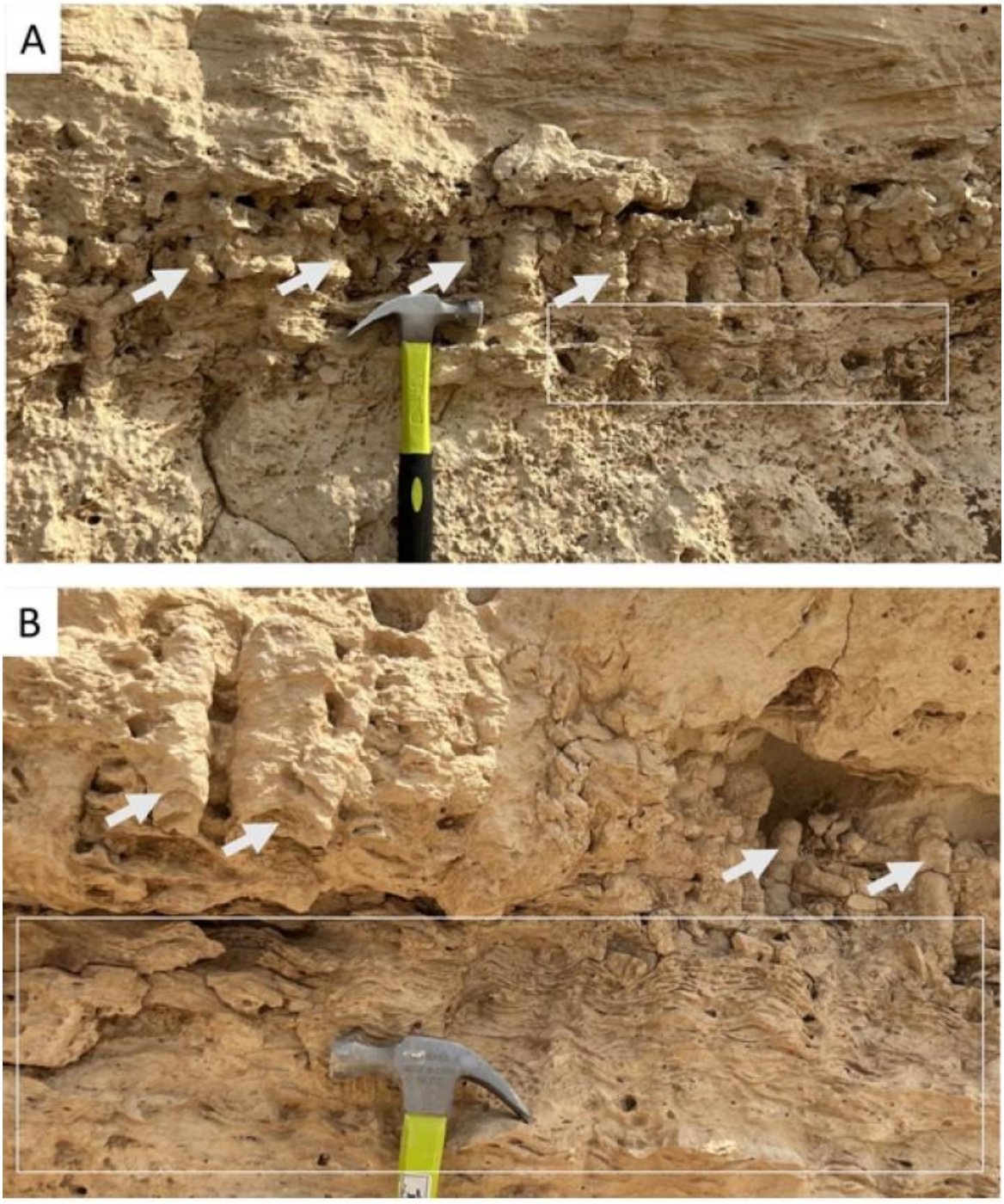

Figure 21: Field photographs showing columnar stromatolite heads positioned above the SB. In both images (A and B), the columnar stromatolite heads (highlighted by white arrows) overlie crinkly laminated stromatolites (outlined by white boxes). Note the vertical axis of this form is markedly longer than the horizontal axis.

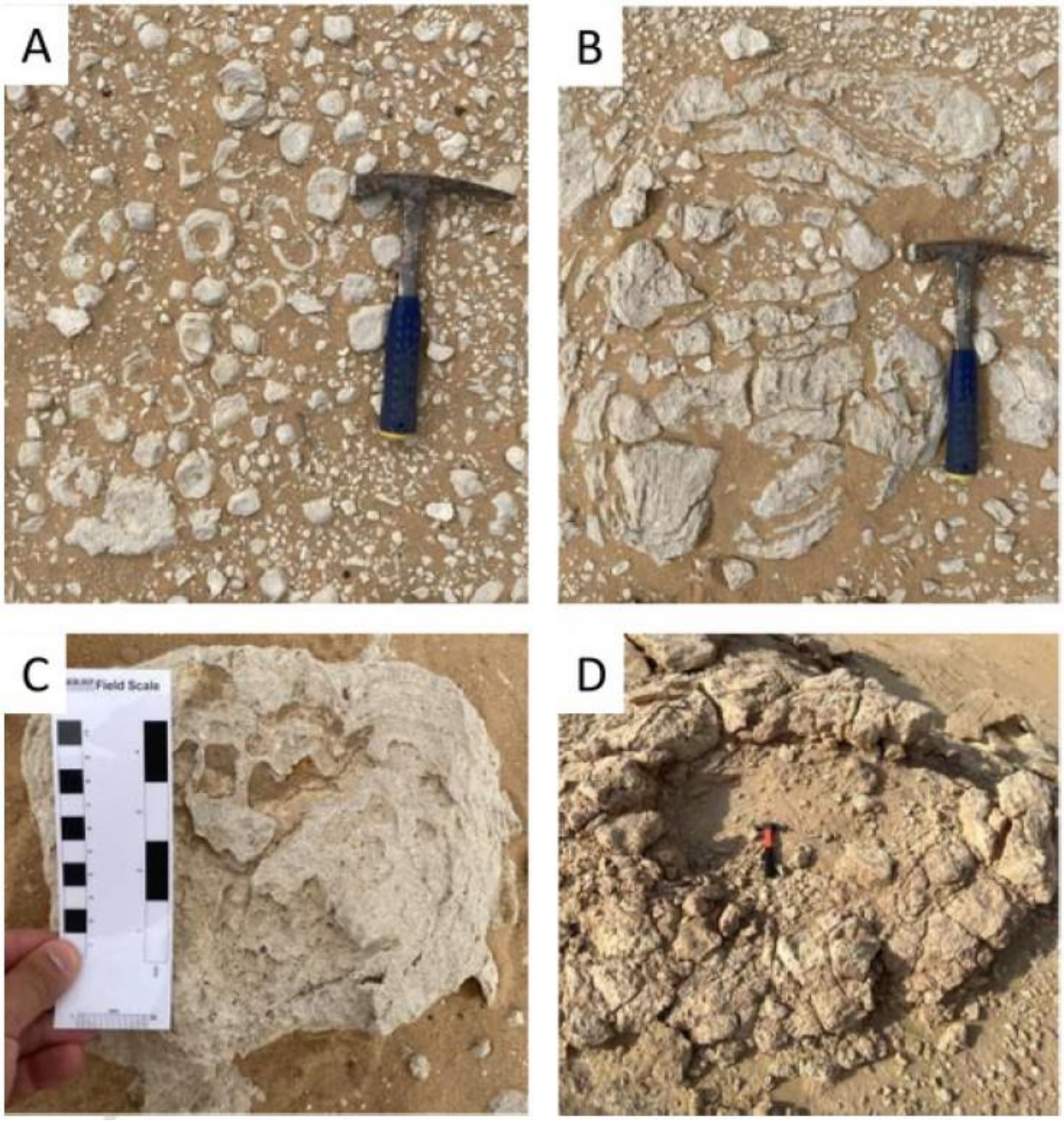

Figure 22: Field photographs showing columnar stromatolite heads positioned below the SB. These stromatolites exhibit a range of sizes, from millimeter scale in (A),centimeter scale in (B) and (C), to meter scale in (D). Note that the horizontal axis is significantly longer than the vertical axis.

suggesting robust wave and current activity that influences its development. 2) Horizontally linked form (Fig. 23): This form exhibits almost horizontal or slightly crinkled lamination, indicative of low to medium wave activity that partially erodes the structure (Fig. 23). It is typically found in the shallow intertidal zone at the boundary with the supratidal zone. 3). Transported form (Fig. 24 A): Found in the lower part of the subtidal zone, this form shows signs of transportation, such as disrupted laminae and a higher mud content, indicating movement and deposition under relatively tranquil conditions. The Burdigalian stage of the Miocene period represents the latest stage before the slowing down of northward movement of the Arabian plate during the Miocene, and temporal ceasing of intraplate extension in the Arabian platform (Hampton et al., 2004). The eastern part of the Arabian plate was located in a subduction zone with Eurasia (Fig. 18 C), and experienced multiple sedimentation sources resulting in the deposition of Dam formation. Consequently, this formation has its respective counterparts from other countries within the eastern part of the Arabian plate such as Al-Nakhash member of Dam Formation in Qatar (Al- Saad and Ibrahim, 2002), Gachsaran Formation in UAE (Sakhavati et al., 2020), the Mutla Member of Lower Fars Formation in Kuwait (Alrefaei et al., 2022), and the Fatha Formation (previously Lower Fars) in Iraq (Al-Juboury and McCann, 2008). Stromatolites in Al-Nakhash member of Dam Formation in southwest Qatar occur mostly as stromatolitic bands in a unit that extends up to 1 m in thickness (Al-Saad and Ibrahim, 2002; Khalifa et al., 2012). Although the Gachsaran Formation in UAE has been shown to be equivalent in age to Dam Formation in both Saudi Arabia and Qatar through foraminifera analysis (Sakhavati et al., 2020), no recognizable stromatolites occurrence has been documented. The same thing applies to the Miocene Lower Fars Formation in Kuwait, even though the

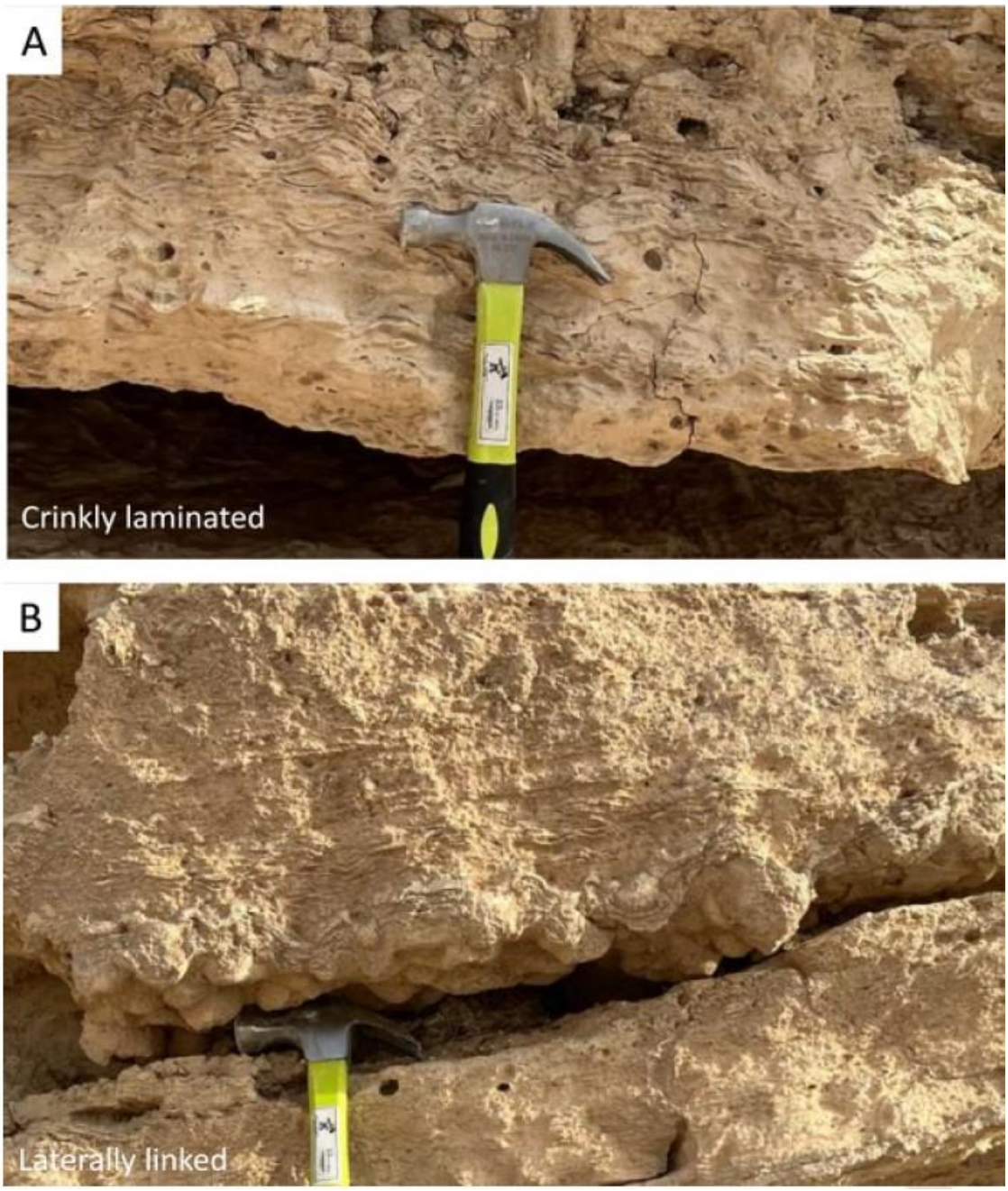

Figure 23: Field photographs showing (A) crinkly laminated stromatolites and (B) laterally linked stromatolites

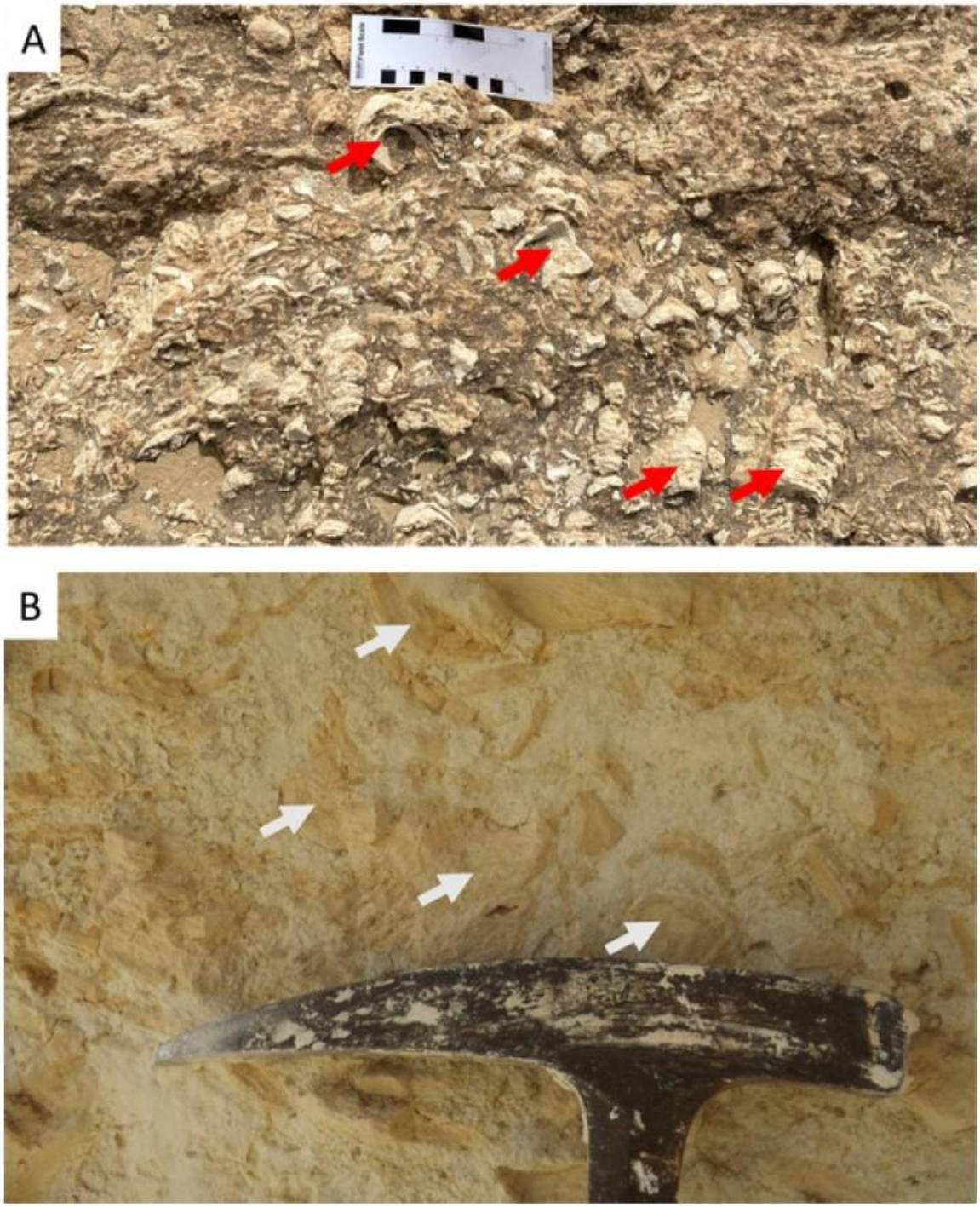

Figure 24: Field photographs showing transported stromatolites in two forms: (A) clast-supported rock texture, where stromatolites act as clasts; and (B) mud-supported rock texture.

supratidal evaporites unit that is equivalent to that of Dam Formation is preserved. In Fatha Formation in northern Iraq, the stromatolites occur in multiple recognized facies, including being present in domal form within the marly limestone facies, and as horizontal lamination within the carbonate mudstone-wackestone microfacies (Al-Juboury and McCann, 2008).

3.3 Methodology

3.3.1 Outcrop measurements

a. Field observations

The methods were designed to test out the hypothesis made for this research which was defined as variation of reservoir quality associated with the same stromatolites' forms, and their location relative to the SB (Fig. 20 B). The investigation started by examining and describing the different forms in the outcrop, specifically their occurrence, sizes, preservation, orientation, and where they occur from a stratigraphic perspective (Fig. 20 B). Multiple outcrops that are present in Jabal Al Lidam were investigated to compare the differences in the stromatolites' forms and abundance. The columnar stromatolite heads above and below sequence stratigraphy of the first composite sequence of the Dam Formation were sampled and cored.

b. Sampling strategy

For the stromatolite heads located both below and above the SB (Fig. 20 B), 20 rock samples were collected from each. Regarding the stromatolite lamination, each set of 20 samples is divided into two groups based on the orientation of the core plug cut (1.5-inch diameter): 10 samples are cut horizontally, and 10 vertically. For the stromatolites situated

above the SB (Fig. 20 B), two additional sets of 20 samples each were gathered—one from the horizontally laminated stromatolites and another from transported stromatolite. These samples are also categorized based on the orientation of the core plug cutting relative to the stromatolite lamination, with 10 samples cut horizontally and 10 vertically.

3.3.2 Laboratory measurements

a. Petrography and petrophysics

Thin sections were prepared for the 40 samples, stained with blue-dyed epoxy to highlight the morphology of the pore system in the stromatolite. The thin sections were imaged using an AxioScan system at the KFUPM laboratory, and the images were processed and analyzed using ZEISS ZEN 3.8 software. Rock texture identification followed the Dunham (1962) classification, while the pore system was classified according to Choquette and Pray (1970). For carbonate components, we applied Flügel's (1981) classification. We used a semi-quantitative method to estimate the percentage and relative abundance of carbonate constituents in each thin section. Porosity and permeability measurements were conducted on the 40 core plugs using a CMS-300TM core measurement system, a pressure decay permeameter and porosimeter that measures pore volume and non-reactive liquid permeability. Velocity measurements were then obtained using Proceq Pundit PL-200 that measures ultrasonic primary waves' (P-waves, [VP]) velocities based on the first arrival time and the plug samples length. Additional considerations were made to ensure the validity of the measurements such as smoothing both ends of the plug samples to ensure consistent travel distances, as well as using coupling gel to enhance contact between the transmitters and the plug ends. The velocity measurements would be cross-referenced with

the porosity-permeability data and petrological findings to explore the origins of any discrepancies.

b. NMR testing

Nuclear magnetic resonance (NMR) testing is also another nondestructive test that was conducted on all the samples using Oxford GeoSpec+ to examine the porosity systems represented within each sample, assisting in explaining any further discrepancies between the rock fabrics and the porosity-permeability data. All plug samples were initially dry; therefore, they were saturated with distilled water before undergoing NMR testing.

c. X-ray diffraction testing

Finally, partial grinding of 16 selected plug samples was performed to produce powder samples that were subsequently subjected to x-ray diffraction (XRD) analysis using PANalytical Empyrean device. The main objective of this test is to quantify the mineralogical composition of the plug samples, aiming to minimize occasional misrepresentation of the thin sections compared to the whole plug samples.

3.4 Results

3.4.1 Field observations

Field examinations of stromatolite columnar form located both below and above the SB revealed distinctive characteristics unique to each (Figs. 21 and 22). Stromatolite heads of the columnar form below the SB are characterized by varying sizes, ranging from a few centimeters up to one meter along their long axis (Fig. 22). Typically, these heads have a horizontal axis (parallel to the bedding plane of the stratum beneath them) that is longer

than the vertical axis (perpendicular to the bedding plane) (Fig. 22). These heads exist in mud-dominated interval above strata with grain-dominated texture that contains skeletal oolitic grainstones.

In contrast to the stromatolite heads of the columnar form below the SB (Fig. 21 A and B), those above the SB are characterized by a horizontal axis that is substantially shorter than the vertical axis (Fig. 21 A). The horizontal spacing between these heads varies from one interval to another, and the filling sediments between the heads also range from being mud-dominated to grain-dominated (Fig. 21 A). Unlike the heads below the SB, which exist solely as columnar heads, those above the SB can coexist with other forms such as horizontally laminated and transported stromatolites (Fig. 21 B).

3.4.2 Petrographic observations

Petrographic analysis revealed the complex internal structure of the studied stromatolites (Figs. 25 A, 26 A). The micritic laminae and the sediments trapped between the stromatolite laminae are evident in several samples, both above and below the SB. An interesting observation is that the laminae in stromatolites above (Fig. 25 A) the SB are remarkably thinner compared to those below the SB (Fig. 26 A).

The main components of the stromatolites are consistent both above and below the SB, though their relative abundances differ (Figs. 25, 26). The five major components are: 1) peloids, 2) coated grains (including ooids and grapestones), 3) skeletal grains (foraminifera and skeletal fragments of mollusks), 4) lime mud, and 5) quartz (Figs. 25 and 26). Notably, the relative abundance of coated grains, quartz, and skeletal grains is substantially higher in stromatolites above the SB compared to those below. In contrast, stromatolites below

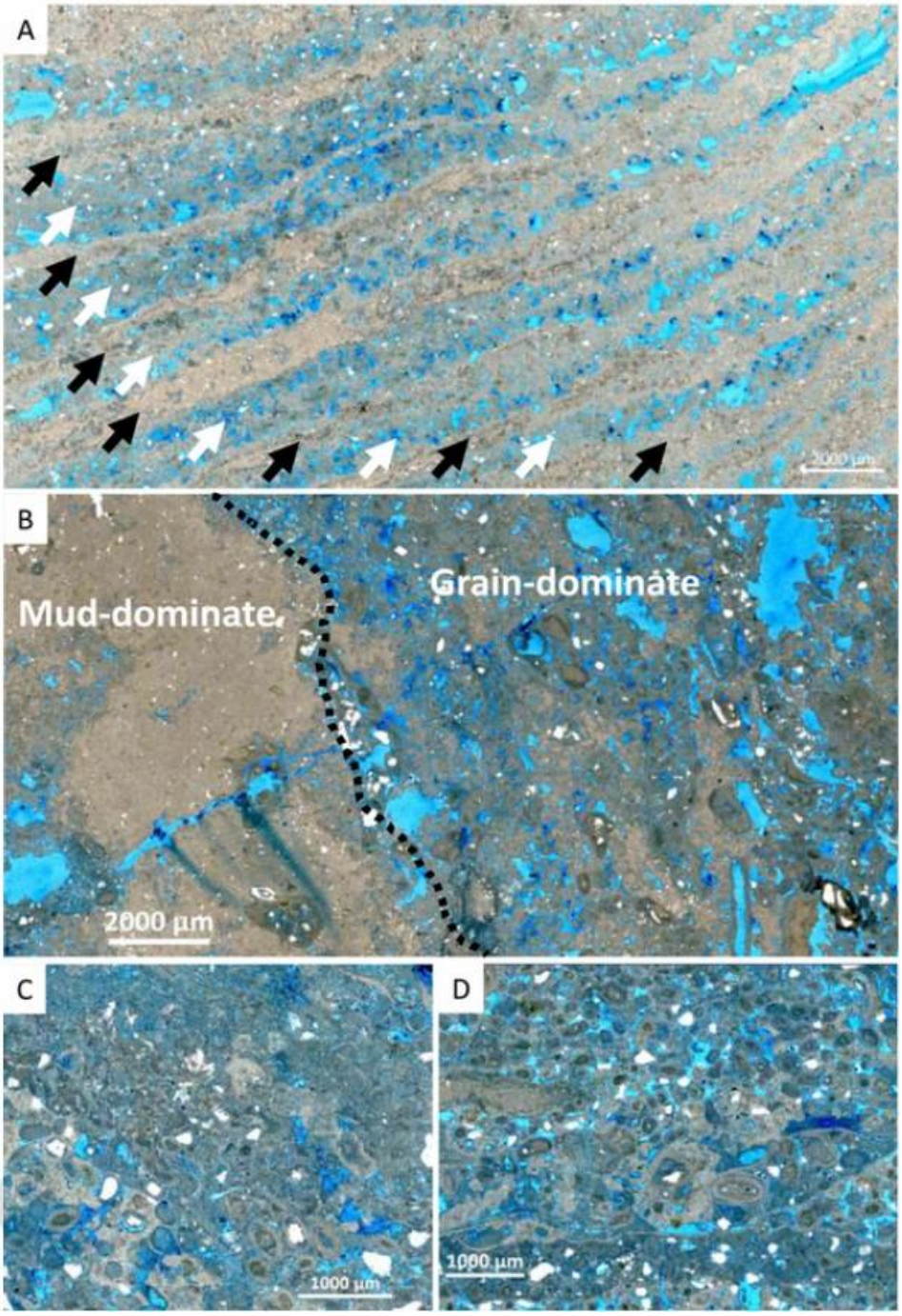

Figure 25: Thin section photomicrographs of columnar stromatolite heads above the SB. (A) Photomicrograph shows algal mats (black arrows) and the entrapped sediments between them (white arrows). Blue coloration indicates porous areas. Note the higher porosity in the lamina between algal mats compared to the mats themselves. (B) Higher resolution image showing the alternation between algal mats and entrapped sediments. The entrapped sediments are grain-dominated, featuring interparticle and moldic pores. (C and D) Microphotographs provide further details of the grain-dominated entrapped sediments, clearly showing interparticle and moldic porosity.

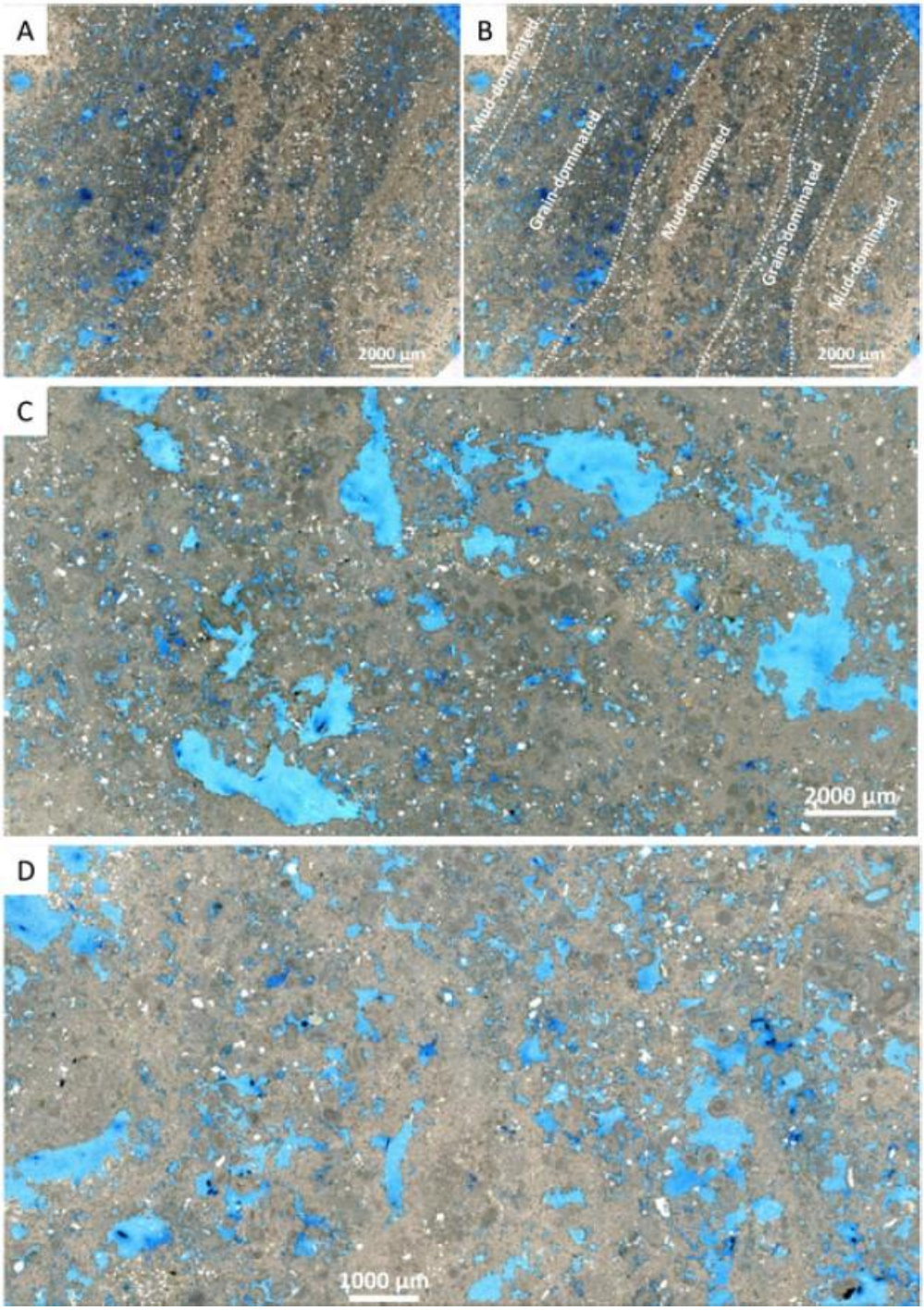

Figure 26: Thin section photomicrographs illustrating the microstructures of stromatolites below the SB. (A) and (B) Photomicrograph and its annotated version showing lamination in the stromatolite below the SB. Note that the laminae are wider compared to those in the stromatolite above the SB. (C) Photomicrograph displaying a mud-dominated texture, with vugs as the predominant pore system. (D) Photomicrograph showing a wackestone to packstone texture within stromatolites below the SB, with localized occurrences of interparticle and moldic pores.

the SB are characterized by a higher relative abundance of lime mud and peloids. The stromatolites above the SB fluctuate between mud-supported and grain-supported matrices (Fig. 25 A and B). Below the SB, the stromatolites are predominantly mud-supported (Fig. 26), with grains constituting up to 50 % in certain instances. As a result, these stromatolites are generally classified as wackestones, with occasional occurrences of grain-dominated wackestones. Both above and below the SB, the dominant pore types in stromatolites include vuggy, interparticle, intraparticle, moldic, and microporosity (Figs. 25 and 26). However, their relative abundance varies significantly depending on their position relative to the SB. Above the SB, interparticle, intraparticle, moldic, and microporosity types are more prevalent compared to vuggy porosity (Fig. 25). Conversely, stromatolites below the SB are dominated by vuggy porosity, reflecting differences in diagenetic processes and depositional environments (Fig. 26).

3.4.3 NMR data

The porosity systems variation between the columnar stromatolites above and below the SB is also clearly seen in the NMR data (Fig. 27 A and B). The NMR results are depicted in a two-axial diagram for all the samples in each form superimposed on each other, where the x-axis corresponds to the T2 relaxation time (in milliseconds), signifying the duration required for hydrogen atoms to revert from a polarized state to their initial state. The hydrogen atoms originate from the water content occupying the internal voids within the samples. The y-axis denotes incremental porosity, implying that during the test the porosity keeps building up with time. The columnar stromatolites heads above the SB shows a bimodal graph with one major peak and one minor peak, representing two different porosity systems (Fig. 27 A). Whereas it is uncertain which peak corresponds to which

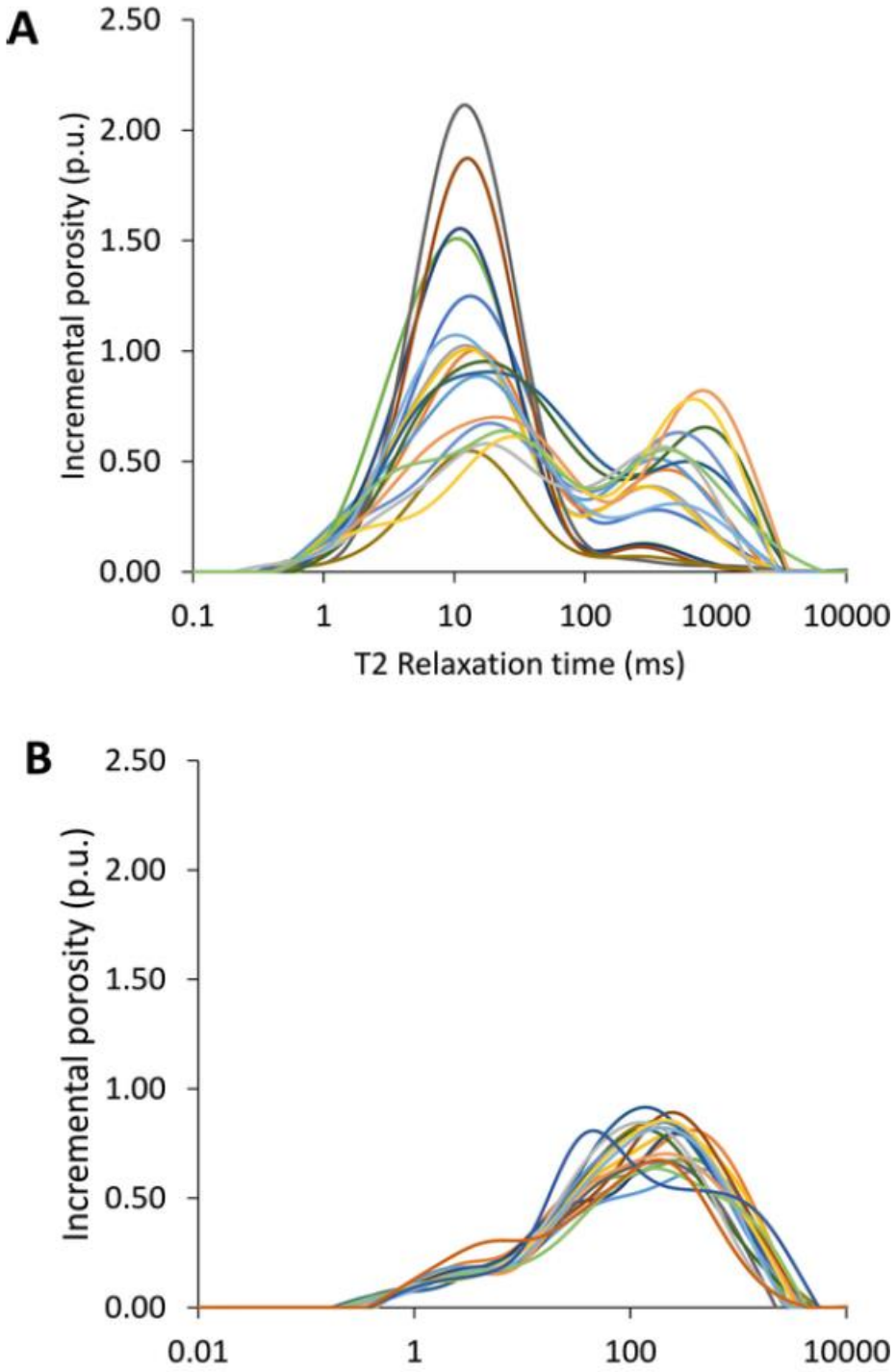

Figure 27: Plots illustrating NMR data for stromatolites above (A) and below (B) the SB. The NMR data for stromatolites above the SB suggest two dominant pore systems, as indicated by the bimodal porosity pattern. In contrast, the NMR data for stromatolites below the SB indicate a single dominant pore system, reflected by the unimodal porosity pattern.

porosity system, integrating the petrographic analysis of the thin section (Fig. 25) can help discern the relationship between the porosity peaks and the respective porosity systems they represent. The primary porosity peaks fell between 10 and 20 ms, whereas the secondary peaks fell between 500 and 1000 ms (Fig. 27 A). The larger peak likely represents the interparticle and vuggy porosity that dominates the columnar stromatolites heads above the SB form, while the smaller peak represents the microporosity porosity. The columnar stromatolites heads below the SB shows overall a unimodal diagram (Fig. 27 B). The primary porosity peaks fell around 150 ms. This NMR pattern represents a singular dominant porosity system. Integrating the NMR data (Fig. 27 B) with petrographic data (Fig. 26) suggest that the NMR unimodal pattern in the columnar stromatolites heads below the SB is likely overwhelmed by the vuggy porosity which is dominated this form as seen from the petrographic analysis.

3.4.4 Distribution of porosity, permeability, and VP

a. Statistical analysis

The porosity, permeability, and VP of columnar stromatolite heads show notable differences above and below the SB (Table 2). For the stromatolite heads above the SB, samples cut horizontally (n = 10) revealed an average porosity of 40.67 % with a standard deviation of 4.12, while their permeability averaged 173.23 mD with a relatively high standard deviation of 267.90. The average value of the VP for these samples was 3113 m/s, with a standard deviation of 672.06. In contrast, the vertically cut samples from the same stromatolite heads above the SB (n = 10) demonstrated a slightly higher average porosity of 41.03 % with a lower standard deviation of 3.57. However, their permeability was

substantially higher, averaging 912.56 mD, but with a large standard deviation of 937.97. The VP in these samples averaged 2809.30 m/s with a standard deviation of 517.73. Comparatively, the stromatolite heads below the SB displayed different characteristics (Table 2). Horizontally cut samples (n=10) from these heads had a lower average porosity of 35.48 % with a standard deviation of 3.02. The permeability in these samples was higher than their counterparts above the boundary, averaging 425.43 mD with a standard deviation of 118.58. The VP was higher as well, averaging 3669.9 m/s with a standard deviation of 609.14. Similarly, the vertically cut samples from the stromatolite heads below the boundary (n = 10) showed a slightly lower average porosity of 35.09 % with a standard deviation of 2.58. Their average permeability was 514.20 mD, with a matching standard deviation. The VP in these samples was 3525.00 m/s with a standard deviation of 390.75, which is lower than in the horizontally cut samples.

b. Graphical analysis

By examining box plots of porosity (and grain density), permeability, and VP for stromatolite, irrespective of sampling direction, we observed substantial differences in these properties based on the stromatolites' stratigraphic position (Fig. 28). Both porosity and grain density are markedly higher in the columnar stromatolite heads above the SB compared to those below (Fig. 28 A and B). Conversely, this trend is reversed for VP, with the columnar stromatolite heads above the SB exhibiting significantly lower values than those below (Fig. 28 C). The permeability data reveal an interesting pattern (Fig. 28 D). In the box plot, the mean value, indicated by a cross, appears nearly identical for both groups

Sample #	Orientation	Porosity (%)	Density (g/cc)	Permeability (mD)	VP (m/s)
CBSB-1	H	32.38	2.81	551.49	4286.00
CBSB-2	H	37.55	2.80	NA	NA
CBSB-3	H	29.48	2.81	232.69	4161.00
CBSB-4	H	33.76	2.80	461.05	3611.00
CBSB-5	H	33.61	2.81	NA	NA
CBSB-6	H	38.20	2.80	350.34	2807.00
CBSB-7	H	37.51	2.81	460.51	3197.00
CBSB-8	H	38.65	2.80	371.79	2883.00
CBSB-9	H	36.31	2.80	556.41	3670.00
CBSB-10	H	37.31	2.82	257.54	3750.00
CBSB-11	V	36.49	2.80	375.13	3401.00
CBSB-12	V	37.49	2.81	973.96	2944.00
CBSB-13	V	33.04	2.81	720.57	4017.00
CBSB-14	V	35.97	2.80	568.50	3182.00
CBSB-15	V	36.02	2.80	477.08	3636.00
CBSB-16	V	37.31	2.80	294.80	3372.00
CBSB-17	V	33.55	2.81	736.54	3631.00
CBSB-18	V	38.05	2.80	419.32	3229.00
CBSB-19	V	30.03	2.81	476.90	4248.00
CBSB-20	V	32.93	2.80	99.23	3590.00
CASB-1	H	38.54	2.84	3.11	3186.00
CASB-2	H	36.69	2.83	12.51	3135.00
CASB-3	H	40.39	2.79	1.80	2941.00
CASB-4	H	44.03	2.84	2.25	2544.00
CASB-5	H	41.33	2.83	2.15	2765.00
CASB-6	H	48.04	2.83	794.74	2109.00
CASB-7	H	33.93	2.83	352.43	4500.00
CASB-8	H	42.65	2.82	117.01	3333.00
CASB-9	H	40.40	2.82	273.04	3504.00
CASB-10	V	38.68	2.83	34.98	3086.00
CASB-11	V	37.94	2.85	22.97	3142.00
CASB-12	V	36.75	2.83	55.83	3133.00
CASB-13	V	40.58	2.83	1.38	3110.00
CASB-14	V	47.30	2.81	2.80	2736.00
CASB-15	V	45.38	2.82	1748.37	2326.00
CASB-16	V	39.01	2.83	1900.50	2048.00
CASB-17	V	43.77	2.84	1784.91	2474.00
CASB-18	V	38.11	2.81	NA	NA
CASB-19	V	42.79	2.83	1788.97	2308.00

Table 2: Data showing porosity, grain density, VP, and permeability of stromatolites, grouped as stromatolites above (CASB) and below (CBSB) the SB. Note that some samples were cut in a vertical orientation (marked as V), while others were cut in a horizontal orientation (marked as H).

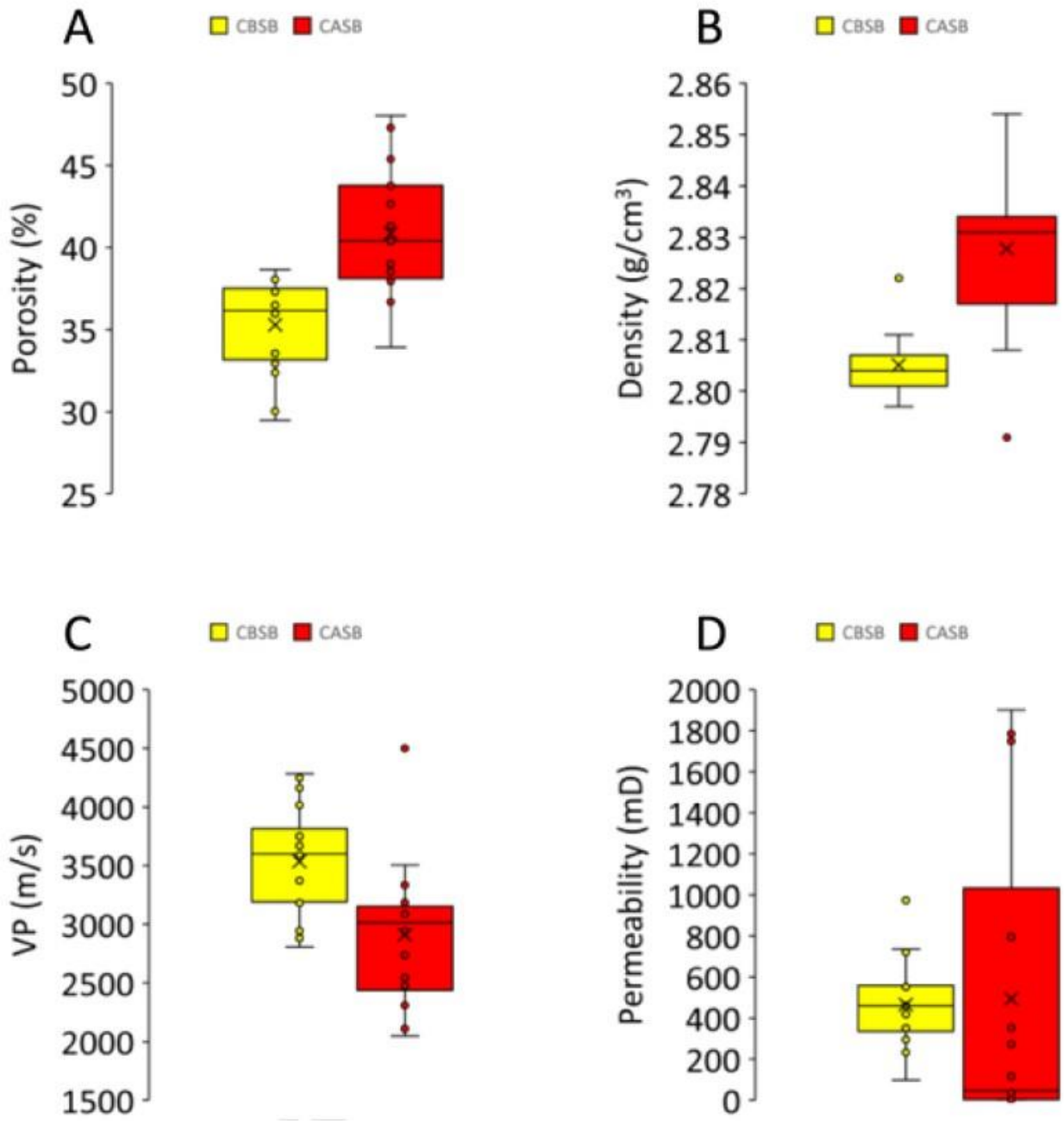

Figure 28: Box plots showing (A) porosity, (B) grain density, (C) VP, and (D) permeability of stromatolites, grouped as stromatolites above and below the SB.

(above and below the SB). However, there are significant differences in the median and range (Fig. 28 D). The permeability data for the columnar stromatolite heads above the SB display a wide range and a median that is noticeably lower than the mean (Fig. 28 D). In contrast, the permeability data for the columnar stromatolite heads below the SB show a narrow range with mean and median values that are nearly the same (Fig. 28 D).

c. ANOVA results

An analysis of variance (ANOVA) was conducted to examine the patterns of stromatolite petrophysical properties observed in the graphical analysis. The results revealed significant differences in porosity, VP, and density between the two groups (stromatolite above and below SB), with p-values less than 0.05 for each variable, indicating statistically significant differences between columnar heads above and below the SB. In contrast, no significant difference was found for permeability, as indicated by a p-value greater than 0.05.

3.4.5 Mineralogy

XRD analysis of eight selected samples, which have comparable porosity measurements but exhibit significant permeability variations, revealed that the columnar forms above and below the SB are predominantly composed of dolomite, with varying amounts of accessory quartz (Table 3). Calcite, palygorskite, and kaolinite are present in trace amounts (less than 1 %) (Table 3). When these samples are classified based on their mineralogy, all but one (sample CASB 6) can be categorized as dolostone, as they contain more than 95 % dolomite (Table 3). Sample CASB 6, however, is classified as quartz dolostone, with a dolomite concentration of 86 % and a quartz concentration of 12.8 %. It is also noteworthy that the

Sample ID	Dolomite [%]	Quartz [%]	Calcite [%]	Palygorskite [%]	Kaolinite 1A [%]
CASB 6	86.4	12.8	0	0.8	0
CASB 13	95.8	3.5	0	0.4	0.2
CASB 16	98.7	0.9	0.1	0.2	0.2
CASB 18	97	2.4	0	0.5	0.1
CBSB 4	98.9	0.9	0	0.2	0.1
CBSB 7	95.8	3	0	0.9	0.2
CBSB 9	99.4	0.3	0	0.3	0
CBSB 12	98.2	1.7	0	0	0.1

Table 3: Data document the XRD analysis results of selected samples from the stromatolites above (CASB) and below (CBSB) the SB.

columnar heads above the SB have a relatively higher average quartz concentration (~5 %) compared to those below the SB (~1.5 %).

3.5 Discussion

Integrating field observations (Figs. 20–24) with petrographic analysis (Figs. 25, 26), NMR data (Fig. 27) and petrophysical measurements (Fig. 28) offers a comprehensive understanding of how petrophysical properties of stromatolites vary within different stratigraphic contexts. This multidisciplinary approach allows for a detailed characterization of the rock textures, mineral compositions, and pore structures of stromatolites, providing valuable insights into how these factors influence properties such as porosity, density, permeability, and velocity. By examining stromatolites both above and below SB, this study aims to reveal the complex interplay between their geological setting and petrophysical behavior, thereby enhancing our knowledge of their potential impact on reservoir quality and fluid flow dynamics.

3.5.1 Variation in stromatolite morphology above and below SB

Alkhaldi et al. (2021) defined three main composite sequences within the Dam Formation, each capped by a SB that separates deepening-upward cycles of marine to nearshore sediments. These SB mark transitions between different depositional environments and play a critical role in the stratigraphic framework of the Dam Formation. Above each SB, sediments are typically indicative of transgressive system tracts, characterized by fluctuating water energy levels that influence the distribution of stromatolites and their associated reservoir properties. In contrast, sediments below the SB represent more restricted environments, where lateral stromatolite growth is favored over vertical

development, leading to distinct differences in porosity and permeability. The SB in the Dam Formation thus defines significant shifts in depositional regimes, with clear implications for reservoir quality. Stromatolites found above these boundaries are typically associated with higher-energy environments and more complex pore systems, while those below the boundaries are more influenced by diagenetic processes, resulting in more uniform but potentially lower reservoir quality.

Field observations at the largest scale reveal a marked difference in stromatolite morphology above and below the SB (Figs. 21, 22). The columnar heads below the SB show considerable variation in size and can form large, laterally extensive stromatolite structures (Fig. 22). In contrast, the columnar heads above the SB are restricted in their ability to develop extensive lateral laminations and instead exhibit vertical growth.

Numerous studies have examined the factors influencing stromatolite morphology (Andres and Reid, 2006; Dupraz et al., 2009; Suarez- Gonzalez et al., 2019). These studies suggest that variations in stromatolite morphology can be attributed to several key controls, including the availability of accommodation space for growth, the hydrodynamic conditions of the depositional environment, and prevailing sedimentation patterns (Andres and Reid, 2006). Considering this previous research, the stromatolite morphology within the Dam Formation, both above and below the SB, is discussed in detail below.

The horizontally expanded morphology of the columnar stromatolite heads below the SB (Fig. 22) can be attributed to the prevailing hydrodynamic conditions. During periods of low sea level, the water depth was shallow, which promoted photosynthesis due to the abundant availability of sunlight. This environmental condition favored lateral expansion

of stromatolites rather than vertical growth, as there was sufficient sunlight without the necessity to grow upwards. However, erosion may have contributed to the limited vertical development of these structures by removing the uppermost layers.

Petrographical analysis indicates that the stromatolite columnar heads below the SB are characterized by a mud-dominated rock fabric (Fig. 25 B). In outcrop exposures, these stromatolites are embedded within a muddy interval that overlies well-defined cross-bedded oolitic grainstone (Fig. 20 A). The stratigraphic and sedimentological characteristics of the strata where these stromatolite columnar heads are found suggest a quiet water environment with some degree of restriction (Bashri et al., 2017; Ali et al., 2021a; Alkhaldi et al., 2021). This setting is comparable to modern analogs, such as Highborne Cay in the Bahamas (Andres and Reid, 2006), where columnar stromatolites are predominantly found in deeper back-reef lagoons behind extensive reef flats. In such environments, restricted water flow and the availability of accommodation space likely contribute to the columnar growth and horizontal expansion of stromatolites. Moreover, the presence of allochthonous fine grain sediments in such settings can facilitate the entrapment of mud by stromatolites.

In contrast, the columnar heads formed above the SB were characterized by a restricted capacity to develop extensive lateral extend laminations (Fig. 21 A). As sea levels rose, these stromatolites adapted by growing vertically to maintain exposure to sunlight and to enhance the structural integrity of the columnar heads. Due to the limited lateral extent, low sediment accommodation space and rapid burial due to rapid sedimentation the algal mats intensified their vertical stacking (Andres and Reid, 2006). This vertical growth resulted in the formation of thin, grainy layers dominated by interparticle porosity,

interspersed with impermeable laminations that formed during periods characterized by high-energy water flow. As water energy decreased, layers characterized by mud and microporosity were more likely to form.

3.5.2 Variation in stromatolite morphology above and below SB

A marked difference in the pore systems of stromatolites above and below the SB is evident, reflecting the distinct morphologies observed in these two settings from petrographic analysis (Figs. 25, 26). NMR data further provide independent evidence to mark such difference (Fig. 27 A and B). The stromatolites below the SB are primarily characterized by vuggy porosity, whereas those above the SB are dominated by interparticle, moldic and micro porosity (Figs. 25–27). This variation in pore types can be attributed to several factors that control stromatolite deposition, such as the hydrodynamic conditions of the depositional environment, and prevailing sedimentation patterns mentioned above. Furthermore, post-depositional processes, including dissolution and cementation, also play a significant role in shaping these differences in the pore systems.

For instance, the dominance of interparticle, moldic and micro porosity above the SB (Fig. 25) can be attributed to the prevalence of a grain-supported versus mud-supported rock fabric, which is itself a result of the high-energy hydrodynamic regime in this setting. The relatively less representation of this pore type below the SB suggests a different control. The prevalence of vuggy porosity in the stromatolites (Fig. 25) provides evidence of diagenetic control. In these stromatolites, diagenesis impacted the rock fabric by promoting internal cementation of grains, which greatly reduced the interparticle, moldic and micro porosity. At the same time, this diagenetic process enhanced vuggy porosity through the enlargement of pores caused by dissolution and the interconnection of initially isolated

voids. These processes most likely occurred in different chronological orders. This dual effect of diagenesis—reducing certain types of porosity while enhancing others—illustrates the complex interplay between post-depositional alterations in determining the ultimate pore architecture of stromatolites in different stratigraphic contexts.

3.5.3 Variation in petrophysical properties

The porosity, grain density, permeability, and VP of columnar stromatolite heads exhibit notable differences above and below the SB. These differences are evident from both graphical representations and statistical analyses, including the results of the ANOVA tests (Fig. 28, Tables 2, 3). These differences are closely related to variations in stromatolite morphology and their associated pore systems. Both porosity and VP show statistically significant differences between stromatolites above and below the SB, likely reflecting the dominance of interparticle, moldic and micro porosity versus vuggy porosity in these stromatolites.

The wider range of porosity and VP values observed in stromatolites above the SB (Fig. 28 A and C), compared to those below (Fig. 28 A and C), can be interpreted as evidence of multiple pore types contributing to the pore system. In contrast, stromatolites below the SB exhibit a more uniform pore system, dominated by vuggy porosity. This interpretation is strongly supported by NMR data (Fig. 10 A and B), which show distinct patterns for the two groups: a unimodal distribution for stromatolites below the SB (Fig. 27 A) and a bimodal distribution for those above (Fig. 27 B). The unimodal distribution below the SB suggests a relatively homogeneous pore system dominated by vugs, while the bimodal distribution above the boundary indicates a more heterogeneous pore structure with a combination of interparticle, moldic, and micro pores.

The observed variations in porosity and VP cannot be attributed to differences in mineralogy, as XRD analysis reveals that nearly all samples are composed of dolomite (Table 3). This consistency in mineral composition suggests that the rock fabric in the stromatolites can be classified as fabric-preserving dolomites, with the variations in rock fabric being the primary factor influencing their petrophysical properties. However, the slight differences in grain density could be linked to mineralogical variations. The slightly lower grain density values in stromatolites below the SB may result from an increased quartz content due to detrital silica input (Fig. 26). This higher silica content is consistent with the depositional environment below the SB, where shallow water levels and proximity to the shoreline would likely result in greater detrital influx.

While porosity, grain density, and VP data show clear distinctions based on stratigraphic position, the permeability data present a different pattern, characterized by noticeable overlap and scatter among stromatolites both below and above the SB (Fig. 28 D). Although the ANOVA results indicate no statistically significant difference in permeability between stromatolites situated above and below the SB (Table 3), the graphical data suggest a wider range of permeability values in stromatolites above the SB compared to those below. This increased variability in permeability may be related to the complex interplay of multiple pore types within the stromatolites above the SB, where interparticle, moldic, and micro pores coexist.

Stromatolites above the SB formed within a transgressive system tract, where water dynamics fluctuated rapidly between high and low energy conditions. These varying water energies likely contributed to the rapid vertical growth of stromatolites and influenced the type of sediment that became entrapped within their structure. In high water energy

settings, stromatolites are more likely to trap grain-dominated sediments, leading to an increased percentage of interparticle and moldic porosity. This condition promotes higher permeability due to the larger pore spaces between the grains. Conversely, in low water energy environments, stromatolites are more prone to trapping mud-dominated sediments, resulting in a higher proportion of microporosity. This finer sediment reduces permeability because of the smaller pore spaces and more compact arrangement. This interpretation could explain the wide range of permeability observed in the stromatolite samples from above the SB. The variability in water energy during formation likely caused differences in the types of sediment entrapped, which in turn affected the porosity and permeability characteristics of the stromatolites.

3.5.4 Implication and limitations

The findings of this study carry several important implications for both academic research and practical applications in the field of reservoir characterization, especially in carbonate systems influenced by stromatolites. Examples of these are highlighted in the below discussion.

The study demonstrates that stromatolite-bearing intervals above and below SB exhibit significant differences in pore types, such as vuggy and interparticle porosity, which in turn affect fluid flow behavior. By incorporating these morphological and stratigraphic insights into reservoir models, geologists can better predict heterogeneity within carbonate reservoirs. This leads to more accurate forecasts of reservoir quality, ultimately improving hydrocarbon recovery efficiency. Moreover, understanding the vertical and lateral variations in stromatolite morphology allows for better decision-making during reservoir simulation and development planning, reducing economic risks associated with drilling.

The study provides practical guidance for optimizing well placement and production strategies in carbonate reservoirs. For example, stromatolites above the SB, which are characterized by interparticle porosity and more heterogeneously distributed permeability, may present zones with higher fluid flow potential, making them ideal targets for well placement. Conversely, the more homogeneous vuggy porosity below the SB may result in more predictable but lower fluid flow rates, which can be leveraged when managing water flooding or secondary recovery methods. Reservoir engineers can thus use the findings to improve field development strategies by anticipating zones of high or low permeability based on stromatolite morphology and stratigraphic positioning. The study highlights the significant role of diagenetic processes, such as cementation and dissolution, in shaping the pore architecture of stromatolites. This knowledge is particularly valuable for predicting areas of the reservoir that may have experienced porosity enhancement due to dissolution or reduction due to cementation. Understanding how diagenesis affects stromatolites both above and below SB provides a framework for assessing the potential diagenetic overprinting in other carbonate reservoirs. This, in turn, aids in the identification of "sweet spots" where secondary porosity from diagenesis may enhance reservoir quality, especially in older or deeper reservoirs where diagenetic processes have had a more pronounced impact.

While this study focuses on stromatolites in the Dam Formation, the results have broader implications for other carbonate systems where stromatolites or microbialites play a significant role. The study's integrated approach—combining field observations, petrographic analysis, NMR, and XRD data—can serve as a model for future research in similar settings. This framework could be applied to other Miocene carbonate formations,

or to formations in different geological time periods, where stromatolites contribute to the reservoir's architecture. The findings can also inform exploration efforts in modern microbialite systems, where similar depositional and diagenetic processes may be influencing reservoir quality.

Despite the valuable insights gained from this study, several limitations must be acknowledged. These limitations highlight areas where further research is necessary to expand the understanding of stromatolite influence on reservoir properties. Examples of these are highlighted in the below discussion.

The study focuses exclusively on stromatolites from the Dam Formation in eastern Saudi Arabia, which is limited both geographically and temporally. The Miocene age of the formation, while important for understanding that specific period's depositional and diagenetic history, may not represent stromatolites in other geologic settings. Stromatolites from different time periods or regions—such as Precambrian or modern stromatolites—might exhibit different morphologies and diagenetic pathways, leading to variations in their influence on petrophysical properties. As such, the generalizability of these findings is constrained by the specific geological and paleoclimatic conditions of the Dam Formation. Future studies that extend the scope to other regions and time periods are necessary to validate and refine these conclusions.

The resolution of the methods employed, while advanced, may still not capture the full complexity of the pore systems within stromatolites. Stromatolites are inherently heterogeneous structures with a wide range of micro- to macro-scale features that influence their petrophysical properties. The limited number of samples, combined with potential

variability in porosity and permeability even within a single stromatolite form, means that small-scale variations may have been overlooked. Increasing the sample size and employing even higher resolution techniques, such as micro-CT scanning or 3D reservoir modeling, could provide a more detailed understanding of the pore architecture within stromatolites.

One of the major challenges in interpreting stromatolite petrophysical properties is the degree to which diagenesis has overprinted the original depositional characteristics. Diagenetic processes, such as cementation and dissolution, have modified the primary porosity and permeability in ways that may obscure the relationship between stromatolite morphology and petrophysical behavior. This introduces uncertainty, especially in distinguishing primary depositional features from secondary diagenetic alterations. For instance, while the study highlights the prevalence of vuggy porosity below the SB, it is difficult to determine whether this porosity is entirely a product of diagenesis or if it reflects primary features of the stromatolites. Future research could benefit from isotopic or geochemical analyses that better constrain the timing and extent of diagenetic modifications.

3.6 Conclusions

This study integrates field observations and laboratory measurements to investigate the difference in petrophysical properties of columnar stromatolite heads in the Dam Formation (Miocene) in eastern Saudi Arabia. The results suggest the following conclusions:

- Stromatolites exhibit different morphologies above and below the SB. Below the SB, stromatolites show large, laterally extensive columnar structures. Above the SB, stromatolites have restricted lateral growth and develop vertical stacking.
- Below the SB, stromatolites are dominated by vuggy porosity. Above the SB, stromatolites have interparticle, moldic, and micro porosity, with more heterogeneity in the pore system.
- Significant differences in porosity, grain density, permeability, and velocity (VP) are observed between stromatolites above and below the SB. Stromatolites above the boundary show wider ranges of porosity and permeability, reflecting the presence of multiple pore types, while those below exhibit more uniform properties.
- The variation in morphology of stromatolites can be linked to hydrodynamic conditions, water depth, and sunlight availability. Lower sea levels favored lateral expansion of stromatolites, while rising sea levels promoted vertical growth to maintain sunlight exposure.
- Variation in pore system and petrophysical properties of stromatolites below and above the SB can be linked to both sedimentological and diagenetic controls.

The insights on stromatolite morphology and pore systems can guide well placement and production strategies in carbonate reservoirs. Moreover, these insights can help understand that diagenetic processes provide a framework for identifying areas with enhanced or reduced reservoir quality due to porosity changes. Thus, the study highlights the need for in depth studies to investigate what controls petrophysical properties within carbonate reservoirs influenced by stromatolites.

CHAPTER 4

Conclusions

Conclusions

This study synergized multi-disciplinary analyses to assess the impact of various stromatolite morphologies, as well as stromatolites with similar morphologies but different stratigraphic positions, on petrophysical properties. The study evaluated two proposed hypotheses: 1) *Stromatolites effects on petrophysical properties vary with different stromatolites forms* 2) *Stromatolites effects on petrophysical properties vary relative to the stratigraphic positioning*. The study concluded that differences in impact, as outlined in the proposed hypothesis, do indeed exist.

Comparing the petrophysical properties of two distinct stromatolite forms—the horizontally-linked form and the columnar form—revealed varying effects on porosity, permeability, and velocity. The horizontally-linked form displayed coarser rock textures, with occasional washout and burial, leading to a lower mud composition. While this did not significantly affect the initial porosity, it noticeably improved permeability compared to the other form. The columnar form exhibited a range of rock textures that did not significantly reduce porosity, but had a variable impact on permeability. The columnar form was deposited in a lower-energy environment and experienced less frequent burial, leading to the preservation of the mud component. The chemical composition did not have a significant impact on the recorded results.

The columnar form, positioned both below and above a major sequence boundary, exhibited some variability in the petrophysical evaluation. Below the sequence boundary, it underwent noticeable diagenesis, which altered some of the initial porosity. While this did not significantly change the porosity values, it improved the connectivity of the initially isolated porosity, resulting in enhanced permeability. Above the sequence boundary, the initial rock textures were preserved, leading to less uniform effects.

The outcomes of this study are important for reservoir characterization and modeling of stromatolite-bearing strata. We propose that the observed effects are globally consistent, provided the depositional conditions, stromatolite morphologies, and laminations are similar. Future studies could further investigate the potential variability in some samples with similar rock textures and micro to macro porosity ratios, but significantly different permeabilities.

References

[1] Al-Enezi, S.B.S.B.M., (2006). Comparison of recent and Miocene foraminifera from Eastern Saudi Arabia, King Fahd University of Petroleum and Minerals.

[2] Al-Juboury, A. I., & McCann, T. (2008). The middle Miocene Fatha (lower fars) formation, Iraq. GeoArabia, 13(3), 141–174. https://doi.org/10.2113/geoarabia1303141

[3] Al-Saad, H., & Ibrahim, M. I. (2002). Stratigraphy, micropaleontology, and paleoecology of the Miocene Dam Formation, Qatar. GeoArabia, 7(1), 9–28. https://doi.org/10.2113/geoarabia070109

[4] Ali, Syed Haroon, Abdullatif, O. M., Babalola, L. O., Alkhaldi, F. M., Bashir, Y., Qadri, S. M., & Wahid, A. (2021a). Sedimentary facies, depositional environments and conceptual outcrop analogue (dam formation, early miocene) Eastern Arabian platform, Saudi Arabia: A new high-resolution approach. Journal of Petroleum Exploration and Production Technology, 11(6), 2497–2518. https://doi.org/10.1007/s13202-021-01181-7

[5] Ali, Syed Haroon, Poppelreiter, M. C., Saw, B. B., Shah, M. M., & Bashir, Y. (2021). Facies, diagenesis and secondary porosity of a miocene reefal platform of Central Luconia, Malaysia. Carbonates and Evaporites, 36(3). https://doi.org/10.1007/s13146-021-00682-0

[6] Alkhaldi, F. M., Read, J. F., & Al-Tawil, A. A. (2021). Mixed carbonate-siliciclastic sequence development influenced by astronomical forcing on a distal foreland, miocene dam formation, eastern Saudi Arabia. Arabian Journal of Geosciences, 14(4). https://doi.org/10.1007/s12517-021-06459-y

[7] Allwood, A. C., Grotzinger, J. P., Knoll, A. H., Burch, I. W., Anderson, M. S., Coleman, M. L., & Kanik, I. (2009). Controls on development and diversity of early Archean stromatolites. Proceedings of the National Academy of Sciences, 106(24), 9548–9555. https://doi.org/10.1073/pnas.0903323106

[8] Allwood, A. C., Walter, M. R., Burch, I. W., & Kamber, B. S. (2007a). 3.43 billion-year-old stromatolite reef from the Pilbara craton of Western Australia: Ecosystem-scale insights to early life on Earth. Precambrian Research, 158(3–4), 198–227. https://doi.org/10.1016/j.precamres.2007.04.013

[9] Alrefaei, A. F., Rahim, M. A., & Pizzio, G. A. (2022). Cytochrome b lineages of Haemoproteus tinniculi in the endangered Saker Falcon (Falco Cherrug) in Saudi

Arabia. Journal of King Saud University - Science, 34(2), 101755. https://doi.org/10.1016/j.jksus.2021.101755

[10] Alsharhan, A. S. (2006). Sedimentological character and hydrocarbon parameters of the Middle Permian to Early Triassic Khuff Formation, United Arab Emirates. GeoArabia, 11(3), 121–158. https://doi.org/10.2113/geoarabia1103121

[11] Altermann, W. (2008). Accretion, trapping and binding of sediment in Archean stromatolites—morphological expression of the antiquity of life. Space Sciences Series of ISSI, 135, 55–79. https://doi.org/10.1007/978-0-387-77516-6_7

[12] Andres, M. S., & Pamela Reid, R. (2006a). Growth morphologies of modern marine stromatolites: A case study from Highborne Cay, Bahamas. Sedimentary Geology, 185(3–4), 319–328. https://doi.org/10.1016/j.sedgeo.2005.12.020

[13] Awramik, S. M. (1992a). The history and significance of stromatolites. Early Organic Evolution, 435–449. https://doi.org/10.1007/978-3-642-76884-2_34

[14] Awramik, S. M., & Riding, R. (1988). Role of algal eukaryotes in subtidal columnar Stromatolite Formation. *Proceedings of the National Academy of Sciences*, *85*(5), 1327–1329. https://doi.org/10.1073/pnas.85.5.1327

[15] Bashri, M., Abdullatif, O., & Salih, M. (2017a). Sedimentology and facies analysis of miocene mixed siliciclastic–carbonate deposits of the dam formation in Al Lidam area, eastern Saudi Arabia. Arabian Journal of Geosciences, 10(21). https://doi.org/10.1007/s12517-017-3244-1

[16] Batchelor, M. T., Burne, R. V., Henry, B. I., & Slatyer, T. (2005). Statistical physics and Stromatolite Growth: New perspectives on an ancient dilemma. Physica A: Statistical Mechanics and Its Applications, 350(1), 6–11. https://doi.org/10.1016/j.physa.2005.01.014

[17] Bellahsen, N., Faccenna, C., Funiciello, F., Daniel, J. M., & Jolivet, L. (2003). Why did Arabia separate from Africa? insights from 3-D laboratory experiments. Earth and Planetary Science Letters, 216(3), 365–381. https://doi.org/10.1016/s0012-821x(03)00516-8

[18] Beydoun, Z. R. (1993b). Evolution of the northeastern Arabian Plate margin and shelf: Hydrocarbon habitat and conceptual future potential. Revue de l'Institut Français Du Pétrole, 48(4), 311–345. https://doi.org/10.2516/ogst:1993021

[19] Bosak, T., Knoll, A. H., & Petroff, A. P. (2013). The meaning of stromatolites. Annual Review of Earth and Planetary Sciences, 41(1), 21–44. https://doi.org/10.1146/annurev-earth-042711-105327

[20] Buick, R., Dunlop, J. S. R., & Groves, D. I. (1981). Stromatolite recognition in Ancient Rocks: An appraisal of irregularly laminated structures in an early Archaean chert-barite unit from North Pole, Western Australia. Alcheringa: An Australasian Journal of Palaeontology, 5(3), 161–181. https://doi.org/10.1080/03115518108566999

[21] Byerly, G. R., Lower, D. R., & Walsh, M. M. (1986). Stromatolites from the 3,300–3,500-Myr Swaziland Supergroup, Barberton Mountain Land, South Africa. Nature, 319(6053), 489–491. https://doi.org/10.1038/319489a0

[22] Cantrell, D. L., & Hagerty, R. M. (1999). Microporosity in Arab Formation carbonates, Saudi Arabia. GeoArabia, 4(2), 129–154. https://doi.org/10.2113/geoarabia0402129

[23] Ceia, M., Missagia, R., Archilha, N., Baggieri, R., Santos, V., Fidelis, S., Oliveira, L., & Lima Neto, I. (2022a). Petrophysical characterization of Lagoa Salgada' stromatolites – a Brazilian pre-salt analog. Journal of Petroleum Science and Engineering, 218, 111012. https://doi.org/10.1016/j.petrol.2022.111012

[24] Chan, S. A., Kaminski, M. A., Al-Ramadan, K., & Babalola, L. O. (2017). Foraminiferal biofacies and depositional environments of the Burdigalian mixed carbonate and siliciclastic dam formation, Al-Lidam area, Eastern Province of Saudi Arabia. Palaeogeography, Palaeoclimatology, Palaeoecology, 469, 122–137. https://doi.org/10.1016/j.palaeo.2016.12.041

[25] Corbett, P., Hayashi, F. Y., Alves, M. S., Jiang, Z., Wang, H., Demyanov, V., Machado, A., Borghi, L., & Srivastava, N. (2015). Microbial carbonates: A sampling and measurement challenge for Petrophysics addressed by capturing the bioarchitectural components. Geological Society, London, Special Publications, 418(1), 69–85. https://doi.org/10.1144/sp418.9

[26] Dupraz, C., Reid, R. P., Braissant, O., Decho, A. W., Norman, R. S., & Visscher, P. T. (2009). Processes of carbonate precipitation in modern microbial mats. Earth-Science Reviews, 96(3), 141–162. https://doi.org/10.1016/j.earscirev.2008.10.005

[27] Ehrenberg, S. N., Nadeau, P. H., & Aqrawi, A. A. M. (2005). A regional comparison of Khuff and Arab reservoir potential throughout the Middle East. International Petroleum Technology Conference. https://doi.org/10.2523/iptc-10222-ms

[28] Eltom, H. A., Abdullatif, O. M., & Babalola, L. O. (2017). Redox conditions through the Permian-triassic transition in the Upper Khuff Formation, Saudi

Arabia. Palaeogeography, Palaeoclimatology, Palaeoecology, 472, 203–215. https://doi.org/10.1016/j.palaeo.2017.01.046

[29] Eltom, H. A., Abdullatif, O. M., & Babalola, L. O. (2018). The elemental geochemistry of Lower Triassic shallow-marine carbonates from central Saudi Arabia: Implications for redox conditions in the immediate aftermath of the latest Permian Mass Extinction. Journal of African Earth Sciences, 139, 283–306. https://doi.org/10.1016/j.jafrearsci.2017.12.020

[30] Esrafili-Dizaji, B., & Rahimpour-Bonab, H. (2014). Generation and evolution of Oolitic Shoal reservoirs in the permo-triassic carbonates, the South Pars Field, Iran. Facies, 60(4), 921–940. https://doi.org/10.1007/s10347-014-0414-4

[31] Ezaki, Y., Liu, J. B., & Adachi, N. (2011). Lower triassic stromatolites in Luodian County, Guizhou Province, South China: Evidence for the protracted devastation of the Marine Environments. Geobiology, 10(1), 48–59. https://doi.org/10.1111/j.1472-4669.2011.00309.x

[32] Farías, M. E., Poiré, D. G., Arrouy, M. J., & Albarracin, V. H. (2011). Modern stromatolite ecosystems at alkaline and hypersaline high-altitude lakes in the Argentinean Puna. Cellular Origin, Life in Extreme Habitats and Astrobiology, 427–441. https://doi.org/10.1007/978-94-007-0397-1_19

[33] Feldmann, M., & McKenzie, J. A. (1998). Stromatolite-thrombolite associations in a modern environment, Lee Stocking Island, Bahamas. PALAIOS, 13(2), 201. https://doi.org/10.2307/3515490

[34] Girdler, R. W. (1984). The evolution of the Gulf of Aden and Red Sea in space and Time. Deep Sea Research Part A. Oceanographic Research Papers, 31(6–8), 747–762. https://doi.org/10.1016/0198-0149(84)90039-6

[35] Grotzinger, J. P., & Knoll, A. H. (1999a). Stromatolites in Precambrian carbonates: Evolutionary mileposts or environmental Dipsticks? Annual Review of Earth and Planetary Sciences, 27(1), 313–358. https://doi.org/10.1146/annurev.earth.27.1.313

[36] Hampton, W. A., White, G. P., O. Hoskin, P. W., L. Browne, P. R., & Rodgers, K. A. (2004). Cinnabar, livingstonite, stibnite and pyrite in Pliocene silica sinter from Northland, New Zealand. Mineralogical Magazine, 68(1), 191–198. https://doi.org/10.1180/0026461046810180

[37] Hempton, M. R., & Barros, J. A. (1992). Mesozoic stratigraphy of Cuba: Depositional architecture of a southeast facing continental margin. Mesozoic and Early Cenozoic Development of the Gulf of Mexico and Caribbean Region: A

Context for Hydrocarbon Exploration: 13th Annual, 193–209. https://doi.org/10.5724/gcs.92.13.0193

[38] Hofmann, H. J. (1973). Stromatolites: Characteristics and utility. Earth-Science Reviews, 9(4), 339–373. https://doi.org/10.1016/0012-8252(73)90002-0

[39] Hoffman, P. (1976). Chapter 10.7 environmental diversity of middle precambrian stromatolites. Developments in Sedimentology, 599–611. https://doi.org/10.1016/s0070-4571(08)71161-0

[40] Hughes, G. W. (2010). Calcimicrobe tubules in uppermost jurassic arab-a carbonates of Saudi Arabia. *GeoArabia*, *15*(1), 17–26. https://doi.org/10.2113/geoarabia150117

[41] Ibarra, Y., & Corsetti, F. A. (2016a). Lateral comparative investigation of Stromatolites: Astrobiological implications and assessment of scales of Control. Astrobiology, 16(4), 271–281. https://doi.org/10.1089/ast.2015.1388

[42] Jackson, J., & McKenzie, D. (1984). Active tectonics of the Alpine--Himalayan belt between Western Turkey and Pakistan. Geophysical Journal International, 77(1), 185–264. https://doi.org/10.1111/j.1365-246x.1984.tb01931.x

[43] Jahnert, R. J., & Collins, L. B. (2012). Characteristics, distribution and morphogenesis of subtidal microbial systems in Shark Bay, Australia. Marine Geology, 303–306, 115–136. https://doi.org/10.1016/j.margeo.2012.02.009

[44] Jahnert, R. J., & Collins, L. B. (2013). Controls on microbial activity and tidal flat evolution in Shark Bay, Western Australia. Sedimentology, 60(4), 1071–1099. https://doi.org/10.1111/sed.12023

[45] Khalifa, M., Mahmoud, E., Ibrahim, M., (2012). Integration of 596 mycorrhiza and calcium treatments for suppression of onion white rot disease. Research Journal of Agriculture and Biological Sciences 8, 385-396.

[46] Knaust, D. (2011). Importance of trace fossils and bioturbation in carbonate reservoir characterization and reservoir quality: Examples from the Khuff Formation. Proceedings. https://doi.org/10.3997/2214-4609.20144063

[47] Kurth, D., Amadio, A., Ordoñez, O. F., Albarracín, V. H., Gärtner, W., & Farías, M. E. (2017). Arsenic metabolism in high altitude modern stromatolites revealed by metagenomic analysis. Scientific Reports, 7(1). https://doi.org/10.1038/s41598-017-00896-0

[48] Lacombe, O., Bellahsen, N., & Mouthereau, F. (2011). Fracture patterns in the Zagros Simply Folded Belt (Fars, Iran): Constraints on early collisional tectonic

history and role of basement faults. Geological Magazine, 148(5–6), 940–963. https://doi.org/10.1017/s001675681100029x

[49] Lindsay, F. R., L. Cantrell, D., W. Hughes, G., H. Keith Harry W. Mueller, T., & S. Duffy Russell, and. (2006). Ghawar Arab-D reservoir: Widespread porosity in shoaling-upward carbonate cycles, Saudi Arabia. GEO 2008. https://doi.org/10.3997/2214-4609-pdb.246.221

[50] Luo, C., & Reitner, J. (2016). 'stromatolites' built by sponges and microbes – a new type of Phanerozoic bioconstruction. Lethaia, 49(4), 555–570. https://doi.org/10.1111/let.12166

[51] Martin, A. Z. (2001). Late permian to holocene paleofacies evolution of the Arabian Plate and its hydrocarbon occurrences. GeoArabia, 6(3), 445–504. https://doi.org/10.2113/geoarabia0603445

[52] Mary, M., & Woods, A. D. (2008). Stromatolites of the Lower Triassic Union Wash Formation, CA: Evidence for continued post-extinction environmental stress in western North America through the Spathian. Palaeogeography, Palaeoclimatology, Palaeoecology, 261(1–2), 78–86. https://doi.org/10.1016/j.palaeo.2008.01.008

[53] McClusky, S., Reilinger, R., Mahmoud, S., Ben Sari, D., & Tealeb, A. (2003). GPS constraints on Africa (Nubia) and Arabia Plate Motions. Geophysical Journal International, 155(1), 126–138. https://doi.org/10.1046/j.1365-246x.2003.02023.x

[54] Mitchell, N. C., & Bosworth, W. (2024). The tectonic stability of Arabia. Rifting and Sediments in the Red Sea and Arabian Gulf Regions, 75–94. https://doi.org/10.1201/9781003321415-6

[55] Monty, C. L. V. (1976). Chapter 5.1 the origin and development of Cryptalgal Fabrics. Developments in Sedimentology, 193–249. https://doi.org/10.1016/s0070-4571(08)71137-3

[56] Muharrag, J., Eltom, H. A., El-Husseiny, A., & AlKhaldi, F. M. (2024). Influence of stromatolites on Petrophysical properties within stratigraphic contexts: A case study from the Dam Formation, eastern Saudi Arabia. Sedimentary Geology, 475, 106781. https://doi.org/10.1016/j.sedgeo.2024.106781

[57] Noennig, G., (2016). Analysis of Stromatolite Reservoir Potential using Computed Tomography, Gustavus Adolphus College.

[58] Noffke, Nora. (2009). The criteria for the biogeneicity of microbially induced sedimentary structures (miss) in Archean and younger, sandy deposits. Earth-Science Reviews, 96(3), 173–180. https://doi.org/10.1016/j.earscirev.2008.08.002

[59] Noffke, Nora, Christian, D., Wacey, D., & Hazen, R. M. (2013). Microbially induced sedimentary structures recording an ancient ecosystem in the ca. 3.48 billion-year-old dresser formation, Pilbara, Western Australia. Astrobiology, 13(12), 1103–1124. https://doi.org/10.1089/ast.2013.1030

[60] Nutman, A. P., Bennett, V. C., Friend, C. R., Van Kranendonk, M. J., & Chivas, A. R. (2016). Rapid emergence of life shown by discovery of 3,700-million-year-old microbial structures. Nature, 537(7621), 535–538. https://doi.org/10.1038/nature19355

[61] Pamela Reid, R., James, N. P., Macintyre, I. G., Dupraz, C. P., & Burne, R. V. (2003). Shark bay stromatolites: Microfabrics and reinterpretation of origins. Facies, 49(1). https://doi.org/10.1007/s10347-003-0036-8

[62] Powers, R. W., Ramirez, L. F., Redmond, C. D., & Elberg, E. L. (1966a). Geology of the Arabian Peninsula: Sedimentary geology of Saudi Arabia. Professional Paper. https://doi.org/10.3133/pp560d

[63] Proctor, J., de Luca, P. H., Pimentel, G. A., Sisk, C., Oliveira, M., Huber, A., Sungkorn, R., Alonso, J. L., Jiménez, R. P., & Silos, V. (2015). Porosity and permeability upscaling in a Lagoa Salgada stromatolite and Codó Formation Stromatolite. 14th International Congress of the Brazilian Geophysical Society & EXPOGEF, Rio de Janeiro, Brazil, 3-6 August 2015, 788–792. https://doi.org/10.1190/sbgf2015-154

[64] Reid, R. P., Macintyre, I. G., Browne, K. M., Steneck, R. S., & Miller, T. (1995). Modern marine stromatolites in the Exuma Cays, Bahamas: Uncommonly common. Facies, 33(1), 1–17. https://doi.org/10.1007/bf02537442

[65] Reid, R. P., Suosaari, E. P., Oehlert, A. M., Pollier, C. G. L., & Dupraz, C. (2024). Microbialite accretion and growth: Lessons from shark bay and the Bahamas. Annual Review of Marine Science, 16(1), 487–511. https://doi.org/10.1146/annurev-marine-021423-124637

[66] Reuter, M., Piller, W. E., Brandano, M., & Harzhauser, M. (2013). Correlating mediterranean shallow water deposits with Global Oligocene–Miocene stratigraphy and Oceanic events. Global and Planetary Change, 111, 226–236. https://doi.org/10.1016/j.gloplacha.2013.09.018

[67] Rezende, M. F., Tonietto, S. N., & Pope, M. C. (2013). Three-dimensional pore connectivity evaluation in a Holocene and Jurassic microbialite buildup. AAPG Bulletin, 97(11), 2085–2101. https://doi.org/10.1306/05141312171

[68] Riding, R. (2002). Microbial carbonates: The geological record of calcified bacterial–algal mats and biofilms. Sedimentology, 47(s1), 179–214. https://doi.org/10.1046/j.1365-3091.2000.00003.x

[69] Sakhavati, B., Yousefirad, M., Majidifard, M. R., Solgi, A., & Maleki, Z. (2020). Age of the gachsaran formation and equivalent formations in the Middle East based on Foraminifera. Micropaleontology, 66(5), 441–465. https://doi.org/10.47894/mpal.66.5.06

[70] Schopf, J. W. (2012). The fossil record of cyanobacteria. Ecology of Cyanobacteria II, 15–36. https://doi.org/10.1007/978-94-007-3855-3_2

[71] Schopf, J. W., Kudryavtsev, A. B., Czaja, A. D., & Tripathi, A. B. (2007). Evidence of archean life: Stromatolites and Microfossils. Precambrian Research, 158(3–4), 141–155. https://doi.org/10.1016/j.precamres.2007.04.009

[72] Schubert, J. K., & Bottjer, D. J. (1992). Early triassic stromatolites as post-mass extinction disaster forms. Geology, 20(10), 883. https://doi.org/10.1130/0091-7613(1992)020<0883:etsapm>2.3.co;2

[73] Sharland, P. R., Casey, D. M., Davies, R. B., Simmons, M. D., & Sutcliffe, O. E. (2004). Arabian plate sequence stratigraphy – revisions to SP2. GeoArabia, 9(1), 199–214. https://doi.org/10.2113/geoarabia0901199

[74] Słowakiewicz, M., Tucker, M. E., Pancost, R. D., Perri, E., & Mawson, M. (2013a). Upper Permian (zechstein) microbialites: Supratidal through deep subtidal deposition, source rock, and reservoir potential. AAPG Bulletin, 97(11), 1921–1936. https://doi.org/10.1306/06181312179

[75] Sprechmann, P., Gaucher, C., Blanco, G., & Montaña, J. (2004). Stromatolitic and trace fossils community of the Cerro Victoria Formation, Arroyo del Soldado Group (Lowermost Cambrian, Uruguay). Gondwana Research, 7(3), 753–766. https://doi.org/10.1016/s1342-937x(05)71061-3

[76] Suarez-Gonzalez, P., Benito, M., Quijada, I., Mas, R., & Campos-Soto, S. (2019). 'Trapping and Binding': A Review of the Factors Controlling the Development of Fossil Agglutinated Microbialites and Their Distribution in Space and Time. https://doi.org/10.31223/osf.io/aymxz

[77] Suarez-Gonzalez, P., Quijada, I. E., Benito, M. I., Mas, R., Merinero, R., & Riding, R. (2014). Origin and significance of lamination in Lower Cretaceous stromatolites and proposal for a quantitative approach. Sedimentary Geology, 300, 11–27. https://doi.org/10.1016/j.sedgeo.2013.11.003

[78] Vahrenkamp, V., Chandra, V., Garuglieri, E., Marasco, R., Hachmann, K., Khanna, P., Daffonchio, D., & Petrovic, A. (2024). Supplemental material: Discovery of modern living intertidal stromatolites on Sheybarah Island, Red Sea, Saudi Arabia. Geology, 52(5), 347–351. https://doi.org/10.1130/geol.s.25180655.v1

[79] Walter, M. R. (1976). Stromatolites (1st ed., Vol. 20). Elsevier Science.

Vitae

Name	:Jaber Muharrag
Nationality	:Saudi Arabian
Date of Birth	:8/3/1993
Email	:Jabir_5005@hotmail.com Jaber.muharrag@aramco.com
Address	:3655 Imam Al Termithy st., Uhud, Dammam 32263, Saudi Arabia
Academic Background	:B.S. in Geosciences from Louisiana State University; with a minor in business administration. M.S. in Geosciences from King Fahad University for Petroleum and Minerals
Research Papers	:The negative impact of Ophiomorpha on reservoir quality of channelized deposits in mixed carbonate siliciclastic setting: The case study of the Dam Formation, Saudi Arabia – 2022 (Co-author). Influence of stromatolites on petrophysical properties within stratigraphic contexts: A case study from the Dam Formation, eastern Saudi Arabia – 2024 (Main author). Petrophysical implications of stromatolite morphologies: 1

A case study of the Dam Formation, Saudi Arabia – 2024 (Main author).

Work Experience :CT scan geologist – Saudi Aramco (Feb 2017 – Feb 2018).

Field geologist – Saudi Aramco (Mar 2018 – Aug 2018).

Reservoir petrophysicist – Saudi Aramco (Sep 2018 – Aug 2019).

CT scan geologist – Saudi Aramco (Sep 2019 – Dec 2022).

Exploration geologist – Saudi Aramco (Jan 2023 – Today).